technische universität
dortmund

Dissertation zur Erlangung des akademischen Grades
Doktor der Naturwissenschaften

Modulation of the transient magnetization of an EuO/Co bilayer by controlled optical excitation

David Mönkebüscher
geboren in Soest

2023

AG Cinchetti
Fakultät Physik
Technische Universität Dortmund

Dissertation zur Erlangung des akademischen Grades Doktor der Naturwissenschaften.
Akzeptiert von der Fakultät Physik der TU Dortmund.

Abgabedatum: 22. September 2023
Disputation: 06. Dezember 2023

Prüfungskommission:
Prof. Dr. Mirko Cinchetti
Prof. Dr. Martina Müller
Jun.-Prof. Dr. Wolfram Helml
Dr. Tim Ruhe

Kurzfassung

Der ferromagnetische Halbleiter Europiummonoxid (EuO) gilt als vielversprechender Kandidat für neuartige spintronische Anwendungen, da er ein großes magnetisches Moment und starke magneto-optische Effekte mit isolierenden Eigenschaften vereint. Obwohl EuO mit $T_C = 69\,K$ die höchste Curie-Temperatur unter den Europiumchalkogeniden aufweist, ist sie für kommerzielle Anwendungen zu niedrig. Viele Ansätze zur Erhöhung von T_C, wie zum Beispiel die Dotierung mit Gd-Ionen oder epitaktische Verformung, wurden bereits erfolgreich untersucht. Jedoch basieren sie alle auf einer Veränderung der Stöchiometrie und Leitfähigkeit des Seltenerdoxids. Das Ausnutzen des Proximity-Effektes könnte eine alternative Herangehensweise für das starke Erhöhen der magnetischen Ordnungstemperatur von EuO darstellen, die gleichzeitig dessen intrinsischen Eigenschaften bewahrt. Dieser Effekt beruht auf der Kopplung an einen Ferromagneten mit hoher Curie-Temperatur und ist in der Literatur für ähnliche System bereits demonstriert worden.

In dieser Arbeit wird ein EuO/Co-Zweischichtsystem dünner Filme mittels des statischen und zeitaufgelösten magneto-optischen Kerr-Effekts (MOKE) untersucht, um einen Nachweis für eine erhöhte Curie-Temperatur von EuO aufgrund der Nähe zum Übergangsmetall Co zu finden. Des Weiteren wird der Einfluss von Co auf die Spindynamik von EuO untersucht. Statische Messungen der Hysterese der EuO/Co-Probe zeigen eine antiferromagnetische Kopplung zwischen den beiden ferromagnetischen Schichten. Aufgrund der Überlagerung des Signals beider Schichten übersteigt die Co-Hysterese einen möglichen Restbeitrag von EuO bei erhöhten Temperaturen. Zeitaufgelöste MOKE-Messungen zeigen eine transiente Verstärkung der EuO-Magnetisierung, die auch dann auftritt, wenn selektiv nur das Übergangsmetall angeregt wird. Dieses Verhalten wird auf die Erzeugung eines superdiffusven Spinstroms von Majoritätselektronen bei der Entmagnetisierung der Co-Schicht zurückgeführt. Der Spinstrom breitet sich in Richtung der EuO-Schicht aus, um deren 5d-Zustände zu besetzen, was zu einer ähnlichen Magnetisierungsverstärkung wie bei einer direkten Photoanregung des Seltenerdoxids führt. Die Beiträge beider Schichten zur transienten Spindynamik zeigen entgegengesetze Vorzeichen. Daher bietet die EuO/Co-Probe ein System, in dem die transiente Kerr-Rotation durch Variation externer Parameter wie der Probentemperatur, des angelegten Magnetfelds und der Pumpstrahlfluenz beeinflusst werden kann. Durch eine starke Anregung der Co-Schicht wird ihre Magnetisierung signifikant verringert, wodurch die Hysterese der EuO-Schicht bei transienten Hysteresemessungen zugänglich wird. Sie ist auch noch bei einer Temperatur von 300 K zu beobachten, was auf eine starke Erhöhung der magnetischen Ordnungstemperatur von EuO, bedingt durch die Nähe zu Co, hindeutet.

Abstract

The ferromagnetic semiconductor europium monoxide (EuO) is a promising candidate for new spintronic applications due to its large magnetic moment and strong magneto-optical effects combined with its insulating properties. Although EuO has the highest Curie temperature among the europium chalcogenides with $T_C = 69\,K$, it still requires excessive cooling in real applications. Many approaches to increase its T_C have been successfully studied, such as doping with Gd ions or epitaxial straining, which inevitably change the stoichiometry and conductivity of the rare earth oxide. An alternative pathway to greatly increase the Curie temperature of EuO while preserving its conductivity and stoichiometry could be based on the magnetic proximity effect. This effect relies on the coupling to a high T_C ferromagnet, and has been demonstrated in the literature for similar systems.

In this thesis, a EuO/Co bilayer of thin films is studied using the static and time-resolved magneto-optical Kerr effect (MOKE) to find an evidence for an elevated EuO T_C due to the proximity to the transition metal Co. Furthermore, the influence of Co on the spin dynamics of EuO is investigated. Static measurements of the EuO/Co bilayer hysteresis reveal an antiferromagnetic coupling between the two ferromagnetic layers. Due to the superposition of the measured signal of both layers, the Co hysteresis exceeds any possible residual EuO contribution to the magneto-optical signal above its bulk T_C. Time-resolved MOKE measurements show a transient enhancement of the EuO magnetization. It is still present when the Co layer is selectively photoexcited by tuning the photon energy of the pump beam below the EuO band gap energy. This behavior is attributed to the generation of a superdiffusive spin current of majority electrons upon demagnetizing the Co layer. It propagates towards the EuO layer to populate its 5d states, inducing a similar magnetization enhancement compared to direct photoexcitation of the rare earth oxide. The two layers of the investigated sample system exhibit a contribution to the transient spin dynamics with opposite signs. Therefore, the EuO/Co bilayer provides a system in which the transient magneto-optical Kerr rotation can be tuned by varying external parameters such as the sample temperature, the applied magnetic field and the pump beam fluence. By strongly exciting the Co layer and thus quenching its magnetization, the EuO hysteresis becomes accessible in transient hysteresis measurements. It persists up to a temperature of $300\,K$, pointing to an experimental evidence for room temperature magnetic order in EuO induced by proximity to Co.

Contents

1 Introduction

The development of the transistor in the first half of the 20th century earned its inventors John Bardeen, William Shockley and Walter Brattain the Nobel Prize in 1956 [1]. It caused a paradigm shift in electronics and marked the onset of the information age, leading to rapid technological advances over the past 60 years [2]. Semiconductor-based transistors replaced vacuum tubes not only by performing all of their functions, like signal amplification and rectification, but also by offering many advantages, such as lower cost and power consumption combined with better reliability and portability [3]. Crucially, the possibility to scale and miniaturize the size of transistors and similar electronic components, and to combine large numbers of elements in integrated circuits (ICs) and microprocessors is the backbone of all information technology in use today, ranging from computers and smart phones to cars and televisions [3, 4]. Since their invention, the number of transistors in ICs has doubled approximately every 18 months, as predicted by the famous Moore's Law, hypothesized by Gordon Moore in 1965 [5]. This development has led to significant performance improvements and thus major technological advances, while simultaneously reducing the cost and power consumption of applications [2, 6].

In recent years, however, this trend has slowed down as the miniaturization of electronic components reaches its physical limits and thus became more complex. It also brings new challenges like increased fabrication costs and an amplified heat generation due to the small size [7, 8]. A direct consequence of the increasing heat accumulation in ICs is the limitation of the microprocessor clock speeds, which have stagnated at values of up to about 5 GHz for nearly 20 years [7, 9]. To overcome this limitation, multi-core processors have been developed that can handle multiple tasks simultaneously. However, since most programs cannot take full advantage of them, the technological progress in processor performance has slowed drastically [8, 10, 11]. Very specialized microchips, like graphics processing units (GPUs) used in personal computers, are less affected by this limitation. The design of their tasks allows them to effectively use up to several thousand cores, and because they are usually stationary, they can be actively cooled [11, 12]. This has led to continuous progress in the development of GPUs with impressive achievements in short periods of time. An example of this development is the relative increase of the processing power of the flagship GPUs of the company Nvidia from 2017 to 2022, which increased by several hundred percent at the expense of an 80 % increase

in power consumption [13, 14]. With the ever-increasing demand for faster data processing, ideally at lower power consumption, new technologies must be explored to support or replace traditional semiconductor-based electronics that carry and manipulate information by controlling the charge of electrons.

The implementation of spintronics (*spin*-based elec*tronics*), which considers electron spin to carry, store, and read information in addition to or instead of the charge, offers a promising alternative for the future of information technology. Utilizing this degree of freedom offers several advantages for electronic devices, such as reduced power consumption, non-volatile data storage, and faster data processing [15]. The discovery of the giant magnetoresistance (GMR) in the late 1980s by Albert Fert [16] and Peter Grünberg [17], for which they were awarded with the Nobel Prize in 2007 [18], marks the beginning of the development of spintronics. GMR describes a significant reduction in the electrical resistance of ferromagnetic multilayers by changing their coupling from antiparallel to parallel, for example by applying a magnetic field. Less than a decade after its discovery, GMR was already utilized in several applications like magnetic sensors and, more importantly, as read heads for hard disk drives, providing a fast and sensitive technique for reading out data. It thus paved the way for major increases in storage density of up to several hundred gigabits per square inch [19, 20]. Another important effect contributing to this development is the tunnel magnetoresistance (TMR), which is widely used in hard disk drives and in magnetoresistive random-access memory (MRAM). TMR relies on two ferromagnetic layers separated by a thin insulating layer that allows electrons to tunnel from one layer to the other. The tunneling probability is greatly enhanced for a parallel orientation of the two ferromagnetic layers, providing control of the electrical resistance by manipulating the orientation of the magnetizations by applying an external magnetic field [21, 22]. Further refinement of this technology led to the spin-transfer torque (STT) technique, which uses spin current instead of magnetic field pulses to switch the orientation of the magnetization. STT is a promising technology for the future of non-volatile data storage due to a better scalability and lower power consumption [23, 24].

Besides continued development to improve data storage capabilities, a lot of research has been conducted on a variety of interesting materials for a new generation of spintronic devices like spin filters [25–27], spin transistors [28–30], or spin diodes [31, 32]. This work is intended to pave the way towards more energy-efficient, smaller, and faster electronics for information technology [33]. A particularly promising class of materials in this regard are magnetic semiconductors. They offer the possibility to combine the magnetic non-volatility of memory with the functionality of high-speed logic, developed over decades for semiconductors. This exciting combination of properties could provide promising new devices for emerging technologies like artificial intelligence and neuromorphic computing [34, 35]. To date, many proposed

spintronic devices, such as spin transistors or spin diodes, rely on the coupling of a ferromagnetic metal to a non-magnetic semiconductor. Replacing the metal with a ferromagnetic semiconductor could solve issues at the interface such as spin scattering and a conductivity mismatch [35]. In addition, this class of materials could ideally merge spintronics with optoelectronics, leading to new devices such as spin lasers with advantages like faster modulation dynamics and better polarization control [36]. Although much research has already been done on various ferromagnetic semiconductors, they are not yet widely used due to major challenges like magnetic ordering temperatures below room temperature and the successful integration with other electronics [36–39].

A particularly promising candidate in this class of materials is the rare earth oxide europium monoxide (EuO), a ferromagnetic semiconductor with a Curie temperature of 69 K and a band gap energy of about 1.2 eV [40]. It offers interesting magnetic properties with a strong magnetic moment of $7\,\mu_\mathrm{B}$ combined with large magneto-optical effects: EuO exhibits a Kerr rotation at least an order of magnitude larger than that of transition metals [41, 42] and one of the largest known Faraday rotations [43]. In addition, it shows intriguing transient properties on the picosecond timescale, with an enhancement of the magnetization upon photoexcitation. This effect is induced by the transition of 4f electrons to 5d states, thus strengthening the ferromagnetic order of the rare earth oxide [44]. This combination of interesting magnetic, magneto-optical and insulating properties makes EuO a promising candidate for a new generation of spintronic applications. It has already been successfully employed as a spin filter, generating electron currents with up to 100 % spin-polarization [26, 45, 46].

The low magnetic ordering temperature of EuO provides a challenge that must be overcome before it can be utilized in real applications. Different approaches, like doping with Gd or inducing oxygen vacancies, have been successful in increasing T_C up to about 170 K, at the expense of altering the stoichiometry and conductivity [47–51]. An alternative approach to greatly increase the magnetic ordering temperature, while preserving the intrinsic magnetic and insulating properties of EuO could rely on the magnetic proximity effect, i.e., the magnetic coupling to a ferromagnet with a high Curie temperature. This effect has been successfully demonstrated for thin films of EuS coupled to the transition metal Co, effectively raising the magnetic ordering temperature of the ferromagnetic semiconductor from 16 K up to at least 300 K [52, 53]. A similar sample system of thin film bilayers of Co grown on EuO is studied in this thesis using the magneto-optical Kerr effect (MOKE) to find evidence for an increased EuO T_C due to proximity to Co. Furthermore, transient MOKE measurements as a function of the time delay and the applied magnetic field are employed to investigate the influence of the transition metal on the EuO spin dynamics on the picosecond timescale. Some of the figures and data discussed in

this thesis are published by Mönkebüscher et al. [54]. The employed measurement approaches are schematically shown in figure 1.1.

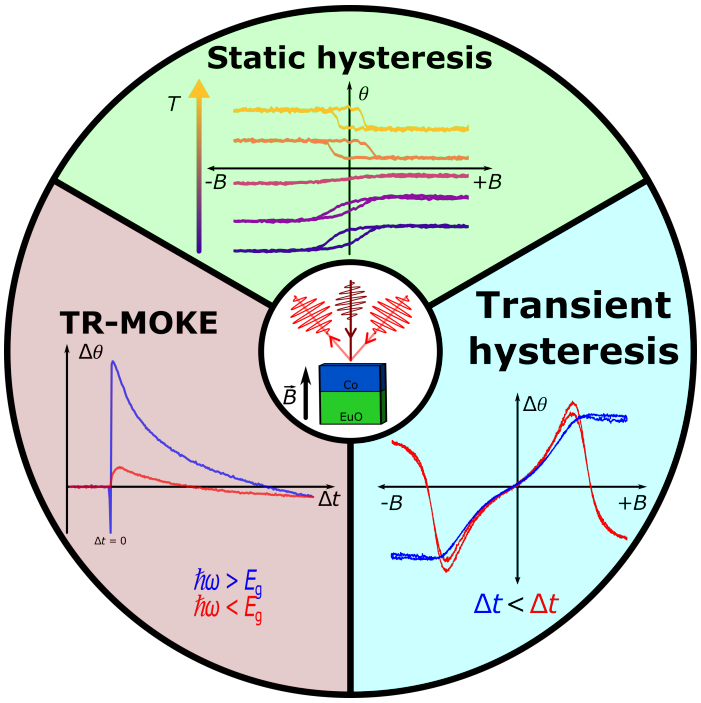

Figure 1.1: Schematic illustration of the different magneto-optical measurement approaches used in this thesis to study the ferromagnetic thin film bilayer consisting of Co grown on EuO.

The thesis is structured as follows: Chapter 2 discusses the most fundamental concepts of magnetism, including magnetic anisotropy and domains as the origin of the magnetic hysteresis curve of ferromagnets. It also provides an overview of the magnetic properties of the europium chalcogenides and discusses different approaches to increase the Curie temperature of EuO. Chapter 3 focuses on static and time-resolved magneto-optical effects, especially the magneto-optical Kerr effect (MOKE), the primary technique employed for this thesis. In addition, the ultrafast demagnetization of transition metals like Co is discussed and the two setups used are described. The sample system and a static characterization by means of MOKE are presented in chapter 4. The spin dynamics of the sample are discussed in chapters 5 and 6 using transient MOKE measurements as a function of the time delay between the pump and probe beam and the magnetic field, respectively. The results of the thesis are summarized in chapter 7, together with an outlook on the future studies.

2 Basics of magnetism

The phenomenon of magnetism has been known since ancient times, and the first reports of simple applications date back to more than 2000 years ago in China [55]. Only with the advances in quantum mechanics over the last hundred years it has become possible to understand the origin and processes of magnetism [56], leading to a plethora of applications ranging from medical uses [57] to data storage [58], transistors and electric motors [59]. Within the scope of this thesis, only the most general concepts of magnetism will be described. A more comprehensive introduction into magnetism can be found in the cited textbooks [55, 59–61].

2.1 Magnetic materials

Materials are classified according to their interactions with external magnetic fields, which differ mainly in the behavior of their magnetic moments. Materials such as H_2O, Cu, Au, or Bi have no permanent magnetic moments and therefore belong to the class of **diamagnets**. By applying an external magnetic field, magnetic moments and thus a magnetization, can be induced. As described by Lenz's Law, the orientation of these induced magnetic moments is antiparallel to the applied magnetic field [62]. If magnetic moments are present in a material even without an external magnetic field, it belong to the class of **paramagnets**. Since there is no interaction between these magnetic moments, their orientation is random and the net magnetization of paramagnets is zero. Contrary to diamagnetic materials, the magnetic moments in paramagnets align in the direction of an applied magnetic field, leading to a finite and positive magnetization. It is defined as the sum of magnetic moments per volume [55]. Examples of paramagnetic materials include most rare earth metals and alkali metals. Both para- and diamagnetism can be distinguished by their respective behavior for insulators (Larmor diamagnetism and Langevin paramagnetism) and metals (Landau diamagnetism and Pauli paramagnetism). They are described in detail in the literature [59, 60], but an elaboration of these topics is beyond the scope of this thesis.

In para- and diamagnetic materials, a finite magnetization can only be achieved by applying an external magnetic field, since the magnetic moments do not interact with each other. This changes in the so-called cooperative magnetism, where a

spontaneous magnetization can occur, even without an external magnetic field. The magnetic moments of this material class interact with each other and arrange into an ordered phase below a material-specific critical temperature. Above this ordering temperature, the ordered phase of the magnetic moments is destroyed by thermal fluctuations. Three types of magnetically ordered materials can be distinguished, as schematically shown in figure 2.1: ferromagnets, antiferromagnets, and ferrimagnets.

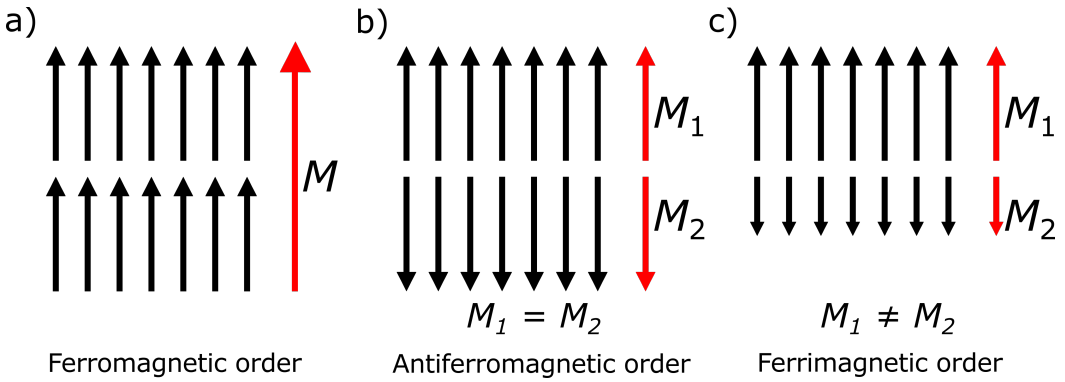

Figure 2.1: Schematic illustration of the basic magnetic order in (a) ferromagnets, (b) antiferromagnets and (c) ferrimagnets in the ordered state. Red arrows depict the total magnetization of the magnetic lattices or sublattices.

In **ferromagnets**, the magnetic moments are ordered parallel to each other below their magnetic ordering temperature, called the Curie temperature (T_C). Due to the parallel ordering, a finite magnetization appears, which is strongly temperature-dependent and disappears above T_C. Well-known elemental ferromagnetic materials are the 3d transition metals Ni, Fe, and Co, all of which have a magnetic ordering temperature well above the room temperature. Other examples are the 4f rare earths, like Gd, Dy, and Ho, which have much lower T_C. **Antiferromagnets** are characterized by two magnetic sublattices with magnetizations of equal amplitude and antiparallel ordering, resulting in a vanishing net magnetization. The magnetic ordering temperature of antiferromagnets is called Néel temperature (T_N). Several oxide materials like NiO, CoO or FeO are examples of antiferromagnets.

Ferrimagnetic materials are similar to antiferromagnets with antiparallel aligned magnetic moments of the magnetic sublattices, which have different magnetizations. Therefore, ferrimagnets have a finite net magnetization below the magnetic ordering temperature, also known as the Curie temperature. A famous example for such a material is magnetite (Fe_3O_4), the first known magnetic material [55]. Other examples for ferrimagnets are transition metal-rare earth (TM-RE) alloys and

iron garnets [63]. There are also synthetic ferrimagnets, which consists of two adjacent ferromagnetic layers with antiferromagnetic coupling, such as Gd/Co multilayers [64, 65]. The varying intrinsic properties of the magnetic sublattices, i.e., the different dependence on the temperature, can give rise to a ferrimagnet-specific phenomenon called compensation temperature T_{Comp} [59]. At this temperature, the antiferromagnetically coupled magnetizations are equal in amplitude, leading to a vanishing net magnetization, as shown schematically for a TM-RE ferrimagnet in figure 2.2. Passing this temperature results in a change of the dominant magnetic contribution and thus, due to the antiferromagnetic coupling, in a change of the sign of the net magnetization of the ferrimagnet [66].

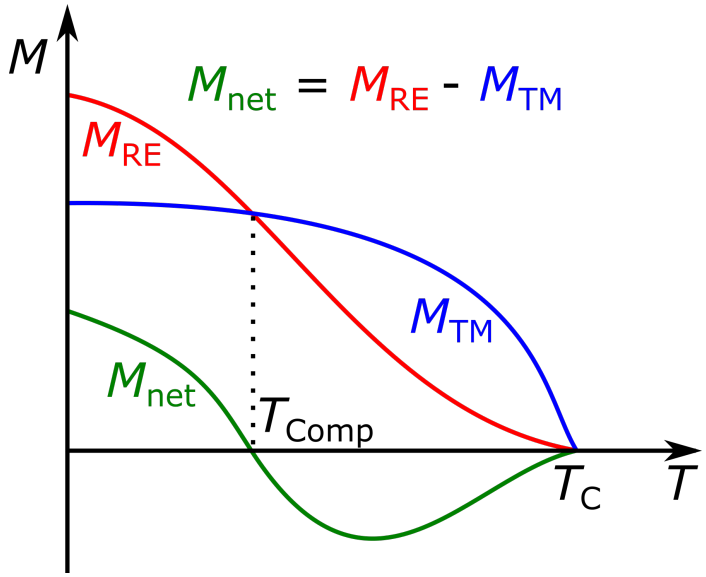

Figure 2.2: Schematic illustration of the temperature dependence of the different magnetizations present in a TM-RE ferrimagnet. The rare earth magnetization M_{RE} is dominant at low temperatures and the transition metal magnetization M_{TM} dominates at higher temperatures. At the compensation temperature T_{Comp}, the antiferromagnetically coupled magnetizations are equal in amplitude, leading to a vanishing net magnetization M_{net}. Passing T_{Comp} changes the sign of M_{net}, as the dominant magnetic contribution in the ferrimagnetic system changes.

2.2 Exchange interaction

The spontaneous magnetization that occurs in ferro-, ferri and antiferromagnets below their respective magnetic ordering temperature relies on the quantum me-

chanical exchange interaction between magnetic moments. It originates from the Coulomb interaction between two electrons from neighboring atoms combined with the Pauli principle, and is described in detail in the literature [59, 60]. Essentially, the wave functions of the electrons overlap and the exchange interaction describes the energy difference between the parallel and antiparallel spin configurations E_p and E_a:

$$J_\mathrm{ex} = E_\mathrm{p} - E_\mathrm{a} \quad . \tag{2.1}$$

The sign of the material-specific exchange constant J_ex determines whether a parallel or antiparallel alignment between the magnetic moments is preferred. A positive J_ex promotes a ferromagnetic order, while a negative J_ex leads to an antiferromagnetic order [60].

Exchange interaction can appear in different forms. It can be direct, i.e., with two overlapping wave functions, but indirect interactions like the superexchange are also possible. In the superexchange, the interaction between two magnetic moments is mediated by a diamagnetic atom separating the two moments. For example, the antiferromagnetic order of MnO between the Mn^{2+} ions is mediated by an overlap of the wave functions of the Mn 3d and the O 2p orbitals [60]. Generally, this indirect exchange interaction can lead to a ferromagnetic or predominantly to an antiferromagnetic alignment between the magnetic moments [59, 67].

A good description of the cooperative magnetism is based on the Heisenberg model, which considers only a pairwise interaction of magnetic moments. In this model, the exchange interaction can be described by the spin-dependent Hamiltonian

$$H_\mathrm{ex} = -2 \sum_{i>j} J_{ij} S_i \cdot S_j \tag{2.2}$$

with the dimensionless spin operators $S_{i,j}$ and the exchange constant J_{ij} interacting between two magnetic moments i and j [59]. The Heisenberg model successfully describes systems with localized electrons like EuO, but it is insufficient for the 3d transition metals Co, Fe and Ni [60, 68]. For these materials, the collective interaction of a single electron with the free electron gas has to be considered in addition to the pairwise interaction of electrons [60]. A model to describe the band magnetism in these materials has been proposed by Stoner, which considers an even split into spin-up and spin-down electrons near the Fermi energy by an internal molecular field [69]. A redistribution of spin-down electrons to spin-up states can lead to a finite magnetization, but is only possible if this process is energetically favorable. This transfer of electrons increases their kinetic energy, but can also lead to a decrease of the potential energy of the system, effectively reducing the total energy [60]. A simple formula that describes whether ferromagnetism is energetically

allowed in metals is the Stoner criterion

$$\frac{1}{2}UD(E_{\mathrm{F}}) > 1 \tag{2.3}$$

with the energy U, which is proportional to the molecular field, and the density of states at the Fermi energy $D(E_{\mathrm{F}})$ [60]. It is only fulfilled by the 3d transition metals Co, Ni and Fe [61].

2.3 Magnetic anisotropy

The magnetization in crystalline ferro-, ferri-, and antiferromagnetic materials tends to have a preferred crystallographic direction, called the easy axis, caused by the magnetic anisotropy. The total magnetic anisotropy of a system is defined as the energy required to rotate the magnetization from the easy axis to the hard axis, e.g. from an in-plane to an out-of-plane geometry [60]. It has three major contributions: the magnetocrystalline anisotropy, the shape anisotropy and the induced anisotropy [55]. The magnetocrystalline anisotropy is an intrinsic material property resulting from the spin-orbit interaction. It couples the spin to the orbital motion of the electrons, and thus also to the anisotropic crystal lattice, inducing a preferential orientation of the spins [60]. The shape anisotropy depends on the specific shape of a sample and the corresponding demagnetization field. A contribution from the induced anisotropy can occur, for example, by uniaxial strain or by annealing a sample with an applied magnetic field [59]. Additional contributions to the magnetic anisotropy can originate for example from mechanical pressure or an external magnetic field [60].

The magnetic anisotropy is an important property of materials. Hard magnetic materials have strong anisotropy, which means that a lot of energy is required to change the direction of magnetization. This makes them ideal candidates for permanent magnets, for example, in electric motors or generators [59]. If the magnetic anisotropy is neglectable, the direction of the magnetization can be changed with hardly any energy required. These materials are called soft magnets, and are often used in electromagnets and transformers [59].

2.4 Domains and hysteresis curves

The net magnetization of ferromagnets below their T_{C} is often smaller than their saturation magnetization, which occurs when all spins are aligned in parallel with an applied magnetic field. In the absence of an applied field, the magnetization breaks

up into small regions called magnetic domains. Within each domain, the spontaneous magnetization is equal to the value of the saturation magnetization. However, since the magnetizations of different domains are not necessarily aligned parallelly, they can compensate for each other, leading to a reduced macroscopic net magnetization. The boundary between adjacent domains is defined by a domain wall, which marks the transition of the orientation of the magnetic moments between the orientations of the different domains. In general, they also appear in antiferromagnets and ferrimagnets [59, 60]. The origin and formation of domains will be discussed only briefly within the scope of thesis, but a comprehensive introduction can be found in the literature [59, 70].

The process of domain formation is schematically shown in figure 2.3 (a). Magnetic domains are formed to minimize the total energy of the system. In the case of a single domain system, where all magnetic moments are aligned parallel, the stray field is large and increases the energy of the system. By forming domains with an antiparallel magnetization orientation, the stray field is reduced. This comes at the cost of an increased exchange interaction. As long as it is energetically favorable, i.e., the total energy of the system is reduced, large domains will split into smaller domains. The formed domains do not necessarily have to be aligned antiparallel to each other, but can also be formed, for example, at a 45° angle to eliminate the stray field outside of the sample. This comes at additional cost of anisotropy energy due to a deviation from the preferred parallel alignment at the domain walls [63].

The Zeeman interaction, which describes the interaction between the magnetic moments and an externally applied field, acts as an additional contribution to the total energy of the system. It depends on the angle between the magnetic moments and the field and is minimized for a parallel alignment along the field direction [60]. Small magnetic fields can induce motion of the domain walls, leading to a growth of domains with a favorable orientation of the magnetization at the expense of domains with an unfavorable orientation. When the magnetic field is increased and exceeds a threshold, the magnetization of the system begins to rotate towards the field direction. If the applied field is sufficiently strong, the sample will reach a single domain state, where all magnetic moments are oriented parallel to the field direction and its magnetization will match the value of the saturation magnetization [60]. The manipulation of domains by applying an externally magnetic field is schematically illustrated in figure 2.3 (b).

The actual behavior of domains in the presence of magnetic fields can be explored by recording magnetization curves, i.e., measurements of the magnetization as a function of the applied field. It manifests itself in a distinct hysteresis, as shown schematically in figure 2.4. This hysteresis arises from the ferromagnetic domain structure, so that its shape depends on the exchange interaction and the magnetic

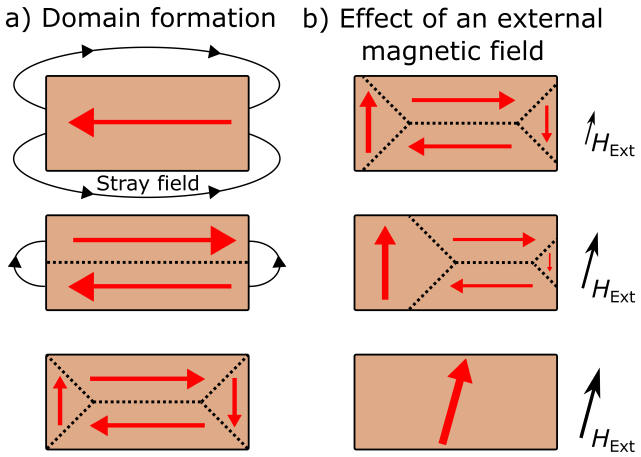

Figure 2.3: Schematic illustration of the domain structure of a ferromagnet. a) Domains are formed to reduce the total energy of the system. Forming domains reduces the stray field, but increases the exchange and anisotropy energies. b) By applying an external field favorably oriented domains will grow at the expense of unfavorably oriented domains. If the external field is sufficiently strong, the sample will reach a single domain state with the magnetization rotated towards the magnetic field direction.

anisotropy [71]. Magnetization curves, often called hysteresis loops, provide insight into various magnetic properties of a sample, such as the presence of a ferromagnetic state, the saturation magnetization, the direction of the anisotropy, the magnetic hardness and more.

The remanent magnetization M_R is an indicator of the spontaneous magnetization present in a ferromagnet in the absence of an external magnetic field. The remanence can be as large as the saturation magnetization M_S, but domain formation leads to a reduction [71]. The remanent magnetization can be removed by applying a sufficiently strong magnetic field in the opposite field direction, which leads to a demagnetization. The magnetic field required to completely demagnetize a ferromagnet is called coercive field, a quantity which can vary from a few microtesla in soft magnetic materials up to several hundred millitesla in hard magnetic materials [71]. As described in section 2.3, ferromagnets tend to have preferential orientations of the magnetic moments, leading to the presence of an easy and a hard magnetization axis. The shape of the hysteresis can differ greatly between these two orientations, as illustrated exemplarily in figure 2.4 in blue and red for the easy and hard axis, respectively. The hysteresis loop performed along the easy axis shows a large coercivity and remanence. The magnetization curve recorded along the hard axis, on the other hand, shows a linear dependence on the applied external field

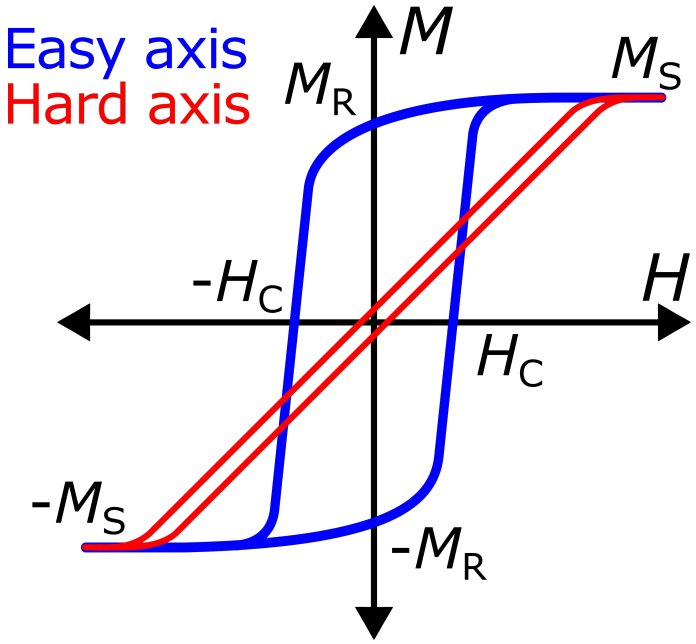

Figure 2.4: Schematic illustration of the hysteresis in the magnetization curve of an arbitrary ferromagnet. The saturation magnetization M_S, the remanence M_R and the coercive field H_C are defined in the main text. The hysteresis loops in blue and red show an example of magnetization curves measured along the easy and hard magnetization axis of a ferromagnet.

between positive and negative saturation magnetization. This behavior can be attributed to the orientation of the domains, which are mostly ordered along the easy magnetization axis. Since they are not necessarily aligned parallel to each other, the typical ferromagnetic hysteresis arises from the growth of favorably oriented domains at the expense of unfavorably oriented domains when an external magnetic field is applied along the easy magnetization axis. If instead the magnetic field is applied along the hard axis, most of the domains are oriented perpendicular to the field. As no domain is in a favorable position, the shape of the magnetization curve arises only from the reversible rotation of the domain magnetizations, as opposed to the irreversible growth of domains along the easy axis [71].

2.5 Magnetism of the europium chalcogenides

EuO, the material studied in this thesis, belongs to the family of the europium chalcogenides EuX (X = O, S, Se, Te). They were among the first magnetic

semiconductors to be discovered and have been extensively studied since the 1960s [48, 49, 72–82]. In this class of materials, an ionic bond is formed between the Eu atoms and the chalcogens using two of the 6s electrons of the rare earth. They saturate the p orbital of the chalcogen and thereby create divalent Eu^{2+} cations with an electronic configuration of [Xe] $4f^7$ [49]. As 4f electrons tend to be very localized, their atomic character is retained even when crystallized, and the effects of the crystal field are negligible [49, 83]. The EuX compounds have a fully polarized ground state with a magnetic moment of $7\mu_B$ due to their half-filled 4f shell. Following the Hund's rules, the angular momentum L is vanishing and the total angular momentum $J = {}^8S_{7/2}$ is equal to the spin angular momentum S [83].

The europium chalcogenides are often described as a model system for the localized Heisenberg exchange interaction, introduced in section 2.2. Their effective Hamiltonian can be approximated via

$$H_{ex} = -\sum_{ij} J_{ij} \left(\vec{S}_i \cdot \vec{S}_j\right) \approx -\sum_{nn} J_1 \left(\vec{S}_0 \cdot \vec{S}_{nn}\right) - \sum_{nnn} J_2 \left(\vec{S}_0 \cdot \vec{S}_{nnn}\right) \tag{2.4}$$

with the nearest-neighbor S_{nn} and next-nearest-neighbor S_{nnn} spins and their corresponding exchange constants J_1 and J_2 [83]. The latter determine the type of coupling between the spins via their magnitude and sign. J_1 and J_2 represent competing exchange mechanisms, that have been described in detail by Kasuya [75]. The ferromagnetic nearest-neighbor exchange interaction J_1, acting between the Eu ions, consists of virtual excitations of 4f electrons to the 5d band. The excited electrons experience a d-f exchange interaction to the nearest-neighbor Eu ion and relax back to the ground state. J_1 is strongly dependent on the lattice constant and is reduced for the larger chalcogenides. The interaction between the next-nearest-neighbor Eu ions is described by J_2 and generally promotes antiferromagnetic ordering. Several exchange mechanisms can play a role in these interactions, such as the superexchange interaction, where an f electron from one Eu ion is transported to the f orbital of a neighboring Eu ion via a chalcogenide cation. Another type of superexchange is also possible, where an electron from the chalcogenide is transferred to the d orbital of a neighboring Eu ion, where it interacts with the 4f electrons. The two interactions can hybridize, which may lead to a ferromagnetic next-nearest-neighbor interaction [75, 84].

The type of the magnetic ordering varies between the different chalcogenides in dependence of the relative values of the two exchange constants, as shown in table 2.1. EuTe is antiferromagnetic, as J_2 is negative and its absolute value exceeds J_1 [81]. In contrast, EuS is ferromagnetic, because J_1 exceeds the negative J_2 [82]. In EuO, the nearest-neighbor interactions are stronger than in EuS, leading to a larger J_1 [81]. In addition, J_2 is positive [81], resulting in a ferromagnetic order with a significantly higher Curie temperature of 69.3 K [78] compared to the 16.6 K in EuS [80]. EuSe

shows a more complicated behavior as J_1 and J_2 are almost equal, but with different signs [81], leading to a metamagnetic behavior with several magnetically ordered phases at different temperatures [74].

Table 2.1: Comparison of different parameters affecting the magnetic ordering of the europium chalcogenides EuX. The values are taken from reference [85].

EuX	Lattice constant	Magnetic ordering	Critical temperature	J_1/k_B	J_2/k_B
EuO	5.141 Å	Ferromagnetic	69.33 K	0.55 K	0.15 K
EuS	5.968 Å	Ferromagnetic	16.57 K	0.22 K	-0.10 K
EuSe	6.195 Å	Antiferromagnetic Ferrimagnetic Antiferromagnetic	4.60 K 2.8 K 1.8 K	0.11 K	-0.09 K
EuTe	6.598 Å	Antiferromagnetic	9.58 K	0.06 K	-0.20 K

2.6 Europium monoxide

Although ferromagnetism in the semiconductor EuO was discovered as early as 1961 [86], it is only in the last two decades that sample growth techniques became sufficiently sophisticated to produce stoichiometric thin films of the high quality required for spintronic applications and suitable for studying interface effects [87–90]. EuO combines the interesting magnetic properties of the europium chalcogenides with a relatively high Curie temperature and the possibility of epitaxial integration with common semiconducting materials such as Si, GaN and GaAs [90–92]. This makes europium monoxide a promising material for a new generation of spintronic materials. In fact, it has already been successfully employed as spin valve [93] and magnetic tunnel barrier, generating almost 100 % polarized electrons [26, 45, 46].

EuO has a lattice constant of 5.14 Å and, like the other europium chalcogenides, it crystallizes in a NaCl structure [72]. The rare earth oxide is known for its large magneto-optical effects, like a Kerr rotation at least an order of magnitude larger compared to transition metals [41, 42] and one of the largest known Faraday rotations with $8.5 \cdot 10^5$ °/cm [43]. It shows a distinct quadratic Kerr effect [94], strong non-linear effects like second- and third-harmonic generation [95–97] and in addition, it exhibits colossal magnetoresistance effects [98].

The density of states of europium monoxide is schematically shown in figure 2.5. EuO has an indirect band gap of about $E_g = 1.2\,\text{eV}$ at room temperature, which

separates the valence band formed by the localized 4f electrons from the 5d-6s conduction band [40]. The crystal field strongly affects the 5d band, splitting it into e_g and t_{2g} states, while the 4f electrons are hardly affected due to their localized nature [76]. Upon decreasing the temperature, EuO becomes ferromagnetic and the band gap undergoes a red shift, i.e., the absorption edge shifts to lower energies [48, 99]. This effect has been attributed to the exchange interaction between the 4f electrons and the 5d-6s states. It induces a spin-splitting of the conduction band of up to 0.6 eV, moving the spin-up bands to lower energies and the spin-down bands to higher energies. As a direct consequence, 5d states close to the band gap energy are almost fully spin-polarized [100].

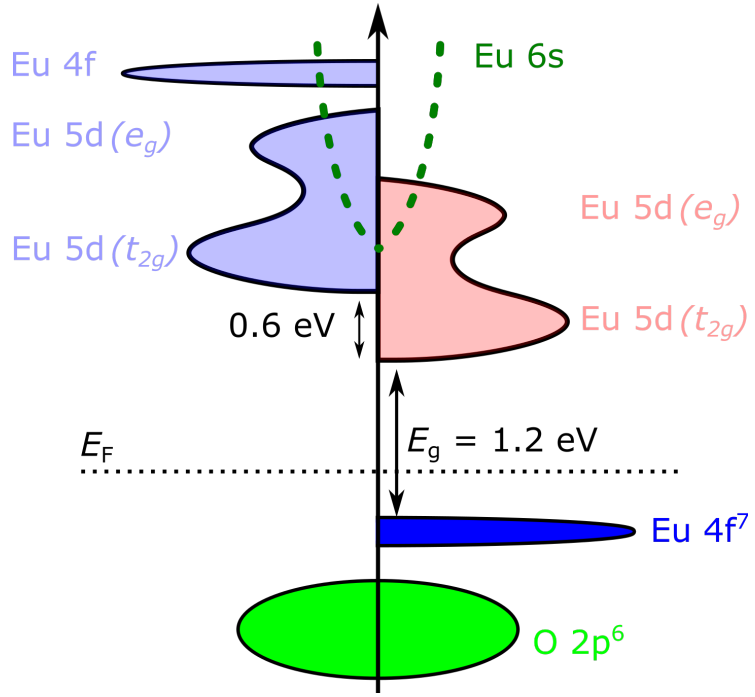

Figure 2.5: Schematic illustration of the density of states of EuO. The 4f valence band and the 5d-6s conduction band are separated by a 1.2 eV band gap. The figure is adapted from reference [54].

2.7 Approaches to increase the Curie temperature of EuO

Although EuO already has the highest Curie temperature of the europium chalcogenides with $T_C = 69.3$ K, it is still too low for technological applications, as helium

cooling is required to reach the magnetically ordered phase. Various approaches such as doping or lattice distortion have been successfully explored in recent decades to increase the EuO T_C, as schematically shown in figure 2.6.

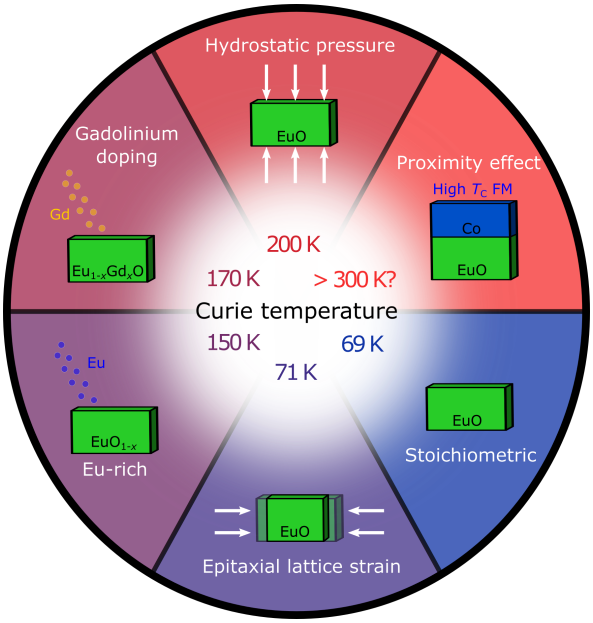

Figure 2.6: Illustration of different approaches to increase the magnetic ordering temperature of EuO, ranging from a small increase of a few Kelvin by applying epitaxial strain, to a large increase of up to 200 K by applying hydrostatic pressure.

Doping with trivalent ions

A significant increase of the magnetic ordering temperature can be achieved by substituting small amounts of the divalent Eu with trivalent rare earth ions. The additional electrons introduced into the system in this way can occupy conduction band states and become spin polarized due to the spin splitting of the conduction band present at low temperatures [100]. They contribute to the indirect exchange interaction, which can strengthen the magnetic order and thus increase T_C [49, 101–103]. In particular, Gd has proven to be a promising dopant due to its similar magnetic configuration with a half-filled 4f shell, which minimizes the impact on the spin system. The effect of substituting a few percent of the Eu ions with Gd has been extensively studied [48, 104–109], and magnetic ordering temperatures of up to 170 K have been achieved [50].

Oxygen-deficiency

Another extensively researched approach is based on the creation of oxygen vacancies, e.g. by excessive Eu deposition, which can lead to an increased Curie temperature of up to 150 K [49, 102–104, 106, 108, 110–113]. This approach is reported to induce additional interesting properties such as an insulator-to-metal transition at low temperatures, with an increase of the electrical conductivity by several orders of magnitude [114–117]. To explain the increased Curie temperature, a model has been proposed that considers the formation of magnetic polarons at the site of oxygen vacancies [47]. Magnetic polarons are quasiparticles, formed by the interaction of a carrier spin with localized spins of magnetic ions [118]. They induce a ferromagnetic order in their vicinity, as schematically shown in figure 2.7. The two conducting electrons introduced into the system are bound to the vacancies and are able to polarize the 4f electrons of the neighboring Eu^{2+} ions, forming a bound magnetic polaron [47, 49, 119]. They are reported to have a relatively large radius due to the high dielectric constant of EuO, and can induce a ferromagnetically ordered state when they overlap due to a sufficiently high doping rate [113]. The additional magnetization induced by the magnetic polarons couples antiferromagnetically to the localized 4f electrons of the Eu ions and becomes the dominant magnetic contribution near the bulk Curie temperature of EuO [51, 113]. It is present up to temperatures of about 150 K, effectively raising the magnetic ordering temperature of oxygen-deficient EuO [47, 51].

Stress and strain

The highest reported Curie temperature of EuO was achieved by means of applying hydrostatic pressure, resulting in a magnetic ordering temperature of about 200 K [120–123]. The applied pressure reduces the lattice constant of the ferromagnet and thereby modifies the exchange interactions and strengthens the magnetic order [123]. A similar approach relies on applying epitaxial strain by growing thin EuO films on substrates with a slightly smaller lattice constant, which can also lead to an increase of the Curie temperature [124]. A magnetic ordering temperature of strained EuO of about 71 K is reported in literature [125].

Magnetic proximity effect

All of the approaches described have been successful in increasing T_C at the cost of altering the stoichiometry or conductivity, and thus changing the promising intrinsic properties of EuO. An alternative way to increase the magnetic ordering

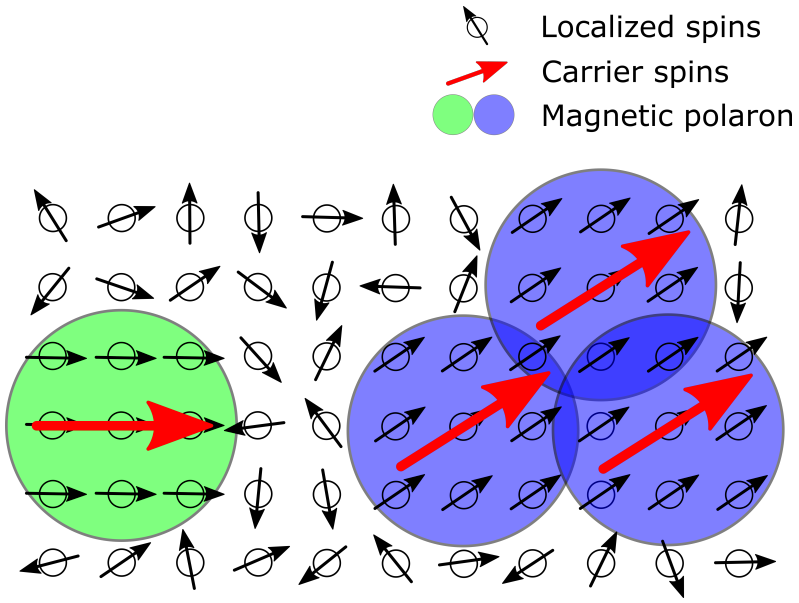

Figure 2.7: Schematic illustration of magnetic polarons. They are formed by the interaction between carriers spins (red arrows) and localized spins of magnetic ions (black arrows). Carrier spins induce a polarization of the nearby magnetic ions in their vicinity, thereby forming a magnetic polaron (green circle) If the radius of several magnetic polarons overlap, they can induce a long-range magnetic order (blue circles).

temperature while preserving the insulating nature of the semiconductor could rely on the magnetic proximity effect. The magnetic properties of a material can be modified when it is in contact with a ferromagnetic layer. The wave functions of the magnetic moments from the ferromagnet do not stop at the interface, but can leak into the adjacent layer [126]. This can lead to a variety of effects for different materials, such as induced spin polarization in non-magnetic materials [127–131] or an exchange bias when the ferromagnet is coupled to an antiferromagnet [132–134]. The latter describes a shift of the center of the ferromagnetic hysteresis loop to a non-zero magnetic field value [135]. Another proximity-induced effect that has been observed for various materials can be a significant increase of the Curie temperature of 100 % and more, when coupled to a high T_C ferromagnetic layer [136–140].

Several studies have been performed on EuS coupled to Co, where the T_C of the ferromagnetic semiconductor was raised from 16 K to room temperature [52, 53, 141–145]. The coupling between the two layers, and thus the origin of the magnetic proximity effect in this sample system, has been attributed to a 3d-5d hybridization. It allows an indirect exchange interaction between the 4f electrons of the rare

earth oxide and the 3d states of the transition metal [144, 146]. Similar studies have also been performed on different EuO bilayer samples. While coupling to the rare earth metal gadolinium did not lead to a significant increase of T_C [147], a recent study on an EuO/Co bilayer system suggests a spin polarization of EuO at room temperature [148]. This sample system will be further investigated by magneto-optical means within the scope of this thesis.

3 Magneto-optical effects

Magneto-optical effects describe the interactions between polarized light and matter in the presence of an applied magnetic field. In 1845, Michael Faraday discovered the rotation of the polarization plane of linearly polarized light upon propagation through matter under the influence of an applied magnetic field [149]. The angle of the rotation, later called the Faraday rotation Θ_{F}, was found to be proportional to the thickness of the medium l and the applied magnetic field H, and can be expressed as

$$\Theta_{\mathrm{F}}(\omega) = V(\omega) \cdot H \cdot l \tag{3.1}$$

with the light frequency-dependent Verdet constant V, which depends on the optical properties of a material [150]. About 30 years later, John Kerr found a similar effect with linearly polarized light being reflected from the surface of a magnetized material, which not only induces a rotation of the polarization plane, but also makes the light elliptical [151]. In contrast to the first described Faraday effect, this interaction, which later on was named magneto-optical Kerr effect (MOKE), is especially sensitive to the surface of materials, and hence is an important tool to observe domain structures or to read out magnetically stored information. The discovery of these possibilities led to significant developments in data storage, such as the development of the compact disk. It even encouraged the emergence of laser diodes, since a reduction in size was necessary to mass-produce devices to read out data [83]. The development of pulsed lasers with ultra-short pulses opened up a whole new field of research with new methods like second-harmonic generation or time-resolved magneto-optical spectroscopy [83]. The latter will be the tool of choice within this thesis to examine the spin dynamics of the EuO/Co bilayer.

3.1 Polarization of light

A plane electromagnetic wave can be described by its electric field vector $\vec{E}$ via

$$\vec{E}(\vec{r}, t) = \vec{E}_0 \exp\left(\mathrm{i}\left(\vec{k} \cdot \vec{r} - \omega t\right)\right) \tag{3.2}$$

with the wave vector $\vec{k}$ and the angular frequency ω. The polarization vector $\vec{E}_0$ determines the state of polarization of the wave. A wave is called linearly polarized

when there is no phase difference between the components of $\vec{E}_0$, i.e., the electric field oscillates perpendicular to the propagation direction. For a propagation along the z-axis and polarization in the xy-plane, the polarization vector can be described by

$$\vec{E}_0 = E_0 \begin{pmatrix} \cos\alpha \\ \sin\alpha \\ 0 \end{pmatrix} \tag{3.3}$$

with the amplitude of the electric field E_0 [83]. For circularly polarized light, the electric field rotates in a plane perpendicular to the direction of propagation. The polarization vector can be expressed as

$$\vec{E}_\pm = \frac{1}{\sqrt{2}} E_0 \begin{pmatrix} 1 \\ \pm i \\ 0 \end{pmatrix} \quad , \tag{3.4}$$

where $\vec{E}_+$ and $\vec{E}_-$ describe a clockwise and counterclockwise rotation, respectively [83]. In dependence on the direction of the rotation, circularly polarized waves are commonly called right or left circularly polarized. If the amplitudes of the electric field components are not equal, or if their phase shift is not 90°, the rotation of the wave perpendicular to the direction of propagation is not circular, but elliptical. This state of polarization is called elliptical polarization [152]. Linearly polarized light can be described as a superposition of left and right circularly polarized light with the same amplitude and phase [83]. Linearly and circularly polarized light are schematically depicted in figure 3.1 in red and green, respectively.

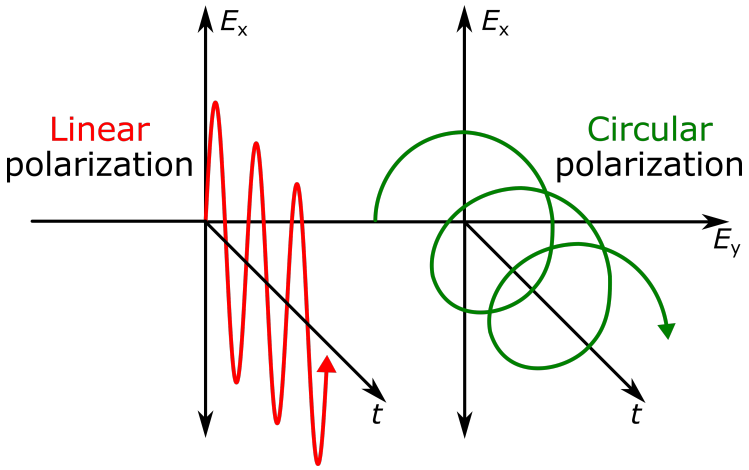

Figure 3.1: Schematic illustration of the propagation of linearly and circularly polarized light in red and green, respectively.

3.2 Magneto-optics

A comprehensive discussion of the theoretical background of the different magneto-optical effects is given in literature by several books [83, 150, 153–156] and articles [157–159]. Within the scope of this thesis, the magnetization-induced anisotropy and its impact on the dielectric tensor are discussed as a macroscopic approach to the Faraday and Kerr effect.

The propagation of light in matter can be described by Maxwell's equations

$$\nabla \cdot D = \rho \tag{3.5}$$
$$\nabla \cdot B = 0 \tag{3.6}$$
$$\nabla \times H = \frac{\partial D}{\partial t} + j \tag{3.7}$$
$$\nabla \times E = -\frac{\partial B}{\partial t} \quad , \tag{3.8}$$

with the electric field E, the electric displacement D, the electric charge density ρ, the magnetic induction B, the magnetic field H and the current density j, combined with the material specific permittivity ϵ and permeability μ [160]. They latter can be described as

$$D = \epsilon E \tag{3.9}$$
$$B = \mu H \quad . \tag{3.10}$$

The permeability is approximated to be $\mu \approx 1$ in ferromagnetic materials in the visible range [157, 161]. Therefore, the macroscopic optical behavior of a material can be described by its permittivity [150]. In the case of a cubic structure, ϵ is given by the tensor

$$\epsilon\left(M,\omega\right) = \begin{pmatrix} \epsilon_{\mathrm{xx}} & \epsilon_{\mathrm{xy}} & \epsilon_{\mathrm{xz}} \\ -\epsilon_{\mathrm{xy}} & \epsilon_{\mathrm{xx}} & \epsilon_{\mathrm{yz}} \\ -\epsilon_{\mathrm{xz}} & -\epsilon_{\mathrm{yz}} & \epsilon_{\mathrm{xx}} \end{pmatrix}, \tag{3.11}$$

in which all elements are complex, and satisfy the Onsager relations

$$\epsilon_{i,j}(-M,\omega) = \epsilon_{j,i}(M,\omega) \quad . \tag{3.12}$$

This means that the diagonal elements of the tensor are even functions of the magnetization M and the off-diagonal elements are uneven functions of M [150, 162, 163]. If a magnetic field is applied along the z-direction, ϵ is simplified to [156]

$$\epsilon\left(M,\omega\right) = \begin{pmatrix} \epsilon_{\mathrm{xx}} & \epsilon_{\mathrm{xy}} & 0 \\ -\epsilon_{\mathrm{xy}} & \epsilon_{\mathrm{xx}} & 0 \\ 0 & 0 & \epsilon_{\mathrm{zz}} \end{pmatrix} \quad . \tag{3.13}$$

The propagation of a plane wave parallel to the magnetization along the z-direction can be described by Maxwell's equations:

$$\nabla \times \nabla E + \epsilon \frac{\partial}{\partial t} E = 0 \quad . \tag{3.14}$$

This gives rise to the eigenvalue problem

$$\begin{pmatrix} N^2 - \epsilon_{\mathrm{xx}} & \epsilon_{\mathrm{xy}} & 0 \\ -\epsilon_{\mathrm{xy}} & N^2 - \epsilon_{\mathrm{xx}} & 0 \\ 0 & 0 & N^2 - \epsilon_{\mathrm{zz}} \end{pmatrix} = 0 \quad , \tag{3.15}$$

solved by

$$N_{\pm}^2 = \epsilon_{\mathrm{xx}} \pm i\epsilon_{\mathrm{xy}} \quad \text{and} \quad \pm iE_{\mathrm{x}} = E_{\mathrm{y}} \quad , \tag{3.16}$$

leading to different refractive indices experienced by left and right circularly polarized light [150, 164]. This circular birefringence is the origin of the Faraday and Kerr effects. The two components of linearly polarized light, which can be seen as a superposition of left and right circularly polarized light of equal amplitude, experience different velocities of propagation and hence, a phase shift appears. Upon exiting the medium and recombining into a linearly polarized wave, this phase shift results in a rotation of the plane of polarization given by

$$\theta_{\mathrm{F}}(\omega) = \frac{\omega}{2c} \cdot \mathrm{Re}(N_+ - N_-) \tag{3.17}$$

with the velocity of light c [150]. In addition to different refractive indices, the absorption coefficient for left and right circularly polarized light may also vary. This can lead to different attenuation rates and an induced ellipticity of the linearly polarized light, given by

$$\nu_{\mathrm{F}}(\omega) = -\frac{\omega}{2c} \cdot \mathrm{Im}(N_+ - N_-) \quad . \tag{3.18}$$

This effect is known as circular dichroism [150].

For the magneto-optical Kerr effect, it is necessary to consider the reflected light, not the transmitted light. The different refractive indices for left and right circularly polarized light lead to two complex reflective coefficients

$$r_{\pm} = \frac{N_{\pm} - 1}{N_{\pm} + 1} \tag{3.19}$$

that can be estimated via the Fresnel relations [164]. Linearly polarized light will generally become elliptical upon reflection, and the complex Kerr rotation is then given by

$$\Theta_{\mathrm{K}} = \theta_{\mathrm{K}} + i\eta_{\mathrm{K}} \approx \frac{i}{2} \ln \frac{r_+}{r_-} \tag{3.20}$$

with the Kerr rotation θ_{K} and the Kerr ellipticity η_{K}. The latter describes the ratio of the minor to the major axis [150, 164].

3.3 Magneto-optical Kerr effect

Due to its sensitivity to surfaces and the ability to measure opaque samples, the magneto-optical Kerr effect (MOKE) is a versatile and widely used tool for measuring thin films [156]. MOKE can be divided into three different categories, depending on the experimental geometry, as schematically shown in figure 3.2. In the polar geometry (P-MOKE), the sample magnetization is perpendicular to the sample surface and parallel to the plane of the incident light. In the longitudinal geometry (L-MOKE), the sample magnetization is parallel to the surface and to the plane of the incident light. The third geometry is transversal (T-MOKE), where the magnetization is parallel to the sample surface and perpendicular to the plane of the incident light. Unlike P- and L-MOKE, the T-MOKE is sensitive to the intensity of the reflected beam [70].

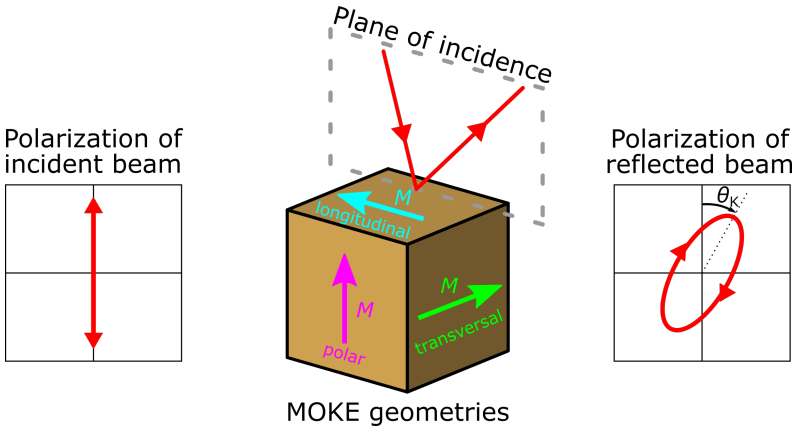

Figure 3.2: Schematic illustration of the different MOKE geometries. In the L-MOKE configuration, shown in cyan, the sample magnetization is parallel to the surface and to the plane of the incident light beam. For P-MOKE, shown in magenta, the sample magnetization is perpendicular to the surface and parallel to the plane of incidence. In T-MOKE, shown in green, the magnetization is parallel to the surface and perpendicular to the plane of incidence. For L- and P-MOKE, an incident beam with linear polarization becomes elliptically polarized upon reflection. The rotation of the polarization plane is called Kerr rotation Θ_K.

All three MOKE geometries offer advantages in different experimental situations. The measured Kerr rotation θ_K is proportional the magnetization M, as expressed via

$$\theta_K = FM \tag{3.21}$$

with the Fresnel coefficient F describing the optical properties of a material. Therefore, P- and L-MOKE can be employed as a probe for the magnetization, for

example for measurements of the magnetic hysteresis in ferromagnets [156]. Due to different magnetic anisotropies of samples, it is useful to not be restricted to a single measurement geometry. Even though the measured rotation is usually the strongest in P-MOKE, especially thin films often have their easy magnetization axis parallel to the surface. In this case hysteresis loops in the P-MOKE geometry might not yield a hysteresis, as it is only sensitive to the hard axis. Measurements in the L-MOKE geometry, on the other hand, are sensitive to the easy axis and hence, might allow access to the hysteresis, even though the measured Kerr rotation is smaller [83]. The T-MOKE geometry can be employed to image domains at the surface of magnetized materials [153] or to investigate element-selective magnetic properties using x-rays [165].

3.4 Time-resolved magneto-optical spectroscopy

The development of femtosecond lasers has led to the new field of time-resolved magneto-optical spectroscopy, allowing the investigation of magnetization dynamics on ultrafast timescales [156]. The most commonly used experimental configuration for such measurements is the pump-probe scheme using two laser beams, as shown schematically in figure 3.3 (a). The more intense pump beam excites the sample to a non-equilibrium state, inducing transient changes in the magnetization that can be monitored by the probe beam. Typically, the intensity of the probe beam is significantly lower than that of the pump beam to prevent a further excitation of the sample. By varying the optical path length of one beam with a mechanical delay line, the time delay Δt between the two beams can be modified, allowing measurements in a stroboscopic scheme.

An exemplary data trace for a pump-probe measurement performed on a Co sample is shown in figure 3.3 (b), where black crosses exemplarily mark a time delay at which the Kerr rotation is recorded. The measured transient rotation of the polarization plane at different time delays provides insight into the induced spin dynamics due to the pump beam excitation. This can include the relaxation time of the magnetization, the coupling between the electron, phonon and spin subsystems, or even photoinduced phase transitions [156]. The temporal resolution of the pump-probe spectroscopy technique is typically limited by the pulse duration of the two beams [166].

Based on equation 3.21, the induced changes in the measured rotation can be expressed by

$$\Delta\theta(t) = F_0\Delta M(t) + M_0\Delta F(t) \tag{3.22}$$

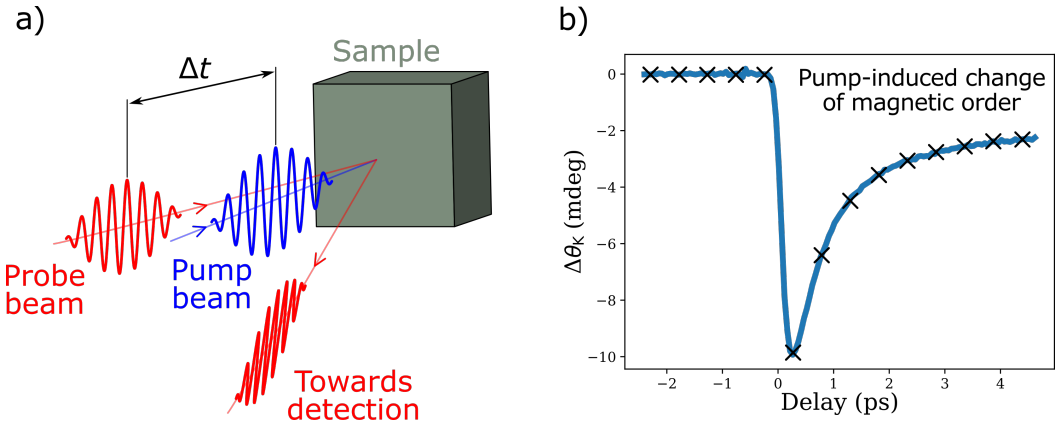

Figure 3.3: Schematic illustration of a) the pump-probe spectroscopy technique and b) exemplary results of time-resolved MOKE measurements performed on a Co single crystal. The black crosses illustrate the stroboscopic method of measurement in the pump-probe technique..

with the ground state magnetization M_0 and Fresnel coefficient F_0, describing the optical properties of the sample, and the induced changes to these two quantities given by ΔM and ΔF. Therefore, the measured transient rotation of the polarization $\Delta\theta(t)$ is not only proportional to the pump-induced changes of the magnetization, but also to the optical properties that can be modified by the pump beam. The latter can cause optical artifacts that may lead to misinterpretation of the data [156]. Optical excitation of a magnetized material can induce different effects. If the sample is absorbing in the photon energy range of the pump beam, its temperature will increase due to laser-induced thermal heating. This can effectively reduce its magnetization by approaching or even exceeding the Curie temperature. Non-thermal effects like the absorption of photons by electronic states that directly affect the magnetization are also possible [167]. This can be seen for example in the antiferromagnetic dielectric NiO, where the excitation with a specific pump photon energy leads to the non-thermal generation of a magnon by absorption of a photon even below the band gap energy [168].

In 1996, Beaurepaire et al. discovered a reduction of the magnetic order of a thin Ni film on a timescale of a few hundred femtoseconds after photoexcitation with an ultrashort laser pulse, which was attributed to an ultrafast demagnetization [169]. Their pioneering work was followed by a plethora of subsequent experiments, which confirmed the presence of an ultrafast demagnetization in several ferri- and ferromagnetic materials [170–174]. In addition, various new effects were discovered such as optically induced phase transitions [175], the generation of coherent magnetic precession [176], all-optical switching, i.e., the reversal of the magnetization

direction with a single pulse [177, 178], and the generation of spin-currents in thin ferromagnetic layers, which can affect the magnetization of adjacent layers [179, 180]. Thus, the discovery of Beaurepaire opened up a new field of research, in which the manipulation and control of magnetic order by light on ultrafast timescales is studied [156, 167].

3.4.1 Three-temperature model

A first phenomenological description of the ultrafast demagnetization, the three-temperature model (3TM), was proposed by Beaurepaire and his coworkers in 1996 [169]. It considers the spins, electrons and lattice as separate thermalized reservoirs that interact with each other, as schematically shown in figure 3.4 (a). Each of the reservoirs $i = \mathrm{s}, \mathrm{l}, \mathrm{e}$ for spins, lattice and electrons, respectively, is in a thermal equilibrium and has an effective temperature T_i and heat capacity C_i. They can be used to describe the temporal evolution of the system via the coupled differential equations

$$C_\mathrm{e}\frac{\mathrm{d}T_\mathrm{e}}{\mathrm{d}t} = -G_\mathrm{el}(T_\mathrm{e} - T_\mathrm{l}) - G_\mathrm{es}(T_\mathrm{e} - T_\mathrm{s}) + P(t) \tag{3.23}$$

$$C_\mathrm{s}\frac{\mathrm{d}T_\mathrm{s}}{\mathrm{d}t} = -G_\mathrm{es}(T_\mathrm{s} - T_\mathrm{e}) - G_\mathrm{sl}(T_\mathrm{s} - T_\mathrm{l}) \tag{3.24}$$

$$C_\mathrm{l}\frac{\mathrm{d}T_\mathrm{l}}{\mathrm{d}t} = -G_\mathrm{el}(T_\mathrm{l} - T_\mathrm{e}) - G_\mathrm{sl}(T_\mathrm{l} - T_\mathrm{s}) \quad . \tag{3.25}$$

These differential equations are connected to each other by the coupling parameters G_{ij}, which control the heat exchange between the three reservoirs, e.g. by electron-phonon scattering processes. An incident laser pulse that interacts with the electron system induces hot electrons, as indicated by the time-dependent term $P(t)$ in the equation describing the electron reservoir. They thermalize at an elevated temperature via electron-electron scattering [167]. Due to electron-phonon interactions, thermal energy is transferred from the electron system to the lattice, leading to a thermal equilibrium between both systems after about 1 ps. The strong coupling between the electron and the spin system leads to a rapid increase of the spin temperature, which decreases the magnetization. The spin system thermalizes on a similar time scale as the equilibration time of the electrons and the lattice due to the coupling to these systems, resulting in a partial restoration of the magnetization [156]. The temporal evolution of the temperature of the three reservoirs is schematically shown in figure 3.4 (b).

The 3TM successfully describes the phenomenological processes involved during the ultrafast demagnetization, without providing information about the microscopic processes. The latter can be, for example, the conservation of angular momentum,

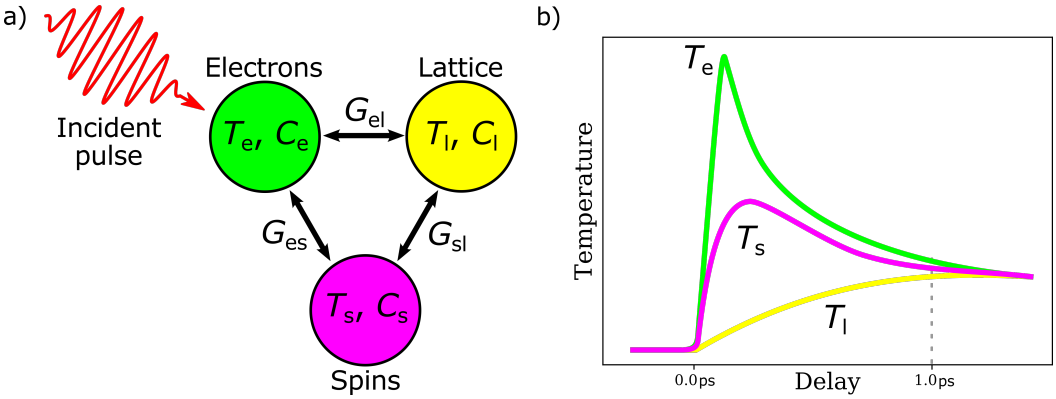

Figure 3.4: Schematic illustration of a) the three-temperature model and b) the temporal evolution of the temperature of the spins, the electrons and the lattice in the three-temperature model during the ultrafast demagnetization. The latter is induced by the interaction of a laser pulse with the electrons system of a sample. The figure is inspired by Kirilyuk et al. [167].

which must be partially removed from the spin system to realize a demagnetization [156, 167]. Over the years, several mechanisms have been proposed to explain the conservation of angular momentum in the ultrafast demagnetization, like spin-lattice relaxation [181], or direct coupling between photons and spins [182]. In 2010, Koopmans et al. proposed a refined version of the 3TM, named the microscopic three-temperature model (M3TM). It considers Elliot-Yafet spin-flip scattering, where electrons have a finite chance to flip their spin when scattering with impurities or phonons [183, 184], as a way to transfer angular momentum from the spin system to the lattice [185]. This process is possible in solids because of the mixed spin character of electronic states in the presence of the spin-orbit coupling. The M3TM provides a differential equation to describe the magnetization dynamics

$$\frac{\mathrm{d}m}{\mathrm{d}t} = Rm\frac{T_\mathrm{l}}{T_\mathrm{C}}\left(1 - m\coth\left(\frac{mT_\mathrm{C}}{T_\mathrm{e}}\right)\right) \tag{3.26}$$

with the Curie temperature T_C, the magnetization $m = M/M_\mathrm{s}$ relative to its value at $T = 0\,\mathrm{K}$, and the proportionality factor $R \propto a_\mathrm{sf}T_\mathrm{C}^2/\mu_\mathrm{at}$ with the atomic magnetic moment μ_at and the spin-flip probability a_sf. It provides information about the material-specific rate of demagnetization. The model developed by Koopmans and coworkers successfully describes the ultrafast demagnetization in different materials like Ni, Co and even Gd, which shows different dynamics than the two transition metals due to its localized 4f electrons dominating the magnetic order [185].

3.4.2 Superdiffusive spin current

Another model describing the microscopic mechanisms of the ultrafast demagnetization relies on the generation of superdiffusive spin currents, that provide a pathway for non-local angular momentum transfer, as proposed by Battiatio et al. [187–189]. Their theory considers the motion of hot electrons in ferromagnetic metals that are photoexcited by an optical pulse, a process that is treated as spin-conserving. Due to the high velocity of the electrons excited into the s and p bands, and the different lifetimes of the minority and majority electrons [190], their mean free paths differ greatly, making the minority electrons less mobile. The longer mean free path of the majority electrons leads to a transfer of magnetization away from the photoexcited surface and thus to a local demagnetization as the electrons diffuse into the ferromagnetic film [187]. During their lifetime, the excited electrons experience different scattering events, like elastic scattering with phonons or impurities and inelastic electron-electron scattering, which can lead to the generation of electron cascades that further contribute to the demagnetization [187, 188]. The motion of such a spin current can be described neither as a diffusive, nor as a ballistic process, but rather as a superdiffusive process, which changes over time from a ballistic behavior at short times to a diffusive behavior at longer times [187]. In heterostructures, the hot electrons generated during the ultrafast demagnetization of a ferromagnetic metal can propagate to adjacent layers and thereby transfer angular momentum [187, 188].

Since their theoretical description in 2010, a variety of observed effects in different thin film sample systems have been attributed to superdiffusive spin currents. In multilayers of ferromagnetic materials separated by a non-magnetic spacer, the generation of a superdiffusive spin current in one layer is reported to affect the magnetization dynamics in the adjacent layer [191–193]. For a parallel coupling between two ferromagnetic layers, a spin current of majority electrons enhances the magnetization of the second layer, and for an antiparallel coupling it induces a demagnetization [192, 194]. If instead the magnetizations between the films are aligned non-collinear, the propagation of superdiffusive spin currents can induce precessional motions of the magnetization in the adjacent layer [179, 180, 195]. This mechanism is called spin-transfer torque and is considered a promising candidate for fast and efficient control of spintronic devices [194, 196]. Further effects like domain wall manipulation [197] and spin injection in non-magnetic metals [198, 199] and semiconductors [200, 201] by means of generating a superdiffusive spin current in an adjacent ferromagnetic layer have also been reported in the literature.

3.5 Experimental setup

Magneto-optical measurements were performed with two different setups, one in the L-MOKE geometry and the other in the P-MOKE geometry. Varying the direction of the magnetic field can provide additional information about the sample system, for example regarding the magnetic anisotropy. The employed L-MOKE setup, located at the Forschungszentrum Jülich, where the magnetic field is applied in parallel to the sample surface to study the in-plane behavior, is shown schematically in figure 3.5. The sample is placed in a helium-cooled cryostat with electrical heating, which allows temperature-dependent measurements in a range from 5 K up to room temperature and above with a precision of ±1 K. The cryostat is placed between the coils of an electromagnet, which can generate a homogeneous magnetic field of up to 100 mT around the sample position. The second harmonic of a Ti:sapphire regenerative amplifier with a repetition rate of 1 kHz, generated by a BBO crystal, is used as a laser beam for the measurements. The pulsed laser with a photon energy of 3.1 eV and an angle of incidence of about 45° is reflected from the sample surface and detected by a balanced photodetector connected to a lock-in amplifier. The detector of the L-MOKE setup has not been calibrated, so the measured rotation of polarization appears in arbitrary units.

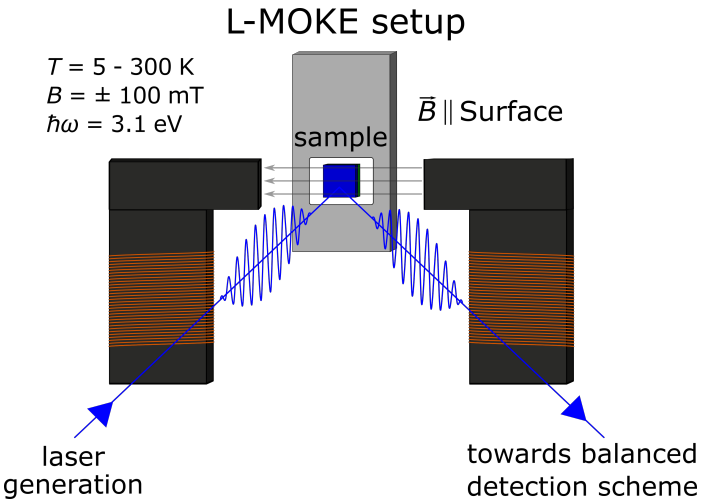

Figure 3.5: Schematic illustration of the L-MOKE setup. A magnetic field of up to ±100 mT can be applied parallelly to the sample surface and the reflection of a beam with a photon energy of 3.1 eV is detected with a balanced detection scheme connected to a lock-in amplifier. Temperature-dependent measurements are possible in the range from 5 K to 300 K and above.

The majority of the measurements discussed in this thesis were performed with the

time-resolved P-MOKE setup shown schematically in figure 3.6 and described in detail in the literature [202, 203]. The employed laser system is provided by the company Light Conversion. An Yb-based 20 W *Pharos* laser amplifier generates pulses with a photon energy of 1.2 eV and a duration of 300 fs at a repetition rate of 200 kHz. A beam splitter is used to separate the laser output into two components to drive two *Orpheus-F/HP* optical parametric amplifiers (OPAs), permitting free tuning of the photon energy in the range from 0.5 eV to 3.5 eV and the compression of the pulse duration to less than 100 fs. The operation of two independent OPAs allows the simultaneous generation of an analyzing probe beam and an exciting pump beam with independent photon energies. Since only the latter is responsible for photoexcitation of the sample, the pump OPA is supplied with an input power of 13 W and the probe OPA with the remaining 7 W. An electro-optical modulator (EOM), which allows the transmission of only a selectable percentage of pulses, is placed in front of the pump OPA. This can be a helpful tool for aligning the pump beam path, but mostly, it is important for time-resolved pump-probe measurements. By allowing every second pulse to pass through the EOM without blocking any probe beam pulses, both the ground state and the photoexcited state of the sample can be probed in a single measurement. In the data analysis, a modulation can be applied to extract the isolated transient response of the sample, and thereby greatly improve the signal-to-noise ratio. This approach and its advantages are described in detail in chapter 6.

The sample is placed in a liquid helium flow *Konti* cryostat provided by the company CryoVac. It is equipped with heating elements that allow temperature-dependent measurements in the range of 4 K to 420 K. Owing to the windows in the front and in the back, measurements can be performed in transmission and reflection. The position of the sample in the cryostat is adjustable over a distance of about 2 cm with a minimum step size of 1 nm using a computer-controlled three-axis piezo stage. The cryostat can be placed in the bore of a solenoid-shaped superconducting magnet, also provided by Cryovac. The magnet has a closed-loop helium cooling and can apply magnetic fields of up to ± 9 T perpendicular to the sample surface. As described in section 3.4, pump-probe measurements are usually performed by varying the optical path difference between the pump and the probe beam. This is achieved by using a mechanical delay line placed in the path of the probe beam, which allows to extend the distance traveled and thereby change the delay between the two beams by up to 4 ns. The delay line is provided by the company Newport and can vary the optical path length of the probe beam with a minimum step size of about 20 fs.

After interacting with the sample, the either reflected or transmitted beam is measured with a balanced detection scheme. The combination of a half-wave plate and a Wollaston prism allows to evenly split the probe beam into its s- and

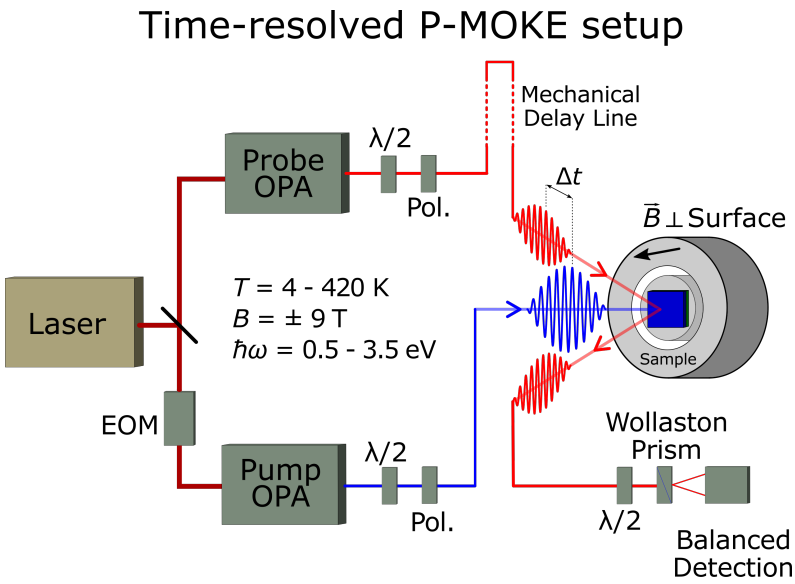

Figure 3.6: Schematic illustration of the time-resolved P-MOKE setup. An Yb-based laser drives two OPAs, allowing the separate tuning of the photon energy of the pump and the probe beam in the range from 0.5 eV to 3.5 eV. Temperature-dependent measurements can be performed between 4 K and 420 K. Magnetic fields of up to ±9 T can be applied perpendicular to the sample surface.

p-polarized components, which get detected by a balanced photodetector. This detector (*PDB450A-AC*, provided by Thorlabs) has three outputs and can transmit the signal measured by the two single photodiodes, i.e., the s- and p-polarized components, and their difference. As described in literature [202], this difference is linearly proportional to the rotation of the polarization plane and is therefore sensitive, for example, to changes of the magnetization of a sample. The balanced photodetector is connected to a PC via a digitizer card that is synced to the repetition rate of the laser and the frequency of the EOM. The latter connection is required for the aforementioned modulation used to isolate the pump-induced changes in the measured rotation of polarization. It can be calculated using

$$\Delta\theta = a \cdot \frac{(U_{\mathrm{A-B}})_{\mathrm{ON}} - (U_{\mathrm{A-B}})_{\mathrm{OFF}}}{(U_{\mathrm{A}})_{\mathrm{OFF}} + (U_{\mathrm{B}})_{\mathrm{OFF}}} \tag{3.27}$$

with the signals U detected by the photodiodes A and B with and without the presence of the pump beam (ON and OFF), their respective difference $U_{\mathrm{A-B}}$ and a calibration factor a, which is specific to the setup [202]. Further details on the setup can be found in the literature [202, 203].

4 Sample growth and static characterization

The ferromagnetic semiconductor EuO is a promising candidate for future spintronic applications due to its combination of a strong magnetic moment, large magneto-optical effects and insulating properties. Its usability in real applications is limited by a low Curie temperature of 69 K, since liquid nitrogen cooling is insufficient to reach the magnetically ordered phase. Although several approaches have been investigated to increase the T_C of EuO (see section 2.7), they all rely on altering its stoichiometry and conductivity [47–51]. A promising alternative approach relies on the magnetic proximity effect, i.e., the coupling to a high T_C ferromagnet, which can change the magnetic properties of a thin film [127–131]. This effect has been successfully demonstrated for EuS coupled to Co, where the Curie temperature of the ferromagnetic semiconductor was raised from 16 K up to room temperature [52, 53]. Recently, an XMCD study performed on EuO coupled to Co suggested a similar increase of the magnetic ordering temperature induced by the proximity to the transition metal [148]. In this work, a similar bilayer system is investigated by magneto-optical means to find evidence for a modified Curie temperature of EuO due to the proximity effect.

4.1 Sample system

The studied sample system consists of a bilayer of 5 nm stoichiometric EuO covered with a 4 nm Co layer as well as a reference sample without Co. Both are shown schematically in figure 4.1. Due to its high bulk Curie temperature of 1360 K [60], which is well above room temperature even for thin films [204], Co is a promising material for increasing T_C of EuO via the proximity effect. In principle, the ferromagnetic transition metals Ni and Fe could also be employed instead of Co, as was shown for granular Fe/EuO films [205] and multilayers consisting of EuS and one of the two materials [143, 206, 207]. However, coupling to Co is reported to induce a larger magnetic moment in EuS at room temperature [207], and it has already been demonstrated for EuO [148].

The samples are prepared by Paul Rosenberger from Martina Müller's group at the University of Konstanz. Eu metal is deposited by thermal heating from a Knudsen cell onto an yttria-stabilized zirconia (YSZ) 0.5 mm thick substrate using

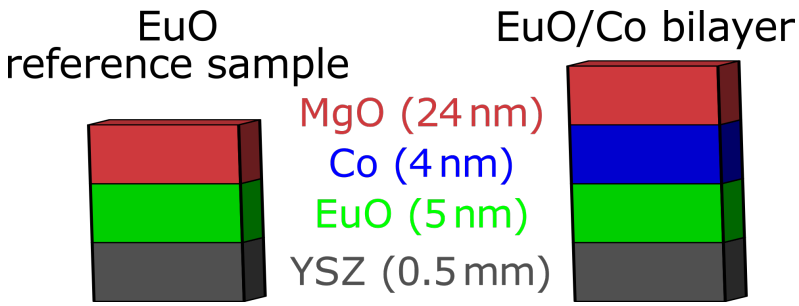

Figure 4.1: Illustration of the two studied sample systems, a 5 nm EuO reference sample and an EuO/Co bilayer with 4 nm Co deposited on a 5 nm EuO film. Yttria-stabilized zirconia (YSZ) with a thickness of 0.5 mm is utilized as the substrate for EuO due to similar lattice constants. To prevent an oxidation of the two ferromagnetic layers of EuO and Co to Eu_2O_3 and CoO, the samples are capped with a 24 nm MgO layer.

the molecular-beam epitaxy (MBE) technique in the adsorption-limited growth mode described in the literature [208, 209]. The lattice constant of YSZ (≈ 5.14 Å) [210] matches that of EuO, making it an ideal substrate for growing thin films without inducing any strain due to a lattice mismatch [211]. As europium monoxide is highly reactive and metastable, it can oxidize to the unwanted paramagnetic Eu_2O_3 phase and thereby lose its interesting properties [209]. Therefore, the chemical composition of the thin film is verified by in-situ X-ray photoelectron spectroscopy. A thin layer of Co is deposited on the EuO film by e-beam evaporation at room temperature. The bilayer system is capped with a 24 nm MgO film to prevent an oxidation of the two ferromagnetic layers for ex-situ handling [212]. Further details on the sample preparation and recent advances in EuO film growth in general can be found in the literature [148, 208, 209, 212].

4.2 Magneto-optical characterization

Magnetic hysteresis measurements are performed on a EuO reference sample and on a EuO/Co bilayer in dependence of the sample temperature to determine changes of the Curie temperature of EuO induced by the proximity to Co. By utilizing both, the L-MOKE and P-MOKE setups described in section 3.5, the in-plane and out-of-plane components of the magnetization can be studied. This approach allows to estimate the magnetic anisotropy of the sample, i.e., the easy and hard axes of magnetization, and the coupling between the two layers. Photon energies of 3.1 eV and 1.55 eV are employed to probe the longitudinal and polar component, respectively. The acquired data have a linear background due to the presence of

para- and diamagnetic contributions in the measurements. They originate from the glass window of the cryostat, the MgO capping layer and the YSZ substrate. This background is removed from the data by placing a linear fit through the data points at saturation magnetization and subtracting it from the data, as visualized in figure 4.2. This approach is performed to improve the visibility of the presented data.

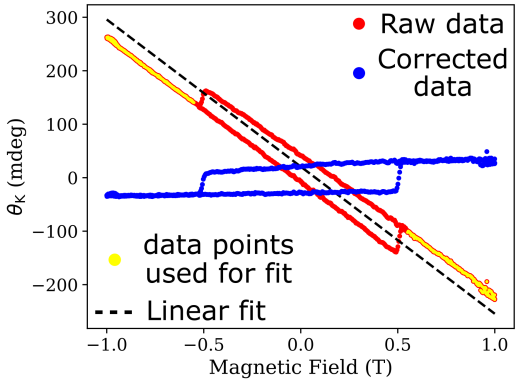

Figure 4.2: Schematic illustration of the background removal procedure. A linear fit (black) is placed through the data points at saturation magnetization (yellow) and subtracted from the raw data (red). The corrected data are shown in blue. The background originates from para- and diamagnetic contributions from the setup and the substrate of the sample system. The figure is adapted from reference [54].

4.2.1 EuO reference sample

The hysteresis loops performed on the EuO reference sample in dependence of the sample temperature are shown in figure 4.3 (a) and (b) in the L- and P-MOKE configurations, respectively. At low temperatures, the EuO reference sample shows a clear hysteresis with a remanence close to 100 % in both geometries. The coercive field recorded in L-MOKE at a temperature of 10 K is as large as 25 mT, which is about 20 times smaller than in P-MOKE, where values of about 500 mT are recorded at $T = 5$ K. The larger field required to reach saturation magnetization in the P-MOKE configuration suggests in-plane anisotropy and, due to the squared hysteresis in both geometries, a single-domain structure.

With increasing temperature, the coercivity and saturation magnetization decrease and disappear upon approaching the EuO bulk Curie temperature of 69 K. Slightly lower magnetic ordering temperatures of EuO have been reported in literature for thin films [213]. There is a small offset of the measurable Curie temperature

along the in-plane and out-of-plane geometry. This can be attributed to a different sensitivity to the temperature in the two setups used for the measurements, e.g. due to different positions of the temperature sensors with respect to the sample.

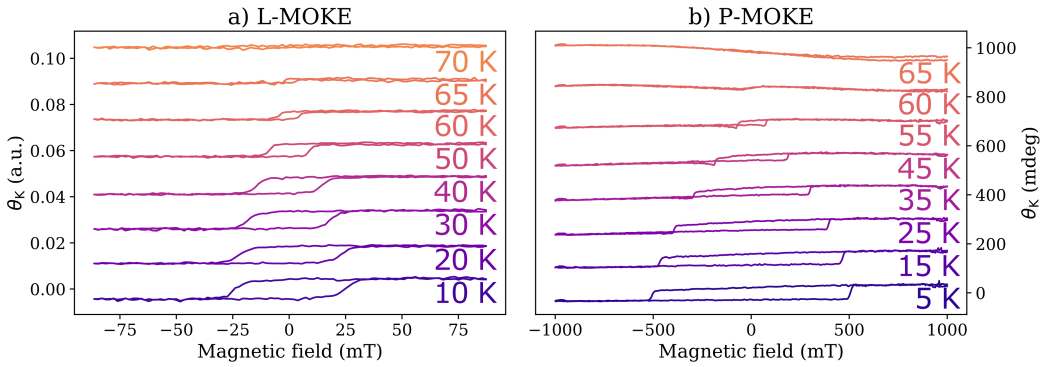

Figure 4.3: Temperature-dependent hysteresis measurements on the EuO reference sample in the (a) L-MOKE configuration and (b) P-MOKE configuration. The photon energy of the laser was 3.1 eV and 1.55 eV, respectively. The figure is adapted from reference [54].

4.2.2 EuO/Co bilayer

The presence of Co drastically changes the shape of the recorded hysteresis loops, as shown in figure 4.4 (a) and (b) for L- and P-MOKE, respectively. The coercive field and saturation magnetization are significantly reduced at low temperatures in the longitudinal MOKE geometry. When the temperature increases, the signal disappears at around 50 K, i.e., at a lower temperature compared to the pristine EuO sample discussed in figure 4.3 (a). Interestingly, as the temperature is further increased, the hysteresis reappears with an inverted orientation and persists up to room temperature. This surprising behavior can be explained by considering the literature values of the Kerr rotation of EuO and Co at saturation magnetization, which are $\theta_{\mathrm{EuO}} \approx 2°$ and $\theta_{\mathrm{Co}} \approx -0.3°$, respectively, at a photon energy of 3.1 eV [154]. Since the Kerr rotations of the two layers have opposite signs, the inversion of the hysteresis upon passing 50 K originates from a substitution of the dominant magnetic contribution. For $T < 50\,\mathrm{K}$, EuO is the dominant magnetic contribution due to its large magnetic moment and strong Kerr rotation [41, 42]. Co becomes dominant at higher temperatures and the inverted hysteresis persists at least up to room temperature owing to its large T_{C} [60]. At $T = 50\,\mathrm{K}$, the measured Kerr rotation from both layers is equal, leading to a vanishing signal since the two contributions have opposite signs.

This behavior is known from antiferromagnetically coupled ferrimagnets, where the net magnetization can disappear, when the components compensate each other at the magnetic compensation temperature T_{Comp}, as described in section 2.1. Upon passing T_{Comp}, the magnetic hysteresis is usually inverted due to a substitution in the dominant magnetic contribution in the ferrimagnet [66]. This comparable behavior suggests a similar antiferromagnetic coupling between EuO and Co in the examined bilayer. An antiferromagnetic coupling has been observed in the literature for similar sample systems, consisting of thin films of transition metals and EuO [148, 214] or EuS [52, 53, 144, 145, 215, 216]. It is described as arising from a hybridization of the transition metal 3d states and the rare earth 5d states [144, 217].

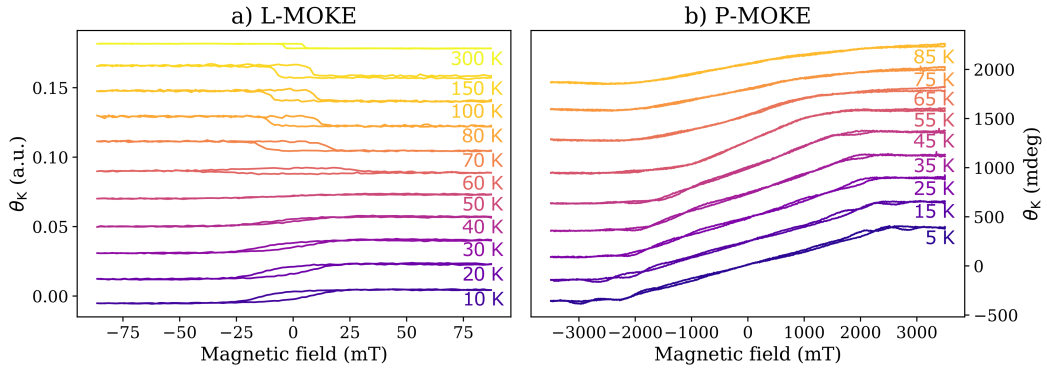

Figure 4.4: Temperature-dependent hysteresis measurements on the EuO/Co bilayer in the (a) L-MOKE configuration and (b) P-MOKE configuration. The photon energy of the laser was 3.1 eV and 1.55 eV, respectively. The figure is adapted from reference [54].

In the P-MOKE geometry, the behavior of the hysteresis loops is quite different. Unlike pristine EuO, where the hysteresis exhibits a broad coercivity and a remanence of about 100 %, the hysteresis obtained from the EuO/Co bilayer is not open. Instead, its shape is comparable to the hard magnetization axis of a bulk crystal magnet like Co [202]. The large difference to the signal of the reference sample suggests that the magnetic interaction with the transition metal changes the magnetic anisotropy of the EuO/Co bilayer system. The shape of the hysteresis loops corresponds to the rotation of the two magnetizations from the in-plane ground state with an antiparallel orientation to a forced parallel alignment along the magnetic field direction. Since the P-MOKE geometry is sensitive to the polar component of the magnetization, the signal disappears when the magnetization of the two layers is parallel to the surface. The magnetic field required to reach saturation magnetization, i.e., where the magnetizations and the field direction are parallel, decreases with increasing

temperature from 2.8 T at 5 K to 1.8 T at 55 K. Above this temperature, the required field remains the same, indicating that the EuO contribution to the signal has largely disappeared and the signal originates mostly from the Co layer.

4.3 Discussion

In agreement with the literature, the EuO reference sample exhibits a magnetic ordering temperature of 65 K to 70 K. In addition, a remanent magnetization of nearly 100 % is observed along the in-plane and out-of-plane geometry. The magnetic behavior of the rare earth oxide changes drastically when it is in contact with the transition metal Co. This alteration is illustrated by the temperature-dependent coercivity and remanence measured in the L-MOKE geometry shown in figure 4.5 (a) and (b), respectively. The black dots correspond to the EuO reference sample and the green dots to the EuO/Co bilayer. For better visualization, the temperature axis is displayed in logarithmic scale.

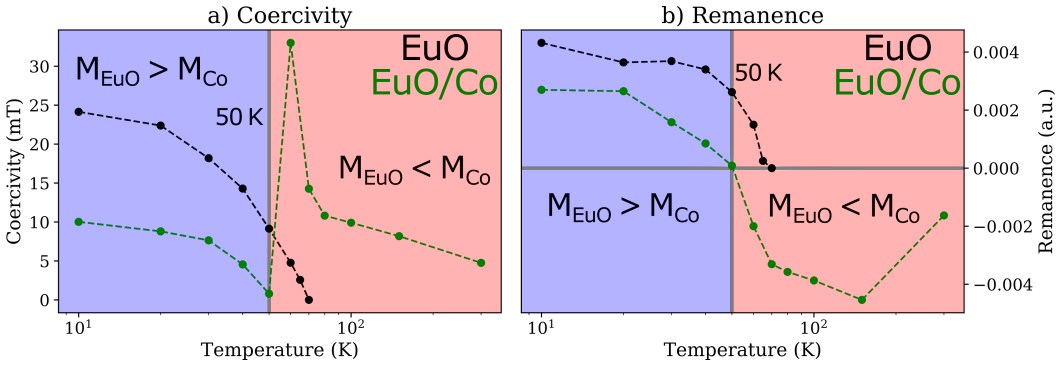

Figure 4.5: Temperature-dependent a) coercivity and b) remanence recorded on the EuO reference sample (black dots) and the EuO/Co bilayer (green dots) in the L-MOKE geometry. For temperatures up to 50 K, EuO is the dominant magnetic contribution in the EuO/Co bilayer ($M_{\mathrm{EuO}} > M_{\mathrm{Co}}$). The large increase of the coercivity and sign change of the remanence due to the hysteresis inversion is attributed to Co becoming dominant for $T > 50\,\mathrm{K}$ ($M_{\mathrm{EuO}} < M_{\mathrm{Co}}$). This transition is illustrated by a change of the background color from blue to red upon passing 50 K, at which both magnetizations equalize ($M_{\mathrm{EuO}} = M_{\mathrm{Co}}$). For better visualization, the temperature axis is displayed in logarithmic scale.

The coercivity and remanence measured on the EuO/Co bilayer decrease with increasing temperature and become zero at 50 K. The hysteresis reappears at higher temperatures with an inverted shape and thus, a negative remanence. A similar behavior can be observed in ferrimagnets, where the sublattice magnetizations can

equalize each other at a specific temperature due to their antiferromagnetic coupling, resulting in a vanishing net magnetization [66]. The measured coercivity is not fully consistent with the behavior of ferrimagnets, where it is expected to diverge at the compensation temperature [218–220], but it still suggests an antiferromagnetic coupling between EuO and Co in the bilayer. For $T < 50\,\mathrm{K}$, EuO is the dominant magnetic contribution ($M_{\mathrm{EuO}} > M_{\mathrm{Co}}$) due to its large magnetic moment and Kerr rotation. Since the rare earth oxide has a significantly lower bulk Curie temperature than Co, as shown in figure 4.3, Co becomes dominant for $T > 50\,\mathrm{K}$ ($M_{\mathrm{EuO}} < M_{\mathrm{Co}}$). This transition is illustrated by the change from a blue to a red background. Due to the large T_{C} of Co [60], the hysteresis persists up to room temperature. At $T = 50\,\mathrm{K}$, the two magnetic contributions are equal ($M_{\mathrm{EuO}} = M_{\mathrm{Co}}$), leading to a vanishing hysteresis. An antiferromagnetic coupling between EuO and transition metals like Fe and Co has already been reported in literature [148, 214].

The presence of the Co layer changes the anisotropy of the sample as indicated by the saturation fields along both experimental geometries, i.e., the field required to reach saturation magnetization. They are shown in figure 4.6 (a) and (b) for the temperature-dependent measurements performed in the L- and P-MOKE geometry, respectively. The green dots correspond to the EuO reference sample and the black dots to the EuO/Co bilayer. For a better comparability between the two geometries, the field is normalized to the maximum value of the reference sample. While the required saturation field is reduced by up to 15 % for $T \leq 30\,\mathrm{K}$ in the in-plane geometry, it is increased by up to 400 % percent in the out-of-plane geometry. This behavior suggests an increased in-plane anisotropy of EuO induced by the presence of the transition metal.

The motivation for the performed measurements was to find evidence for an increased Curie temperature of EuO due to the proximity to Co. However, since the transition metal provides the dominant magnetic contribution in the EuO/Co bilayer for $T > 50\,\mathrm{K}$ and the measured Kerr rotation is a superposition of the signals from both layers, any potential residual signal from the rare earth oxide is greatly exceeded. Thus, by static magneto-optical means, it is not possible to draw a conclusion about a modification of the EuO magnetic ordering temperature, which was suggested by Lömker [148]. A promising alternative approach to investigate the nature of the coupling between the two layers and to find potential modifications of the EuO T_{C} is to study the spin dynamics of the EuO/Co bilayer. The two materials show a distinctly different transient behavior, as described in the next chapter.

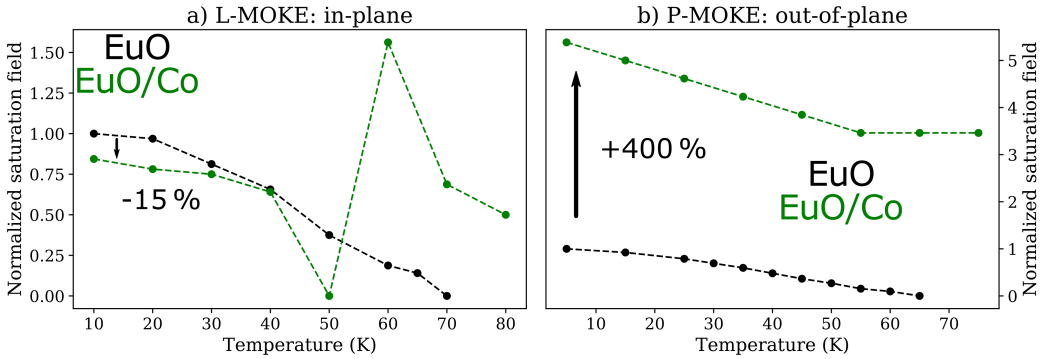

Figure 4.6: Temperature dependence of the magnetic field required to reach saturation magnetization in the a) L- and b) P-MOKE geometries. The black dots correspond to the EuO reference sample and the green dots to the EuO/Co bilayer. The saturation field is normalized to the maximum value of the respective EuO measurement. There is a large increase in the saturation field in the out-of-plane geometry, and a decrease in the in-plane geometry for $T \leq 30\,\mathrm{K}$, suggesting an increased in-plane anisotropy induced by the presence of the Co layer.

5 Time-resolved characterization

EuO and Co, the two ferromagnetic materials in the bilayer sample studied in this thesis, exhibit a distinctly different behavior on the picosecond timescale. This opens up the possibility of disentangling the two coupled magnetizations in time-resolved pump-probe experiments. As described in section 3.4.1, the transition metal Co undergoes an ultrafast demagnetization upon photoexcitation with a femtosecond laser pulse, followed by a subsequent remagnetization within a few picoseconds [202, 221–223]. EuO, on the other hand, does not experience an ultrafast demagnetization, but its magnetization is reported to be enhanced upon photoexcitation above its band gap energy [44, 224]. This remarkable effect of the rare earth oxide is explained by the transition of 4f electrons to 5d states, forming magnetic polarons [44]. They are similar to the bound magnetic polarons formed in oxygen-deficient EuO_{1-x} that are introduced in section 2.7. The ferromagnetic exchange interaction of EuO relies on virtual excitations of 4f electrons to the unoccupied 5d band in the ground state, as described in section 2.5. By occupying a 5d state with an electron, the f-d exchange interaction is enhanced, resulting in a measurable enhancement of the magnetization [44].

The photoenhancement of EuO is followed by a slower thermal demagnetization, which becomes the dominant transient contribution after several hundreds of picoseconds. Upon photoexcitation, the temperature of the 5d electrons increases rapidly. However, since the magnetization in EuO is determined by the effective temperature of the 4f electrons, demagnetization occurs only gradually as the temperature of the 4f and 5d electrons equilibrate [44]. The time-resolved behavior of the magnetizations of EuO and Co upon photoexcitation is schematically shown in figure 5.1. The magnetization of the transition metal is shown in blue and the net magnetization of the rare earth oxide in black. The magnetization enhancement and thermal demagnetization components of EuO are shown in green and red, respectively.

A similar enhancement of magnetization has already been found in a variety of materials, mostly ferromagnetic semiconductors, where it has been explained by comparable mechanisms [225–230]. For example, photoexcitation of EuS induces electron-hole pairs, which enhance the magnetization due to an additional contribution to the exchange interaction [228]. In GaMnAs, photoexcitation enhances the p-d

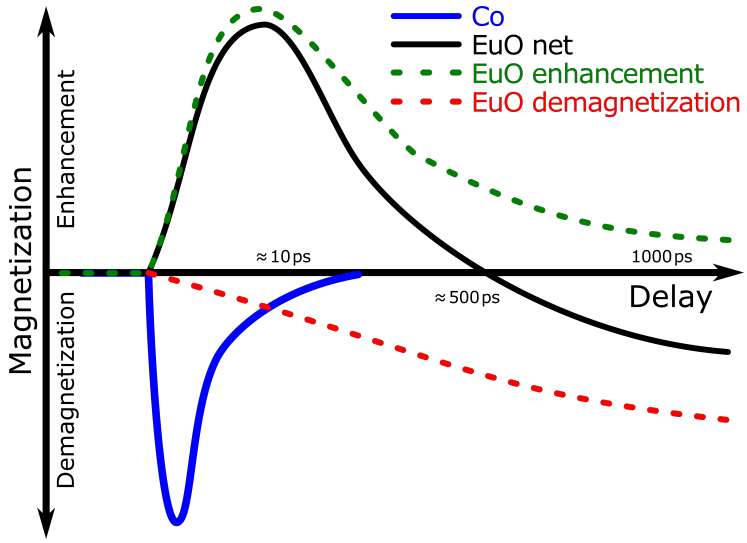

Figure 5.1: Schematic illustration of the magnetization behavior of EuO (black) and Co (blue) upon photoexcitation. The magnetization enhancement and thermal demagnetization components of EuO are represented by dashed lines in green and red, respectively. While Co undergoes an ultrafast demagnetization upon photoexcitation and remagnetizes within several picoseconds, EuO experiences an enhancement of the magnetization. Upon photoexcitation, the EuO 5d electrons heat up and slowly increase the temperature of the 4f electrons in an equilibration process, inducing a thermal demagnetization on a longer timescale. It will exceed the magnetization enhancement after several hundred picoseconds, leading to a negative net magnetization, i.e., a demagnetization. The figure is inspired by Liu et al. [44].

exchange interaction between laser-induced holes and Mn spins [226]. Other mechanisms leading to a photoinduced magnetization enhancement are also known, like a laser-induced change in the anisotropy of layered organic-inorganic hybrids [229].

To confirm the presence of the EuO magnetization enhancement effect [44] and to study the changes in the spin dynamics of EuO induced by the proximity to Co, time-resolved MOKE measurements are performed in this work using the polar MOKE pump-probe setup. The setup allows to vary the photon energy of the pump beam, providing the possibility to excite either both layers in the EuO/Co bilayer or only the Co layer. Thus, the spin dynamics of the transition metal can be isolated by selectively exciting the sample above and below the EuO band gap energy of 1.2 eV. Measurements are performed in dependence of the sample temperature T, the pump beam fluence F and the applied magnetic field B. By studying the spin behavior on short and long timescales of up to 20 ps and 2000 ps,

respectively, with different delay step sizes, further insight into the coupling of the two ferromagnetic layers can be gained. For all measurements, the photon energy of the probe beam is set to 1.55 eV with a negligible fluence of less than 10 µJ/cm². To ensure that the sample is in magnetization saturation, a magnetic field of 3.5 T is applied perpendicular to the sample surface. As shown in section 4.2, with such a magnetic field the magnetizations of the two layers are in a forced parallel alignment along the field direction. For each measured data point, 16000 pulses are acquired and the measurements are averaged over at least two consecutive scans. Details on the photon energy and fluence of the pump beam are given separately for each set of measurements.

5.1 Photoinduced magnetization enhancement

Time-resolved magneto-optical measurements in dependence of the pump photon energy performed on the EuO reference sample and the EuO/Co bilayer are shown in figure 5.2 (a) and (b), respectively. The pump fluence is set to 0.5 mJ/cm² and its photon energy is varied from above the EuO band gap energy with 1.65 eV ($\hbar\omega > E_g$) to below the EuO band gap energy with 0.73 eV ($\hbar\omega < E_g$). The traces plotted in blue and red correspond to a pump photon energy of $\hbar\omega > E_g$ and $\hbar\omega < E_g$, respectively. By tuning the pump photon energy between values above and below the EuO band gap, it is possible to excite only the Co layer and thus isolate its transient response.

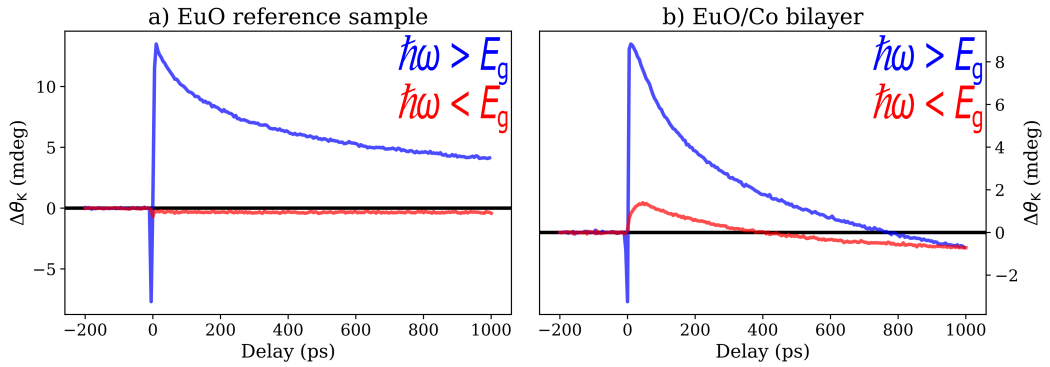

Figure 5.2: Time-resolved MOKE measurements performed in the polar configuration on a) the EuO reference sample and b) the EuO/Co bilayer at $T = 5$ K. A magnetic field of 3.5 T is applied perpendicular to the sample surface and the pump fluence is set to 0.5 mJ/cm². The blue traces correspond to a pump photon energy set to $\hbar\omega > E_g$ and the red trace to $\hbar\omega < E_g$. The figure is adapted from reference [54].

5.1.1 EuO reference sample

For a pump photon energy of $\hbar\omega > E_g$, the measured transient Kerr rotation of the EuO reference sample increases rapidly on a short timescale of a few tens of picoseconds, as shown by the blue trace in figure 5.2 (a). It decreases to about 50 % of its maximum value within 350 ps, but remains well above the equilibrium magnetization even after 1000 ps. Since the transient rotation $\Delta\theta_K$ is sensitive to pump-induced changes of the magnetization, the observed strong positive and long-lasting signal can be attributed to a photoinduced enhancement of the magnetization of EuO, in agreement with the literature [44]. The positive values of $\Delta\theta_K$ even after 1000 ps indicate that the magnetization enhancement still suppresses the thermal demagnetization. Note that the amplitude of the spin dynamics is expected to decrease with an increasing delay, since the electrons photoexcited into the 5d states will relax to the 4f ground state after some time.

In the first few picoseconds, $\Delta\theta_K$ becomes negative, before rising to large positive values. This feature appears at the same time delay Δt in the transient reflectivity, which is not shown here. Since photoexcitation can not only induce changes to the magnetization of a sample, but also alter its optical properties, as described in section 3.4, this artifact is most likely of an optical origin. The employed modulation approach (pump on - pump off) isolates the transient response of the sample, but it cannot remove pump-induced features that have no magnetic origin.

The time-resolved behavior of the EuO reference sample changes drastically for an excitation with the pump photon energy set to $\hbar\omega < E_g$, as shown by the red trace in figure 5.2 (a). Since the sample is mostly transparent at this photon energy [76], the 4f to 5d transition is suppressed and no photoinduced magnetization enhancement can occur. Nevertheless, the measured transient Kerr rotation is not zero, but the signal is rather slightly negative for a duration of at least 1000 ps. This derivation from the equilibrium ground state could originate from an indirect excitation process like impulsive-stimulated Raman scattering (ISRS), which can even be observed for optical excitation below E_g [231, 232].

5.1.2 EuO/Co bilayer

The measurements performed with the same parameters on the EuO/Co bilayer are shown in figure 5.2 (b). For an excitation above the EuO band gap energy ($\hbar\omega > E_g$), the transient behavior of the bilayer is similar to that of the EuO reference sample. The transient rotation $\Delta\theta_K$ increases strongly on a short timescale, which again indicates the photoinduced magnetization enhancement described in the literature [44]. The maximum value of $\Delta\theta_K$ is about 32 % smaller than that

observed in figure 5.2 (a), and it decays to 50 % already after 180 ps, which is almost twice as fast as for the EuO reference sample. This reduced EuO magnetization enhancement in the bilayer is attributed to the partial absorption of the pump beam in the Co layer. When propagating through 4 nm of Co, its intensity is expected to decrease by 29 % at the employed photon energy [233], which approximately matches the observed behavior.

For $\Delta t \geq 750$ ps, the measured transient rotation becomes negative. As shown schematically in figure 5.1, this indicates that the thermal demagnetization exceeds the EuO magnetization enhancement. A sign change appears only in measurements performed on the EuO/Co bilayer, suggesting a stronger demagnetization channel due to the presence of the transition metal. The negative peak at zero delay does not correspond to the ultrafast demagnetization of Co, since the step size of the delay is 5 ps and thus too large to resolve it. It is rather the same optical artifact that is also present in the measurement performed on the EuO reference sample for a pump photon energy of $\hbar\omega > E_g$.

By performing measurements with the pump photon energy set to $\hbar\omega < E_g$, the influence of Co on the spin dynamics of the EuO/Co bilayer can be isolated. EuO is mostly transparent at this photon energy and no photoinduced magnetization enhancement occurs, as shown by the red trace in figure 5.2 (a). The results of this measurement are depicted by the red trace in figure 5.2 (b). Surprisingly, the sample again shows an enhancement of the magnetization, indicated by a positive transient rotation at short delays. $\Delta\theta_K$ reaches its maximum at about 50 ps, which is slower than for a pump photon energy set to $\hbar\omega > E_g$, where the magnetization enhancement is established within about 10 ps. Similar to the excitation of both layers, the transient rotation changes its sign after 350 ps, indicating that the thermal demagnetization exceeds the magnetization enhancement.

The role of superdiffusive spin currents

Since Co is not known to exhibit a magnetization enhancement upon photoexcitation, the positive signal has to originate in the EuO layer, even though it is not photoexcited. This unexpected behavior suggests a magnetic interaction at the EuO/Co interface that allows the manipulation of the neighboring spin system as a consequence of incident pump pulses. It could either rely on an indirect excitation of the rare earth oxide by the generation of a thermal current [234], or on the transfer of majority spins from Co to EuO. Heating of EuO due to the generation of a thermal current can be excluded as an interaction mechanism in our sample system, since it would cause a demagnetization of the rare earth oxide. On the other hand, a transfer of the majority electrons from the Co 3d states to the unoccupied EuO

5d band via superdiffusive spin currents would induce the observed magnetization enhancement and thus explain the behavior. A direct excitation of the EuO 4f electrons to the 5d band is not possible with a photon energy of 0.73 eV ($\hbar\omega < E_g$). However, the photon energy is sufficiently large to promote transitions of Co 3d electrons into excited states, that are on a similar energy level as the unoccupied EuO 5d band. A number of electrons will migrate from the transition metal into the EuO layer, populating its 5d band and thereby inducing the observed magnetization enhancement. This process is shown schematically in figure 5.3.

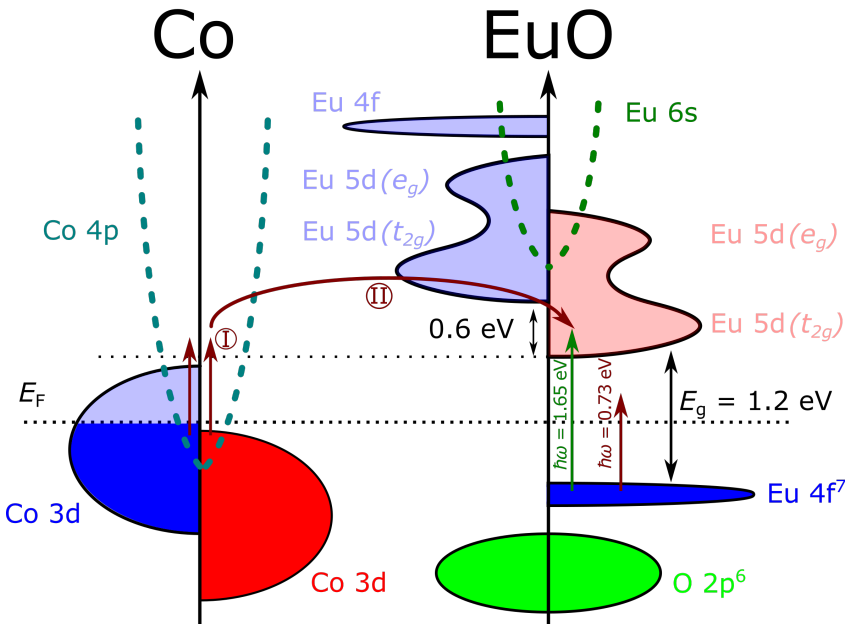

Figure 5.3: Schematic illustration of the density of states of EuO and Co, together with the electronic transitions induced by the employed pump photon energies used during the measurements. By exciting EuO above its band gap energy (1.65 eV, green arrow), transitions of 4f electrons to the 5d band will be promoted. This process is not possible for an excitation below the band gap energy (0.73 eV, dark red arrow). In the EuO/Co bilayer, this process becomes possible as an indirect excitation due to photoexcitation of Co. First, 3d electrons of Co will populate excited states (I), which then will propagate towards the EuO layer to populate the 5d band of the rare earth (II). The figure is adapted from reference [54].

Since both minority and majority electrons are excited, the spin current generated by the photoexcitation of Co can generally have a mixed character. Due to the longer lifetime of majority electrons with respect to minority electrons [190] and the spin-splitting of the EuO conduction band [100], the spin current is expected to

consist mainly of majority electrons. As described in section 3.4.2, superdiffusive spin currents provide a pathway for angular momentum transfer during the ultrafast demagnetization of transition metals. They have been observed in literature to affect the magnetization of layers adjacent to the one where they are generated [191–193]. For a parallel coupling, superdiffusive spin currents can induce a magnetization enhancement, while for an antiparallel coupling they induce a demagnetization [192, 194]. We are able to observe the enhancement of magnetization in EuO as a consequence of the generation of a superdiffusive spin current, because both magnetizations in the bilayer are forced into a parallel alignment by the external magnetic field. This allows majority electrons originating from the Co 3d states to populate the spin-split EuO 5d states.

5.2 Magnetization enhancement: Temperature dependence

The EuO magnetization enhancement and the influence of Co on the spin dynamics of the rare earth oxide are further investigated by temperature-dependent measurements. The results are depicted in figure 5.4 (a) and (b) for the EuO reference sample and the EuO/Co bilayer, respectively. The pump photon energy is set to $\hbar\omega > E_g$ so that the results of both samples can be compared. The pump fluence is again set to 0.5 mJ/cm².

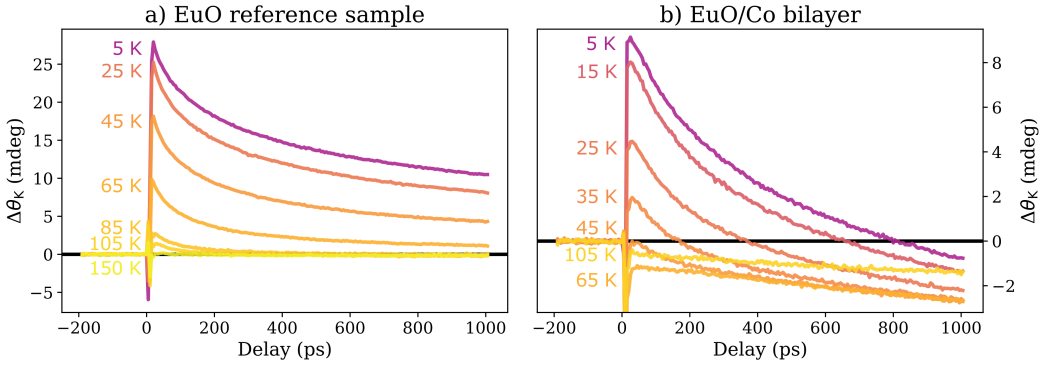

Figure 5.4: Time-resolved MOKE measurements performed in the polar configuration on a) the EuO reference sample and b) the EuO/Co bilayer in dependence of the sample temperature. The pump photon energy is set to $\hbar\omega > E_g$ in both sets of measurements with a fluence of 0.5 mJ/cm². A magnetic field of 3.5 T is applied perpendicular to the sample surface.

5.2.1 EuO reference sample

The photoinduced magnetization enhancement of EuO is strongly dependent on the temperature, as indicated by the measurements performed on the reference sample shown in figure 5.4 (a). The positive transient rotation $\Delta\theta_K$ attributed to the enhanced magnetization is largest for $T = 5\,K$ and gradually decreases with increasing temperature. For $T < T_C$, the measured signal is long-lasting and does not decay to the ground state even after 1000 ps. Upon passing the Curie temperature of 69 K, the magnitude and lifetime of the signal greatly decrease and the equilibrium magnetization is recovered within a few hundred picoseconds. The signal disappears completely for temperature above $T = 150\,K$.

The diminishing trend of the (transient) magnetization enhancement for $T < T_C$ is expected, since the (static) magnetic order of EuO decreases upon increasing the temperature. For a better comparability between these two quantities, the temperature-dependent behavior of both is shown in figure 5.5. The green dots correspond to the maximum value $\Delta\theta_K$ of the transient magnetization enhancement, taken from figure 5.4 (a). The black dots show the Kerr rotation θ_K at the saturation magnetization from the static measurements performed on the EuO reference sample shown in figure 4.3 (b) as a probe of the EuO magnetic order. θ_K and $\Delta\theta_K$ are normalized to their respective value at $T = 5\,K$. For temperatures up to 35 K, the decrease of the Kerr rotation in both measurements is nearly identical. Only for higher temperatures the offset between $\Delta\theta_K$ (green) and θ_K (black) increases, with a vanishing signal in the static measurement at 65 K. Although EuO is not expected to be in a magnetically ordered phase above this temperature, the photoinduced magnetization enhancement persists up to $T = 150\,K$. This different behavior in the time-resolved measurements is most likely caused by the photoinduced magnetic polarons responsible for the magnetization enhancement. As reported in the literature [44], optically generated magnetic polarons can polarize 4f electrons even above the EuO bulk Curie temperature, leading to a photoinduced increase of T_C.

5.2.2 EuO/Co bilayer

The results from the temperature-dependent measurements performed on the EuO/Co bilayer are shown in figure 5.4 (b). The bilayer exhibits a similar behavior compared to the EuO reference sample with a decreasing magnitude of the magnetization enhancement for increasing temperatures. This effect is accompanied by a reduction of the delay, at which the transient rotation changes its sign and the EuO magnetization enhancement is exceeded by the thermal demagnetization. While

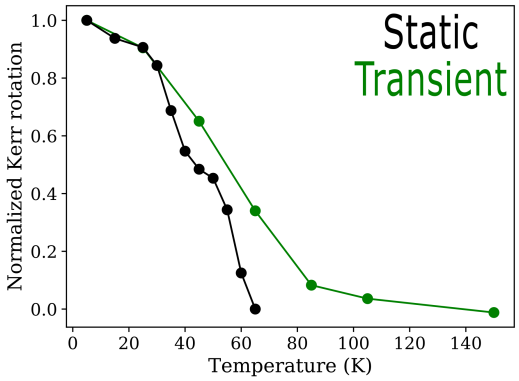

Figure 5.5: Comparison of the temperature-dependent behavior of the transient EuO magnetization enhancement and the Kerr rotation at saturation magnetization of hysteresis measurements as a probe of the magnetic order of EuO. The green data points correspond to the maxima of the pump-probe measurement from figure 5.4. The black data points are taken from figure 4.3. Both are normalized to their respective maximum at $T = 5\,\mathrm{K}$. Up to $T = 35\,\mathrm{K}$, $\Delta\theta_\mathrm{K}$ (green) and θ_K (black) decay in a similar fashion. While the static magnetic order decays to zero near 65 K, the transient signal persists up to 150 K. This behavior is attributed to the presence of photoinduced magnetic polarons that can polarize EuO 4f electrons even above its bulk T_C [44].

at $T = 5\,\mathrm{K}$, the sign change occurs at $\Delta t = 800\,\mathrm{ps}$, at $T = 35\,\mathrm{K}$ the demagnetization becomes dominant after 170 ps. For even higher temperatures, the transient rotation becomes negative regardless of the delay. The typical shape of the magnetization enhancement with a peak at short delays vanishes above $T > 45\,\mathrm{K}$. As shown for the time-resolved measurements performed on the EuO reference sample depicted in figure 5.4 (a), the magnetization enhancement is still expected to be present at this temperature, but it is greatly exceeded by the demagnetization component. The thermal demagnetization continues to increase in magnitude even after 1000 ps, and still appears at 105 K, well above the EuO Curie temperature. Although a transient signal of the EuO layer is possible at this temperature, it is expected to relax to the equilibrium magnetization after about 300 ps, as shown in figure 5.4 (a). Therefore, this long-lasting signal in the EuO/Co bilayer might originate from the transition metal. A demagnetization for more than 1000 ps is highly atypical for Co, but can be explained by the laser-induced heating of the thin film, which has no heat sinks since it is deposited between two insulating materials (EuO and MgO).

A similar temperature-dependent behavior is observed for a pump photon energy below the EuO band gap ($\hbar\omega < E_\mathrm{g}$), i.e., when only the Co layer is photoexcited, as shown in figure 5.6. The pump fluence is set to $1\,\mathrm{mJ/cm^2}$ for these measurements.

As the temperature increases, the positive component of $\Delta\theta_K$ continues to decrease and it changes its sign at a shorter delay. Since increasing the temperature has only a small effect on the Co spin dynamics [202], this behavior is attributed to a reduced EuO magnetization enhancement. At $T = 100\,\mathrm{K}$, $\Delta\theta_K$ is negative independent of the delay, and its value increases even after 2000 ps, suggesting that the magnetization enhancement of the rare earth oxide has largely disappeared due to exceeding its Curie temperature. The transient rotation is thus dominated by the thermal demagnetization of the transition metal. Interestingly, at $T = 200\,\mathrm{K}$, the signal is still present after 2000 ps, but its magnitude is significantly decreased ($\ll 1\,\mathrm{mdeg}$). Since this temperature is still far below the Curie temperature of Co, such a large decrease of its spin dynamics is unlikely. Instead, the long-lasting signal that is present for $T < 200\,\mathrm{K}$ could be a combined thermal demagnetization effect of both layers, indicating a residual magnetization of EuO above its bulk T_C, most likely at the EuO/Co interface.

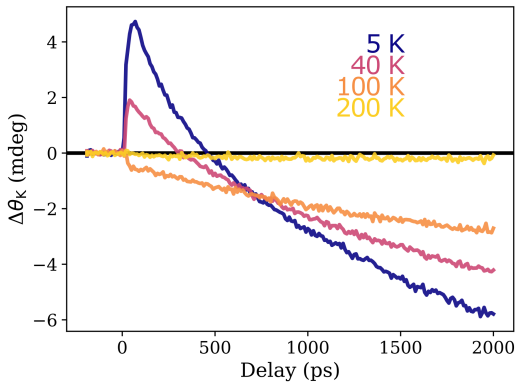

Figure 5.6: Time-resolved MOKE measurements performed in the polar configuration on the EuO/Co bilayer in dependence of the sample temperature. The pump photon energy is set to $\hbar\omega < E_g$ with a fluence of $1\,\mathrm{mJ/cm^2}$. A magnetic field of 3.5 T is applied perpendicular to the sample surface.

5.3 Magnetization enhancement: Pump fluence dependence

To further study the indirect excitation of EuO by demagnetizing Co, a set of pump-probe measurements are performed on the EuO/Co bilayer in dependence of the pump fluence for an excitation above and below the EuO band gap energy. To achieve higher fluences with the employed setup, the pump photon energy below the EuO band gap energy ($\hbar\omega < E_g$) is changed from 0.73 eV to 0.82 eV. This

is necessary due to experimental reasons, as the efficiency of the OPAs is highly wavelength dependent. The measurements are performed at a temperature of 5 K. The results are shown in figure 5.7 (a) and (b) for a pump photon energy of $\hbar\omega > E_g$ and $\hbar\omega < E_g$, respectively. Figure 5.7 (c) and (d) show a zoomed-in version of the data depicted in figure 5.7 (a) and (b). Note that a new sample was fabricated for this set of measurements, which nominally has the same thickness of the EuO and Co layers. However, small variations in the chemical composition are possible, which could result in slight changes in the timescales of the transient behavior compared to the previously discussed results.

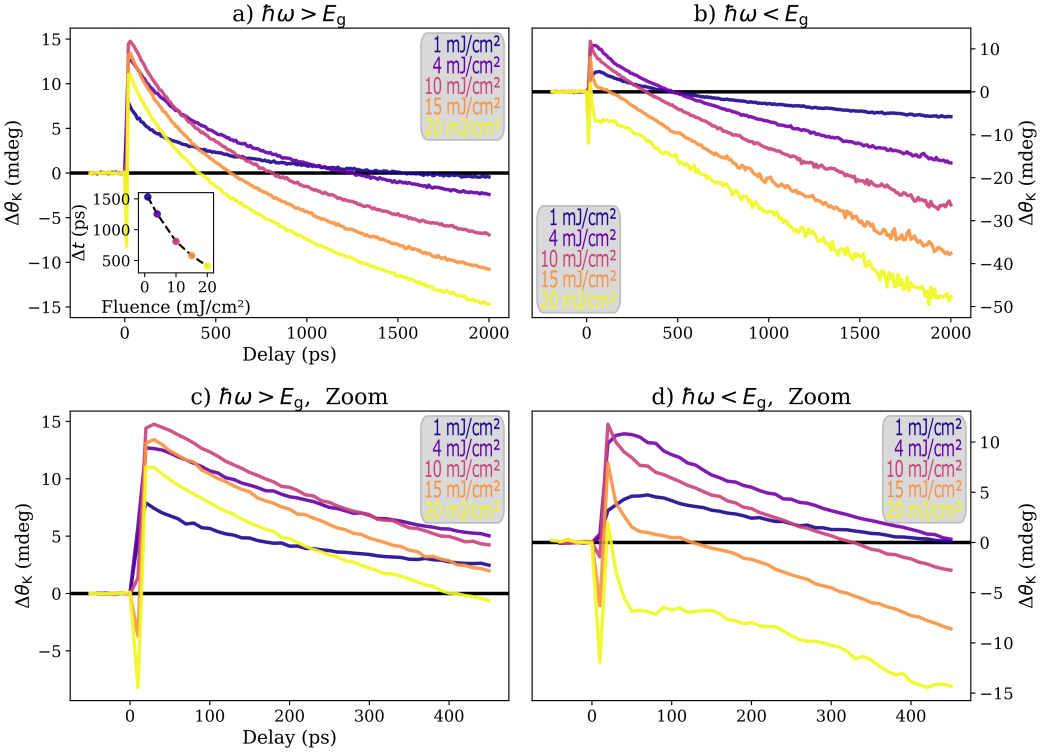

Figure 5.7: Time-resolved MOKE measurements performed at $T = 5\,\mathrm{K}$ in the polar configuration on the EuO/Co bilayer in dependence of the pump fluence for a pump photon energy of a) $\hbar\omega > E_g$ and b) $\hbar\omega < E_g$. In both cases, a magnetic field of 3.5 T is applied perpendicular to the sample surface. The inset in a) shows the fluence-dependent delay at which $\Delta\theta_K$ changes its sign. c) and d) show a zoom-in of a) and b).

For $\hbar\omega > E_g$, the EuO magnetization enhancement increases proportionally to the fluence up to 10 mJ/cm², as can be clearly seen from the transient rotation signal

at short delays in figure 5.7 (a) and (c). For fluences above 10 mJ/cm², the peak value of the transient rotation decreases. Simultaneously, each increase in fluence decreases the delay required to change the sign of the transient rotation, suggesting that the demagnetization becomes the stronger transient contribution at shorter delays. While for $F = 1\,\mathrm{mJ/cm^2}$ this happens at $\Delta t = 1500\,\mathrm{ps}$, for $F = 20\,\mathrm{mJ/cm^2}$ the delay is reduced to 400 ps, as shown in the inset. The behavior up to a few hundred picoseconds appears to result from a varying scaling of the different spin dynamics with respect to the pump fluence. For fluences up to 10 mJ/cm², the magnetization enhancement, i.e., the positive contribution to $\Delta\theta_\mathrm{K}$, increases faster than the thermal demagnetization, i.e., the negative contribution to $\Delta\theta_\mathrm{K}$, and vice versa for higher fluences. This could be due to an increased laser-induced thermal heat, and thus, a reduced magnetic order in EuO. Another explanation might be that the effect of the photoinduced magnetization enhancement is limited and the magnetization can only be increased up to a certain level, while the demagnetization may continue to increase.

The results of the fluence-dependent measurements performed on the EuO/Co bilayer for $\hbar\omega < E_\mathrm{g}$ are depicted in figure 5.7 (b) and (d). Up to $F = 5\,\mathrm{mJ/cm^2}$, the behavior is similar to a photoexcitation above the EuO band gap energy. The transient rotation shows a positive peak at a short delay, subsequently decreases and changes its sign when the thermal demagnetization becomes the dominant contribution to the transient signal. As discussed in section 5.1, for a photoexcitation with $\hbar\omega < E_\mathrm{g}$, the magnetization enhancement of EuO cannot occur as a direct process, since the rare earth oxide is mostly transparent at this photon energy. Instead, a superdiffusive spin current of majority electrons generated in the Co layer upon photoexcitation will propagate towards the rare earth oxide, populating its 5d band and thereby induce the observed magnetization enhancement. By increasing the fluence to 10 mJ/cm², the shape of the magnetization enhancement peak changes drastically and becomes sharper with a faster decay of the transient rotation. In addition, the transient rotation changes its sign at shorter delays. This effect becomes more pronounced as the fluence is further increased, and at $F = 20\,\mathrm{mJ/cm^2}$ it becomes negative already after about 20 ps. The magnetization enhancement is still present at this delay, as indicated by the positive peak at $\Delta t = 10\,\mathrm{ps}$, but the negative demagnetization component is dominating the spin dynamics.

A similar behavior was observed in the temperature-dependent measurements (see figure 5.6), where for $T \geq 100\,\mathrm{K}$ the transient rotation also becomes negative, independent of the delay. This suggests that the vanishing magnetization enhancement with increasing fluence observed for a pump photon energy of $\hbar\omega < E_\mathrm{g}$, could be of thermal nature. Increasing the temperature of the bilayer, either by direct photoexcitation or by the transfer of majority electrons, induces fluctuations in the magnetizations, which in turn reduce the parallel alignment of the two layers. Since

the indirect excitation of EuO relies on such a parallel alignment between EuO and Co, as described in section 5.1, increasing the fluence will reduce the efficiency of the superdiffusive spin current and thus the magnetization enhancement. This effect is not observed for a pump photon energy of $\hbar\omega > E_g$, because the magnetization enhancement of EuO is induced as a direct photoexcitation of the rare earth oxide.

5.4 Ultrafast behavior

So far, measurements have been performed on a long timescale of up to 2000 ps to study the EuO magnetization enhancement and the changes to the spin dynamics induced by the proximity to the Co layer. Time-resolved MOKE measurements on a shorter timescale ($\Delta t \leq 20$ ps) with a much smaller step size in the time domain can provide insight into the ultrafast spin dynamics of the sample and the interaction between the two layers. By varying the pump photon energy, the influence of the photoexcitation of the Co layer can be isolated, which may provide information about the superdiffusive spin currents responsible for the indirect excitation of the EuO layer. The results are shown in figure 5.8 (a) for a pump photon energy of $\hbar\omega > E_g$ and $\hbar\omega < E_g$ in red and blue, respectively. The fluence of the pump beam is set to 10 mJ/cm^2 and the sample temperature is $T = 5$ K. A magnetic field of 3.5 T is applied perpendicularly to the sample surface. Figure 5.8 (b) shows a zoom-in scan using the same parameters with a reduced step size of the delay.

The measured transient rotation shows an oscillatory behavior with several different peaks, which are especially pronounced for an excitation below the EuO band gap energy. We will first discuss the optical artifacts and peaks of technical origin. Around zero delay, the transient rotation shows a structure with positive and negative peaks, marked with black asterisks in figure 5.8 (a). These peaks arise from a photoinduced change in the optical properties of the sample during the cross-correlation of the pump and the probe beam. This behavior is commonly referred to as "coherent artifact" in the literature [235]. The peaks can be neglected as they do not provide any information about the magnetic behavior of the sample. Note that this does not apply to the peak marked with an orange asterisk at a delay of $\Delta t \approx 0.8$ ps, best visible in figure 5.8 (a). Another peak appears in both traces before zero delay, leading to a small deviation from the equilibrium magnetization ($\Delta\theta_K = 0$) at negative delays. At about the same distance after zero delay, there is another peak, which can be best seen in the red trace in figure 5.8 (a). These peaks, both marked with a green asterisk, could be due to internal reflections inside the sample. The time delay between them and zero delay is approximately the time it takes for light to pass twice through the YSZ substrate of the sample ($d = 0.5$ mm) [236]. This could, for example, lead to additional reflections of the probe beam arriving at

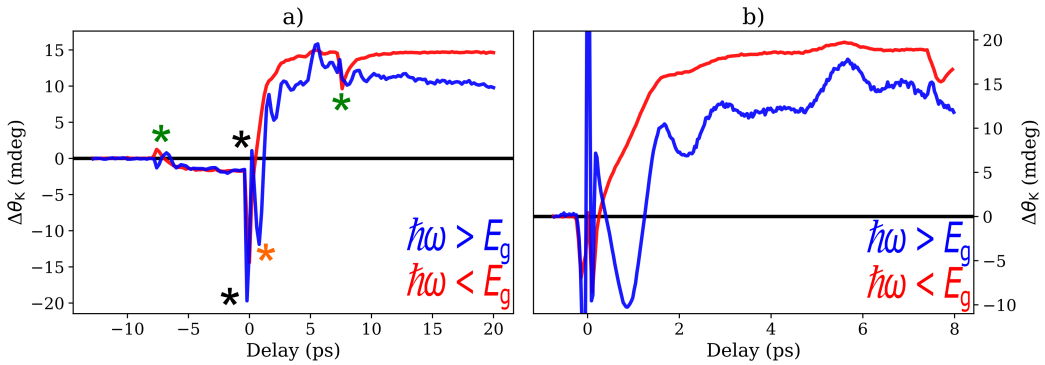

Figure 5.8: Time-resolved MOKE measurements performed in the polar configuration on the EuO/Co bilayer at a temperature of 5 K. The blue traces correspond to a pump photon energy set to $\hbar\omega > E_g$ and the red traces to $\hbar\omega < E_g$. The pump beam fluence is set to 10 mJ/cm² and a magnetic field of 3.5 T is applied perpendicular to the sample surface. In b), the stepsize of the delay is reduced compared to a) and the y-axis is zoomed-in to focus on the oscillations. The green and black asterisks in a) mark peaks of the transient rotation that correspond to optical and technical artifacts, respectively. The orange peak is of magneto-optical origin. Further details are given in the main text.

the photodetector with a small temporal shift of a few picoseconds after interaction with the sample. However, since a similar behavior with additional peaks before and after zero delay has also been observed in measurements performed on another sample system not discussed in this work, it most likely originates from a double pulse in one or both of the beams. The transmission of a laser beam through optics may induce reflections that are collinear with the beam, but offset in time by a short duration. These double pulses can lead to a different transient behavior of a sample, for example due to a second photoexcitation in the time frame of a measurement. The additional peaks before and after zero delay appeared in all measurements, even though the photon energies of both beams were varied and all optical elements were checked to prevent the generation of double pulses. Since they induce only minor variations in the transient rotation, the influence of these artifacts can be neglected.

The remaining peaks in between $\Delta t = 0.5$ ps and $\Delta t = 7$ ps show a periodic behavior with a frequency of about 0.9 THz. These peaks are of greater interest because they are most likely not of purely optical origin, but rather magneto-optical and thus carry information about the sample magnetization. Their positions appear independently of the pump photon energy, although they are only vaguely visible for an excitation with a pump photon energy of $\hbar\omega > E_g$, for example at $\Delta t = 1.6$ ps and $\Delta t = 5.6$ ps. The blue trace shows maxima of the oscillation at the same delays,

so the frequency is the same for both pump photon energies. The large minimum at about $\Delta t \approx 0.8\,\mathrm{ps}$ most likely corresponds to the ultrafast demagnetization of the Co layer, as its delay roughly matches data reported in literature [223]. This peak is only observable when the EuO magnetization is not directly excited ($\hbar\omega < E_\mathrm{g}$), because the onset of the EuO magnetization enhancement exceeds the transient contribution of the transition metal for a photoexcitation with $\hbar\omega > E_\mathrm{g}$. For $\hbar\omega < E_\mathrm{g}$, the magnetization enhancement of the rare earth oxide is established during the subsequent oscillations, indicated by the transient rotation becoming positive. As described in section 5.1, this indirect excitation of EuO relies on a superdiffusive spin current generated by the ultrafast demagnetization of Co. From the different behavior and amplitude of the oscillations at different photon energies, it can be concluded that they originate from the demagnetization of the transition metal. Most likely, the generated spin current is responsible for the observed behavior, but the exact mechanism is unclear.

Spin currents transfer angular momentum and can exert a torque on the magnetization. This can lead to a precessional motion of the magnetic moments of neighboring layers, as described in section 3.4.2. Especially in synthetic ferrimagnets, this precession is reported to exceed frequencies of several hundreds of GHz due to the antiferromagnetic coupling between the layers [237, 238]. However, this is an unlikely explanation for the observed behavior, since it only occurs when the spin current is generated in a non-collinear magnetic multilayer [239], which is not the case in the examined sample system. Due to the large magnetic field in the performed measurements, the magnetizations of EuO and Co are aligned parallely along the field direction. Instead, it is possible that the oscillation originates from a magnon or phonon excited by the spin current, although a frequency of 0.9 THz is highly atypical for a ferromagnet.

5.4.1 Temperature, fluence and field dependence

To gain further insight into the origin of the observed oscillations, measurements are performed in dependence of the sample temperature, the pump fluence and the magnetic field. The measurements are conducted with the pump photon energy set to $\hbar\omega < E_\mathrm{g}$. The results from the **magnetic field dependence** are shown in figure 5.9 (a). The measurements are performed at $T = 5\,\mathrm{K}$ with a pump fluence of $0.5\,\mathrm{mJ/cm^2}$. Varying the magnetic field between $B = 0.5\,\mathrm{T}$ and $B = 3.5\,\mathrm{T}$ does not induce changes in the frequency of the oscillations, as indicated by the vertical lines placed at different peak positions at fixed delays. The only observable effect of reducing the magnetic field is a reduction of the measured $\Delta\theta_\mathrm{K}$. This is due to reduced polar magnetization components of EuO and Co when the field is not

sufficiently large to induce a parallel alignment along the hard anisotropy axis of the bilayer. The independence of the frequency from the magnetic field suggests that the oscillation does not originate from a magnon mode.

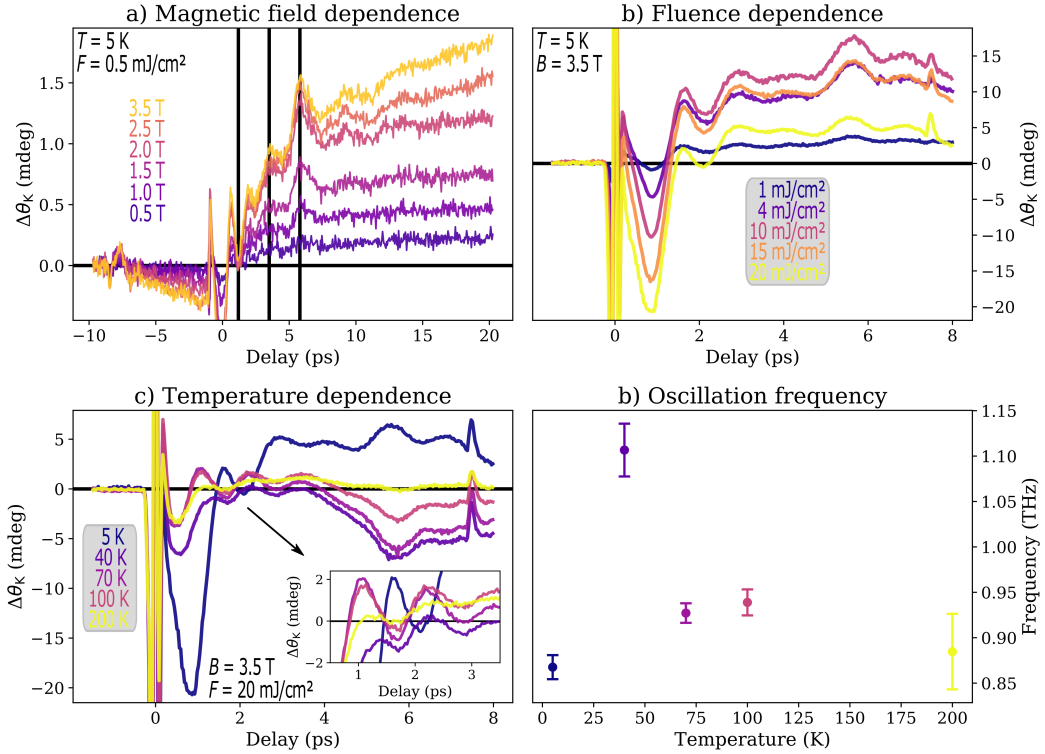

Figure 5.9: Time-resolved MOKE measurements performed in the polar configuration on the EuO/Co bilayer in dependence of a) the applied magnetic field, b) the pump fluence and c) the sample temperature. The pump photon energy is set to $\hbar\omega < E_g$. The used parameters for the pump fluence, the magnetic field and the temperature are given in the respective figure. The inset in c) shows a zoom-in for delays ranging from 0.5 ps to 3.5 ps to better visualize the varied behavior for increasing temperatures. d) shows the variation of the oscillation frequency in dependence of the sample temperature. The frequency is extracted from the pump-probe traces shown in c) with the fit function described in equation 5.1

The results of the **pump fluence dependence** performed at $T = 5\,\mathrm{K}$ are shown in figure 5.9 (b). Increasing the fluence from $1\,\mathrm{mJ/cm^2}$ up to $20\,\mathrm{mJ/cm^2}$ gradually decreases $\Delta\theta_K$ at the Co demagnetization peak at a delay of $\Delta t = 0.8\,\mathrm{ps}$, i.e., increasing the fluence leads to a stronger demagnetization of the transition metal. Similar to the behavior observed in figure 5.7, the transient rotation at $\Delta t > 0.8\,\mathrm{ps}$ increases up to $10\,\mathrm{mJ/cm^2}$ and decreases for higher values. This behavior, which is

attributed to the demagnetization of the bilayer exceeding the EuO magnetization enhancement, also occurs in the amplitude of the oscillations. It increases up to $4\,\mathrm{mJ/cm^2}$, but decreases for $F > 15\,\mathrm{mJ/cm^2}$. This can bee seen for example at a delay of $\Delta t = 1.8\,\mathrm{ps}$. However, the frequency of the oscillations does not depend on the pump fluence, as indicated by the vertical lines placed at different peak positions at fixed delays.

A more drastic change in the ultrafast behavior occurs in the **temperature dependence** shown in figure 5.9 (c). The measurements are performed with a pump fluence of $20\,\mathrm{mJ/cm^2}$. Upon increasing the temperature, the Co demagnetization peak shrinks significantly and appears already at $\Delta t = 0.5\,\mathrm{ps}$ for $T \geq 40\,\mathrm{K}$, earlier than for $T = 5\,\mathrm{K}$. In contrast to changing the pump fluence or the applied magnetic field, varying the temperature also induces changes in the frequency of the observed oscillations, as indicated by the inset and shown explicitly in figure 5.9 (d). The frequency increases slightly to 1.1 THz at $T = 40\,\mathrm{K}$ and decreases again for higher temperatures to about 0.9 THz, similar to the value observed at $T = 5\,\mathrm{K}$. The value of the frequency is extracted from the data with a fit using the function

$$f(t) = \underbrace{a + b \cdot t + c \cdot \mathrm{e}^{-d \cdot t}}_{\text{Background}} + \underbrace{e \cdot \cos\left(2\pi \cdot f \cdot t + g\right)\mathrm{e}^{-h \cdot t}}_{\text{Oscillations}} \quad . \tag{5.1}$$

The parameters a up to d describe the linear and exponential background present in the respective pump-probe trace. The remaining parameters describe different properties of the oscillations, namely the amplitude e, the frequency f, the phase g and the lifetime h [168].

The oscillation persists at least up to 200 K, although with greatly reduced amplitude. The shift to positive values of the transient rotation occurring simultaneously with the oscillation is most pronounced at 5 K and decreases with increasing temperature, but is present for all studied temperatures. Due to the reduced magnetic order of EuO upon increasing the temperature, the magnetization enhancement decreases, as observed in figure 5.4 and 5.6. It does not vanish above the bulk EuO Curie temperature because the photoinduced magnetic polaron may induce a spin polarization even above T_C, as shown for the EuO reference sample in figure 5.4 (a). Since the studied temperature range is well below the magnetic ordering temperature of Co, the changed behavior observed for increasing the temperature up to 200 K is most likely related to the reduced magnetic order of EuO.

5.5 Discussion

Time-resolved MOKE measurements have been performed on the EuO reference sample and on the EuO/Co bilayer to study the changes in the EuO spin dynamics

induced by the proximity to Co. By tuning the pump photon energy from above ($\hbar\omega > E_g$) to below ($\hbar\omega < E_g$) the EuO band gap, the influence of Co on the spin dynamics can be isolated. The transition metal experiences an ultrafast demagnetization within hundreds of femtoseconds and relaxes to the ground state within several picoseconds when photoexcited [202, 221–223]. EuO, on the other hand, undergoes a magnetization enhancement within tens of picoseconds, as described in literature [44] and confirmed by the presented measurements. Occupying the 5d conduction band with 4f electrons strengthens the ferromagnetic f-f exchange interaction between neighboring ions, which relies on virtual excitations to the 5d band in the ground state. The photoexcited 5d electrons form magnetic polarons and can polarize nearby 4f electrons, further strengthening the ferromagnetic order of EuO. On a longer timescale of several hundred picoseconds, EuO is expected to demagnetize, due to a thermal equilibration of the 4f and the hot 5d electrons [44]. As shown in figure 5.4 (a), the magnetization enhancement is strongly dependent on the temperature. However, it does not vanish at the EuO bulk T_C, because the photoinduced magnetic polarons can polarize nearby electrons even above the magnetic ordering temperature.

Our experiments show that the EuO magnetization enhancement also occurs in the EuO/Co bilayer, even when only the Co layer is photoexcited ($\hbar\omega < E_g$). This unexpected behavior is explained by the generation of a superdiffusive spin current of majority electrons by the ultrafast demagnetization of Co. It propagates toward the EuO layer and populates the unoccupied 5d band to form the magnetic polarons responsible for the magnetization enhancement of the rare earth oxide. This process is possible, because the magnetizations of EuO and Co are in a forced parallel alignment along the magnetic field direction. Time-resolved measurements examining the ultrafast behavior of the EuO/Co bilayer show the demagnetization peak of Co, followed by oscillations with a frequency of about 1 THz. During these oscillations, the (indirect) magnetization enhancement of EuO is established for an excitation below the EuO band gap ($\hbar\omega < E_g$). The oscillations are also present for a photoexcitation with $\hbar\omega > E_g$, but they are greatly exceeded by the onset of the EuO (direct) magnetization enhancement, since the rare earth oxide is directly photoexcited. Due to the different oscillatory behavior of $\Delta\theta_K$ for different excitation conditions, their origin can be ascribed to the superdiffusive spin current. However, it is unclear why this spin current would induce oscillations in the measured transient Kerr rotation. Magnetic field dependent measurements confirm that the oscillations do not originate from an excited magnon mode, as the frequency is independent of the applied field. Only by increasing the temperature, the frequency of the oscillations can be modified, as shown in figure 5.9. This suggests that they are related to the magnetic order of EuO, as the spin dynamics of Co should not be affected in this temperature range since it is far from its T_C. The oscillations could

be related to a phonon or the magnetic coupling between the two layers, but this remains unclear.

The transient behavior of EuO and Co is expected to appear on different timescales, as the magnetization enhancement and subsequent demagnetization of EuO is reported to exceed several hundred picoseconds [44]. By examining the spin dynamics of the EuO/Co bilayer on long timescales, the transient contributions of both layers can be disentangled. This opens up the possibility to find evidence for an increased T_C of EuO, since only the rare earth oxide is expected to have a transient response for $\Delta t \geq 100\,\mathrm{ps}$. Temperature-dependent measurements show a long-lasting demagnetization of the bilayer for at least up to $T = 200\,\mathrm{K}$, which is not present in the EuO reference sample. This could be a hint of an increased Curie temperature of EuO due to the proximity to Co, but it could also originate from a long-lasting thermal demagnetization of the transition metal. The latter would be highly atypical, but possible, since the Co layer is interfaced to two insulators without any heat sinks. Furthermore, since EuO shows a transient signal even above its T_C, it is difficult to distinguish between a signal originating from magnetic polarons and from the proximity to Co. An approach to differentiate these two possible origins of a transient signal of EuO above its T_C is to perform transient hysteresis loops, i.e., pump-probe measurements performed at a fixed delay in dependence of the applied magnetic field. As only a long-range magnetic order is expected to give rise to a magnetic hysteresis, it cannot originate from the photoinduced magnetic polarons. Even though they can form such a magnetically ordered state in the EuO layer, it is only transient and disappears as the sample relaxes to the ground state after each pulse.

6 Transient hysteresis measurements

The EuO/Co bilayer is further investigated by measuring transient hysteresis loops, i.e., pump-probe measurements at a fixed delay as a function of the applied magnetic field. This kind of measurement can provide an additional insight into the spin dynamics of the two layers, as well as a possible increase of the magnetic ordering temperature of EuO induced by the proximity to Co. As mentioned in section 3.5, the employed P-MOKE pump-probe setup utilizes an electro-optical modulator that can be set to block every second pulse of the pump beam. In combination with the used digitizer card, this allows for the simultaneous acquisition of the Kerr rotation of the equilibrium magnetization θ_K and the Kerr rotation of the excited state $\theta_\mathrm{K} + \Delta\theta_\mathrm{K}$. The transient Kerr rotation $\Delta\theta_\mathrm{K}$ can be isolated by taking the difference of these two quantities. It is proportional to the pump-induced changes of the magnetization component oriented perpendicularly to the sample surface due to the polar measurement geometry of the setup. An example of the data analysis is shown in figure 6.1 (a) and (b) for a pump-probe measurement as a function of the delay and the magnetic field, respectively. The measured transient response ($\theta_\mathrm{K} + \Delta\theta_\mathrm{K}$) is plotted in red, the static signal (θ_K) in blue and their difference, the isolated transient Kerr rotation ($\Delta\theta_\mathrm{K}$) in black.

The isolation of $\Delta\theta_\mathrm{K}$ offers different advantages for pump-probe measurements performed in dependence of the delay and the applied magnetic field. Since the former are generally performed with a static magnetic field, the signal acquired from the equilibrium magnetization θ_K is small and, neglecting accumulated heat, static. However, electronic noise may induce artifacts in θ_K, which are also observable in the excited state $\theta_\mathrm{K} + \Delta\theta_\mathrm{K}$, as shown by the blue and red trace in figure 6.1 (a). By applying the modulation to isolate $\Delta\theta_\mathrm{K}$, the signal-to-noise ratio can be greatly improved, as demonstrated by the black trace. The advantage of the employed modulation is even more important for the transient hysteresis measurements. Since both the equilibrium magnetization M and the pump-induced change of the magnetization ΔM vary with the magnetic field, $\Delta\theta_\mathrm{K}$ is small compared to the static signal θ_K. As shown in figure 6.1 (b), the measured static and transient signals θ_K and $\theta_\mathrm{K} + \Delta\theta_\mathrm{K}$ are nearly identical. Only by taking their difference, i.e., by applying the modulation, can the transient Kerr rotation $\Delta\theta_\mathrm{K}$ be accessed and made visible. Since the signal of this transient rotation is about 10 times weaker in amplitude in this example, it is additionally plotted in gray with a separate scale to emphasize

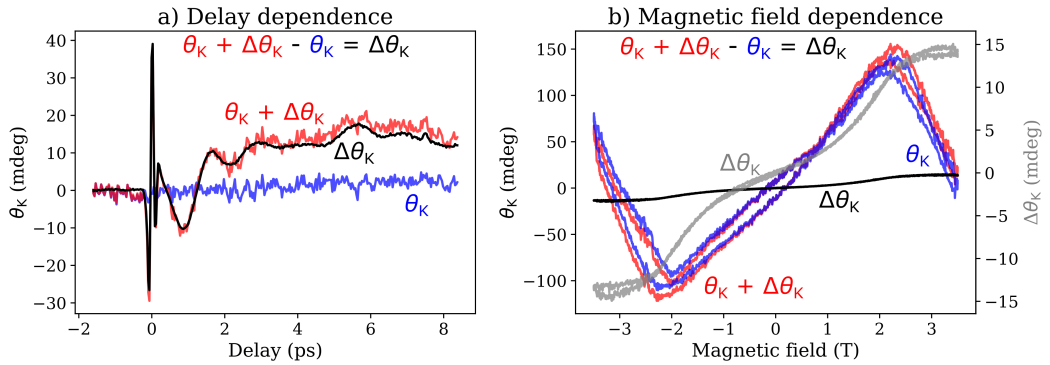

Figure 6.1: Schematic visualization of the employed modulation to isolate the transient Kerr rotation $\Delta\theta_K$ for pump-probe measurements performed in dependence of a) the delay and b) the applied magnetic field. The latter is called transient hysteresis within this thesis. The static Kerr rotation θ_K is shown in blue, the transient response of the sample $\Delta\theta_K + \theta_K$ in red and the isolated transient Kerr rotation $\Delta\theta_K$ in black. In b), $\Delta\theta_K$ is plotted additionally in gray with a separate y-scale to emphasize its shape.

its different shape. For the estimation of transient hysteresis loops, the procedure for removing the background from the static hysteresis data described in section 4.2 is not applied.

6.1 Behavior of transient hysteresis loops

Transient hysteresis loops are not as commonly presented as conventional time-resolved measurements at a fixed magnetic field. The variation of the magnetic field can give rise to complicated shapes of the transient rotation, so their possible behavior and the information they can provide must first be discussed. In the simplest case of a single ferromagnetic layer, a negative transient rotation $\Delta\theta_K$ at the positive saturation magnetization indicates a reduced magnetic order and thus a demagnetization. Positive values of $\Delta\theta_K$ can be attributed to an increase of the magnetization. The magnetization enhancement and demagnetization observable in transient hysteresis loops are schematically shown in figure 6.2 in green and red, respectively. The full response of the system ($\theta_K + \Delta\theta_K$) is depicted on the left, and the transient hysteresis, i.e., the isolated transient response ($\Delta\theta_K$), on the right. Photoexcitation can strengthen or weaken the magnetic order, leading to a larger ($\Delta\theta_K > 0$) or smaller ($\Delta\theta_K < 0$) Kerr rotation with respect to the static hysteresis shown in blue ($\Delta\theta_K = 0$). The transient hysteresis of a magnetization enhancement is a hysteresis loop with the same orientation as the static hysteresis

loop. A demagnetization, on the other hand, will show an inverted hysteresis, since $\Delta\theta_K$ is negative. The magnitudes of the magnetization enhancement and the demagnetization are arbitrary in this example. Typically, ferromagnets experience a demagnetization upon photoexcitation ($\Delta\theta_K < 0$) [169–174, 202], with a few exceptions like the semiconductors EuO and EuS, which exhibit an enhancement of the magnetization ($\Delta\theta_K > 0$) [44, 224, 228], as discussed in chapter 5.

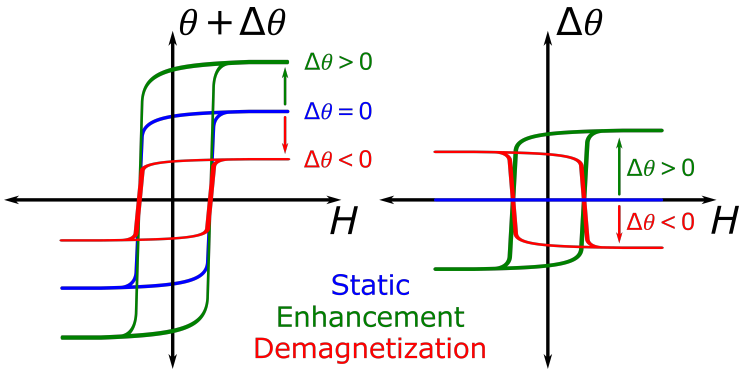

Figure 6.2: Schematic illustration of a magnetization enhancement (green) and a demagnetization (red) observable in transient hysteresis loops. The complete response of the system ($\theta_K + \Delta\theta_K$) is shown on the left, the transient hysteresis loop, i.e., the isolated transient response ($\Delta\theta_K$), on the right. The static hysteresis ($\Delta\theta_K = 0$) is shown in blue. For a magnetization enhancement, the transient response is positive, leading to a larger hysteresis, and vice versa for a demagnetization. The transient hysteresis for the former shows a hysteresis with the same orientation as the static hysteresis, the one from the demagnetization is inverted.

6.1.1 EuO/Co bilayer

The behavior of the transient hysteresis loops becomes more complicated for the EuO/Co bilayer, since the two materials are antiferromagnetically coupled in the ground state and exhibit distinctly different spin dynamics. In addition, the orientation of their separate magnetizations with respect to the applied magnetic field can vary due to different intrinsic magnetic anisotropies of the two layers. Performing transient hysteresis loops at different time delays provides the possibility to disentangle the magnetic contributions to the transient rotation $\Delta\theta_K$ by utilizing the different characteristic timescales of the spin dynamics. As discussed in the previous chapter, photoexcitation of Co induces an ultrafast demagnetization with a subsequent remagnetization within a few picoseconds [169]. EuO, on the other hand, experiences an enhancement of its magnetization on a short timescale of a few tens

of picoseconds [44]. On a longer timescale of several hundreds of picoseconds, the EuO/Co bilayer undergoes a thermal demagnetization. It might originate from a long-lasting thermal demagnetization of the Co layer due to being interfaced to two insulators without heat sinks. An example of two transient hysteresis loops recorded at $T = 5\,\mathrm{K}$ at a short delay of $\Delta t = 6\,\mathrm{ps}$ and a long delay of $\Delta t = 2000\,\mathrm{ps}$ are shown in figure 6.3 (a) and (b), respectively. The pump photon energy is varied between $0.83\,\mathrm{eV}$ ($\hbar\omega < E_\mathrm{g}$, red trace) and $1.65\,\mathrm{eV}$ ($\hbar\omega > E_\mathrm{g}$, blue trace) with a fluence of $2\,\mathrm{mJ/cm^2}$ to excite the sample below and above the EuO band gap, respectively. The corresponding background-corrected static hysteresis loop is depicted in gray with a separate y-scale. Due to the strong in-plane anisotropy of the EuO/Co bilayer, both the static and the transient hysteresis show no coercivity, i.e., they have no opening around zero field.

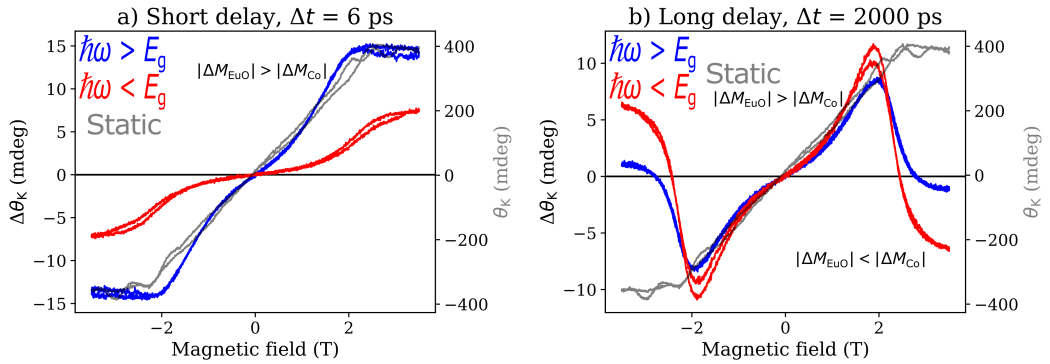

Figure 6.3: Examples for transient hysteresis loops recorded at $T = 5\,\mathrm{K}$ for a fixed time delay of a) $\Delta t = 6\,\mathrm{ps}$ and b) $\Delta t = 2000\,\mathrm{ps}$. The blue and red trace correspond to a pump photon energy of $\hbar\omega > E_\mathrm{g}$ and $\hbar\omega < E_\mathrm{g}$, respectively, with a fluence of $2\,\mathrm{mJ/cm^2}$. The corresponding static hysteresis loop is shown in gray.

Behavior at a short delay

At a short delay of $\Delta t = 6\,\mathrm{ps}$ (see figure 6.3 (a)), the transient rotation is positive for positive magnetic fields for both pump photon energies and vice versa for negative fields. This indicates the expected photoinduced EuO magnetization enhancement that exceeds the demagnetization of the Co layer: $|\Delta M_\mathrm{EuO}| > |\Delta M_\mathrm{Co}|$. The transient rotation gradually increases with the magnetic field up to $B = \pm\,2\,\mathrm{T}$, where the measured signal reaches a plateau. This behavior is similar to that of the static hysteresis loop, which shows a linear increase of the Kerr rotation θ_K up to magnetic field values of about $B = 2.4\,\mathrm{T}$, where it also reaches a plateau, namely the saturation magnetization. Note that the description of the transient

hysteresis loops will be limited to the positive magnetic fields, because the behavior is identical for negative fields. As discussed in section 4.2, the shape of the static hysteresis loop corresponds to the rotation of the magnetization of EuO (M_{EuO}) and Co (M_{Co}) from an antiparallel in-plane ground state to a forced parallel alignment along the magnetic field direction at saturation magnetization. Since the transient hysteresis loops follow the trend of the static hysteresis, it can be concluded that the pump-induced changes of the magnetization have a longitudinal character, i.e., ΔM_{EuO} and ΔM_{Co} are parallel to M_{EuO} and M_{Co}, respectively.

The main difference between the two transient hysteresis loops in figure 6.3 (a) is the slope of $\Delta\theta_{\mathrm{K}}$ for $B < 1\,\mathrm{T}$. For a photoexcitation with $\hbar\omega > E_{\mathrm{g}}$ the slope is relatively large, even at the remanence, while for a photoexcitation with $\hbar\omega < E_{\mathrm{g}}$ it is significantly smaller and increases only gradually for larger magnetic fields. The different behavior of the slopes of the transient rotation is attributed to the different excitation processes of EuO. When the rare earth oxide is directly photoexcited ($\hbar\omega > E_{\mathrm{g}}$), the magnetization enhancement process is independent of the magnetic field, because it does not rely on the coupling to the Co layer. This results in a large slope of $\Delta\theta_{\mathrm{K}}$ even for small magnetic fields, reflecting the increase of the polar component of the EuO magnetization with an increasing magnetic field. For a photoexcitation of the EuO/Co bilayer below the EuO band gap ($\hbar\omega < E_{\mathrm{g}}$) on the other hand, the magnetization enhancement can only occur as an indirect process. It relies on the generation of a superdiffusive spin current of majority electrons in the transition metal upon demagnetization. This process, described in detail in section 5.1, is expected to appear independent of the pump photon energy, but requires a parallel alignment of the two magnetizations M_{EuO} and M_{Co}. It thus becomes more efficient for increasing magnetic fields, as can be seen from the increasing slope of $\Delta\theta_{\mathrm{K}}$ in both traces in figure 6.3 (a) for magnetic fields above 1.5 T.

Interestingly, the slope for small magnetic fields is not zero for a photoexcitation with $\hbar\omega < E_{\mathrm{g}}$, but finite, even though the magnetizations of the two layers are expeceted to be aligned antiparallel to each other. In this configuration, hardly any majority electrons should be able to populate the EuO 5d band, since it is spin-split by 0.6 eV [100]. As described in section 3.4.2, the superdiffusive spin current generated when Co is demagnetized generally has a mixed character consisting of majority and minority electrons. The still present finite slope of $\Delta\theta_{\mathrm{K}}$ can therefore be attributed to minority electrons populating majority states of the EuO 5d band, a process only allowed for small magnetic fields due to the antiparallel coupling of the two layers. Since minority electrons have a short lifetime compared to majority electrons [190], only a small number of them propagate toward the EuO layer. The thereby induced magnetization enhancement is rather weak, resulting in a small slope of $\Delta\theta_{\mathrm{K}}$. As the magnetic field increases, the angle between M_{Co} and M_{EuO} becomes smaller,

allowing majority electrons of Co to populate majority states of the EuO 5d band. This leads to a stronger magnetization enhancement of the rare earth oxide and thus to a larger slope of $\Delta\theta_K$.

Behavior at a long delay

The transient hysteresis loops recorded at a delay of $\Delta t = 2000\,\text{ps}$ are depicted in figure 6.3 (b). They show a distinctly different behavior than those measured at $\Delta t = 6\,\text{ps}$. As discussed in chapter 5, a long-lasting thermal demagnetization attributed to the Co layer exceeds the EuO magnetization enhancement at long delays, resulting in a negative transient rotation ($|\Delta M_{\text{Co}}| > |\Delta M_{\text{EuO}}|$). Surprisingly, this is only the case for magnetic field values above a critical field threshold of $B_{\text{Crit}} \approx 2.7\,\text{T}$, nearly independent of the pump photon energy. For smaller fields, the transient rotation is positive, and increases with the field up to a peak at $B = 1.9\,\text{T}$, before decreasing and changing sign as the critical field is passed. Above an applied field of 3 T, the transient rotation reaches a plateau, again due to the saturation magnetization of the EuO/Co bilayer.

The positive transient rotation for $B < B_{\text{Crit}}$ corresponds to the EuO magnetization enhancement exceeding the thermal demagnetization ($|\Delta M_{\text{Co}}| < |\Delta M_{\text{EuO}}|$), even after a long delay of 2000 ps. This can be understood as an effect of the different magnitude of the magnetic anisotropies of the two layers. As shown by the static hysteresis measurements in figures 4.3 (b) and 4.4 (b), EuO reaches its saturation magnetization at smaller magnetic fields than Co. This means that for $B < B_{\text{Saturation}}$, the angle between M_{EuO} and the external field is smaller than between M_{Co} and the field. Due to the longitudinal nature of the pump-induced variation of the magnetization, this behavior can also be ascribed to ΔM_{EuO} and ΔM_{Co}, and their respective angle to the magnetic field. Consequently, even though $|\Delta M_{\text{Co}}| > |\Delta M_{\text{EuO}}|$ is true, independent of the magnetic field, the polar component of the transient EuO magnetization can exceed that from the Co layer up to B_{Crit}, thus providing a positive transient rotation. This behavior is schematically explained in figure 6.4. It does not appear for transient hysteresis loops recorded at a short delay, because $|\Delta M_{\text{EuO}}|$ greatly exceeds $|\Delta M_{\text{Co}}|$.

6.1.2 Structure of this chapter

To gain further insight into the behavior of the transient hysteresis loops, and thus the spin dynamics of the sample system, measurements are performed in dependence of the sample temperature, the pump fluence and the delay. First, the measurements performed with a pump photon energy of $\hbar\omega > E_g$ are discussed in section 6.2,

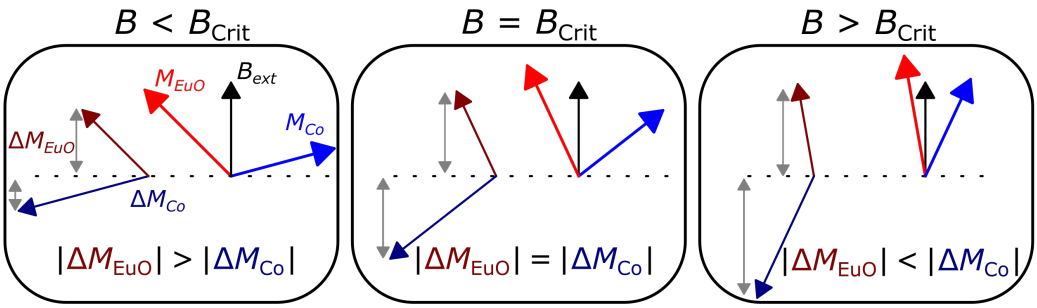

Figure 6.4: Schematic illustration of the rotation of the magnetizations and their transient components of the EuO and Co layer in respect to the magnetic field B_{ext}. ΔM_{EuO} is an enhancement of the static EuO magnetization M_{EuO}, and is therefore parallel to it. ΔM_{Co}, on the other hand, originates from a demagnetization of Co, resulting in an antiparallel alignment to M_{Co}. Even though $|\Delta M_{\mathrm{Co}}|$ exceeds $|\Delta M_{\mathrm{EuO}}|$, the transient polar component from EuO might exceed the one from Co up to a critical field due to the different magnetic anisotropies of the two layers. Since the P-MOKE geometry is only sensitive to the polar component, this can lead to a positive transient rotation even at long delays. The figure is adapted from reference [54].

followed by the results for a pump photon energy of $\hbar\omega > E_{\mathrm{g}}$ discussed in section 6.3. The pump photon energy is varied to selectively excite both layers and only the Co layer. An additional set of high fluence measurements is performed with a pump photon energy of $\hbar\omega > E_{\mathrm{g}}$ in dependence of the delay and sample temperature to explore the origin of the oscillations observed in section 5.4. Besides providing information on the spin dynamics of the EuO/Co bilayer, the conducted transient hysteresis loops will reveal any increase of the Curie temperature of EuO due to its proximity and magnetic coupling to Co.

6.2 Transient hysteresis loops for $\hbar\omega > E_{\mathrm{g}}$

The results of the transient hysteresis measurements performed in dependence of the delay, the sample temperature and the pump fluence with the pump photon energy set to 1.65 eV ($\hbar\omega > E_{\mathrm{g}}$) are discussed in this section. The probe photon energy is set to 1.55 eV with a negligible fluence of $F < 10\,\mu\mathrm{J/cm^2}$ to avoid a further excitation of the sample. A magnetic field of up to $\pm$ 3.5 T is applied perpendicular to the sample surface. The measurements are conducted with the pump-probe P-MOKE setup described in section 3.5

6.2.1 Delay dependence

Transient hysteresis loops recorded at $T = 5\,\mathrm{K}$ in dependence of the delay are depicted in figure 6.5 (a). The pump photon energy is set to $\hbar\omega > E_g$ with a fluence of $10\,\mathrm{mJ/cm^2}$. The delay is gradually increased from -20 ps up to 2000 ps, as visualized by the equally colored vertical bars in the time-resolved trace shown in figure 6.5 (b). The measurements are conducted using the same parameters and a static magnetic field of 3.5 T applied along the hard axis.

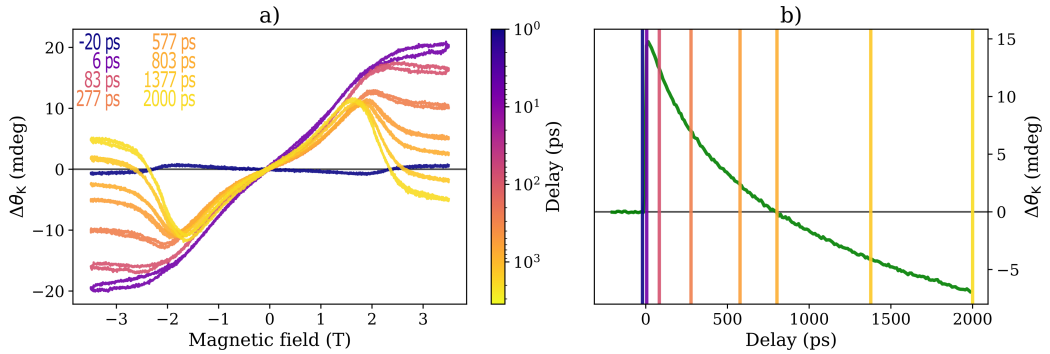

Figure 6.5: a) Transient hysteresis loops recorded on the EuO/Co bilayer in the P-MOKE geometry at $T = 5\,\mathrm{K}$ in dependence of the delay. The pump photon energy is set to $\hbar\omega > E_g$ with a fluence of $10\,\mathrm{mJ/cm^2}$. The delay is gradually increased from -20 ps up to 2000 ps. It is visualized by the equally colored vertical bars in b), where a corresponding time-resolved measurement is shown, captured with the same parameters and a field of 3.5 T applied perpendicular to the sample surface.

The shape of the transient hysteresis loops recorded for positive delays of up to 300 ps resembles the shape discussed for figure 6.3 (a) with a positive transient rotation up to the saturation magnetization. This behavior is explained by the EuO magnetization enhancement exceeding the thermal demagnetization of Co ($|\Delta M_{\mathrm{Co}}| < |\Delta M_{\mathrm{EuO}}|$). By further increasing the delay, a local maximum of the transient rotation appears at $B \approx 2\,\mathrm{T}$. Above this magnetic field threshold, the measured $\Delta\theta_{\mathrm{K}}$ decreases, indicating that either the transient contribution of the thermal demagnetization increases, or that of the magnetization enhancement decreases. A combination of both processes is also possible. The position of this peak shifts to smaller field values, down to $B = 1.6\,\mathrm{T}$ at $\Delta t = 2000\,\mathrm{ps}$, as the delay is increased. In addition, the subsequent decrease of $\Delta\theta_{\mathrm{K}}$ becomes gradually stronger, leading to negative values at the saturation magnetization upon passing a delay of about 1100 ps. Starting from this delay, the long-lasting demagnetization exceeds the EuO magnetization enhancement ($|\Delta M_{\mathrm{Co}}| > |\Delta M_{\mathrm{EuO}}|$) when passing a critical field B_{Crit}. Generally, the

transient hysteresis loops recorded in dependence of the delay show the decreasing EuO magnetization enhancement and increasing thermal demagnetization of the Co layer for increasing delays. Thus, they illustrate the transition between the two blue-colored transient hysteresis loops discussed in figure 6.3 (a) and (b).

An additional transient hysteresis loop recorded at a negative delay of $\Delta\theta_K$ = -20 ps, i.e., before zero delay, unexpectedly also shows a non-zero signal. Its shape is similar to that measured at long delays, but mirrored along the x-axis. The transient rotation is negative at small magnetic fields and becomes positive only when a critical field is passed. This shape is surprising, but might be related to a long demagnetization time of the bilayer, which appears to exceed 5 µs due to the 200 kHz repetition rate of the setup. In literature, even longer spin dynamics have been reported for Co/Pt multilayers, where a signal was observed after up to 5 ms [240].

6.2.2 Fluence dependence

Pump fluence-dependent transient hysteresis loops recorded at Δt = 6 ps and Δt = 2000 ps are shown in figure 6.6 (a) and (b), respectively. The photon energy of the pump beam is set to 1.65 eV ($\hbar\omega > E_g$) and the fluence is varied from 2 mJ/cm² to 25 mJ/cm². The measurements are performed at T = 5 K.

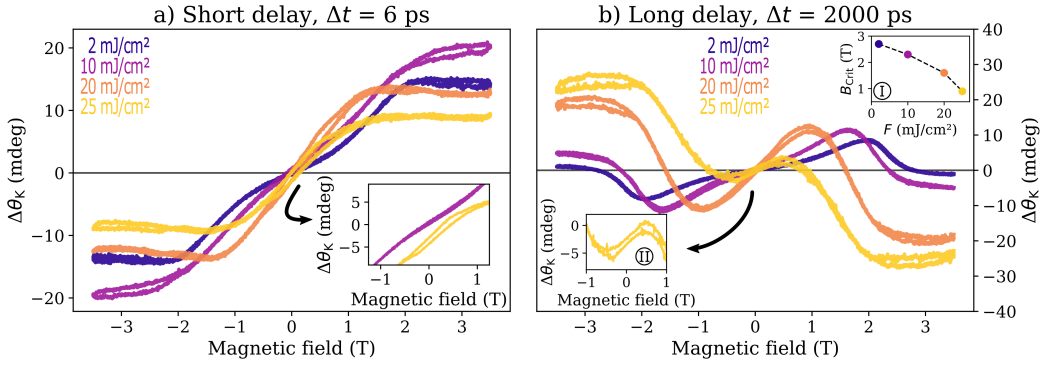

Figure 6.6: Transient hysteresis loops recorded at T = 5 K in dependence of the pump fluence at a) a short delay of Δt = 6 ps and b) a long delay of Δt = 2000 ps. The pump photon energy is set to $\hbar\omega > E_g$. The inset in a) shows a zoom-in around zero magnetic field for the measurements performed with F = 10 mJ/cm² and F = 25 mJ/cm². Inset I in b) shows the reduction of the critical field B_{Crit} for increasing fluences F. Inset II in b) shows a zoom-in for small magnetic fields for the 25 mJ/cm² measurement.

Fluence-dependent behavior at a short delay

The transient hysteresis loop recorded at a short delay of $\Delta t = 6\,\mathrm{ps}$ with a fluence of $2\,\mathrm{mJ/cm^2}$ resembles the blue trace discussed in figure 6.3 (a). It shows a positive transient rotation up to the saturation magnetization, i.e., the EuO magnetization enhancement is the dominant transient contribution. Increasing the fluence to $10\,\mathrm{mJ/cm^2}$ increases the slope of $\Delta\theta_K$ and also the measured signal at the saturation magnetization. This increase is due to a stronger photoexcitation of EuO, leading to a greater magnetization enhancement. Similar to the time-resolved measurements discussed in section 5.3, increasing the pump fluence above $10\,\mathrm{mJ/cm^2}$ does not further increase the transient signal at the saturation magnetization, but rather reduces it. The accumulated heat in the sample scales with the fluence, resulting in stronger demagnetization that effectively reduces the measured transient rotation.

Interestingly, for fluences of $F \geq 20\,\mathrm{mJ/cm^2}$, the transient hysteresis loops show an opening around zero magnetic field, i.e., the hysteresis has a small coercivity. This can be seen in the inset of figure 6.6 (a), which shows a zoom-in of the measurements conducted with a fluence of $10\,\mathrm{mJ/cm^2}$ and $25\,\mathrm{mJ/cm^2}$. For a better visualization, the latter is slightly shifted along the y-axis. Considering that the magnetic hysteresis of Co measured along the hard anisotropy axis is not reported to show a coercivity [202], this signal is attributed to the EuO layer. By strongly quenching the Co magnetization, i.e., by using a high fluence pump beam, the in-plane anisotropy of the sample is reduced, as indicated by the reduced magnetic field required to reach the saturation magnetization. While for $F \leq 10\,\mathrm{mJ/cm^2}$ a magnetic field of $B \approx 2.3\,\mathrm{T}$ is necessary to achieve saturation magnetization, for $F \geq 20\,\mathrm{mJ/cm^2}$ the field is reduced to $B \approx 1.6\,\mathrm{T}$. This decrease of the in-plane anisotropy allows the detection of the magnetic hysteresis of the underlying rare earth oxide in the EuO/Co bilayer, even in the out-of-plane geometry. Note that the emerging hysteresis is unlikely to originate from the photoinduced magnetic polarons responsible for the EuO magnetization enhancement. Even though they can form a long-range magnetic order in the ferromagnetic semiconductor, it is transient and disappears after each pulse as the sample relaxes to the ground state. Therefore, the magnetic polarons cannot be the origin of the hysteresis. Instead, the observed behavior is attributed to the static magnetization of EuO. Its contribution to the Kerr rotation is only accessible in the transient signal due to the strong quenching of the Co magnetization.

Fluence-dependent behavior at a long delay

The transient hysteresis loops recorded at a long delay of $\Delta t = 2000\,\mathrm{ps}$ are shown in figure 6.6 (b). The pump fluence is again varied between $2\,\mathrm{mJ/cm^2}$ and $25\,\mathrm{mJ/cm^2}$. Similar to the blue trace discussed in figure 6.3 (b), for $F = 2\,\mathrm{mJ/cm^2}$, $\Delta\theta_\mathrm{K}$ is positive and gradually increases with the field up to a peak at $B = 2\,\mathrm{T}$. For larger fields, the transient rotation decreases and becomes negative above a critical field of 2.7 T. This behavior is attributed to different rotation rates of the two magnetization vectors in the EuO/Co bilayer with respect to the magnetic field as a result of different magnetic anisotropies of the two layers, as schematically shown in figure 6.4.

Similar to increasing the delay (see figure 6.5), increasing the pump fluence at $\Delta t = 2000\,\mathrm{ps}$ reduces the critical field at which the measured transient rotation changes its sign. While for $F = 2\,\mathrm{mJ/cm^2}$ the critical field is $B_\mathrm{Crit} = 2.7\,\mathrm{T}$, for a larger fluence of $F = 25\,\mathrm{mJ/cm^2}$ it is significantly reduced to $B_\mathrm{Crit} = 0.9\,\mathrm{T}$. This is visualized by the inset in figure 6.6 (b), which is marked with I. In addition, the negative transient rotation at the saturation magnetization increases with the fluence. Both effects arise from an increasingly strong thermal demagnetization of Co induced by the amplified heat accumulation in the Co layer. This negative transient contribution can exceed the positive contribution to $\Delta\theta_\mathrm{K}$, the photoinduced EuO magnetization enhancement, even at gradually decreasing magnetic fields for an increasing fluence. Similar to the measurements performed at $\Delta t = 6\,\mathrm{ps}$ with $F \geq 20\,\mathrm{mJ/cm^2}$, the transient hysteresis recorded at $\Delta t = 2000\,\mathrm{ps}$ shows a small coercivity around zero field in the same fluence range. A close-up of this hysteresis opening from the measurement conducted with $F = 25\,\mathrm{mJ/cm^2}$ is shown in the inset in figure 6.6 (b), which is marked with II. As explained above, it arises from the magnetization of the underlying EuO layer and is visible due to the strong quenching of the Co magnetization.

6.2.3 Temperature dependence

Transient hysteresis loops recorded with high fluences show the promising possibility of accessing the magnetic hysteresis of EuO in the EuO/Co bilayer by strongly quenching the Co magnetization and thereby reducing the in-plane anisotropy. To further investigate this interesting effect and to find evidence for an increased Curie temperature of the rare earth oxide due to its proximity to the transition metal, additional measurements are performed in dependence of the sample temperature. The pump photon energy is again set to 1.65 eV ($\hbar\omega > E_\mathrm{g}$) with a fluence of $20\,\mathrm{mJ/cm^2}$. The results for measurements performed at a short delay of $\Delta t = 6\,\mathrm{ps}$ and a long delay of $\Delta t = 2000\,\mathrm{ps}$ are shown in figure 6.7 (a) and (b), respectively.

The temperature is varied in the range from $T = 5\,\mathrm{K}$ up to $T = 70\,\mathrm{K}$. As this temperature range is far from the Curie temperature of Co [60], changes in the behavior of the transient hysteresis loop most likely originate from the EuO layer.

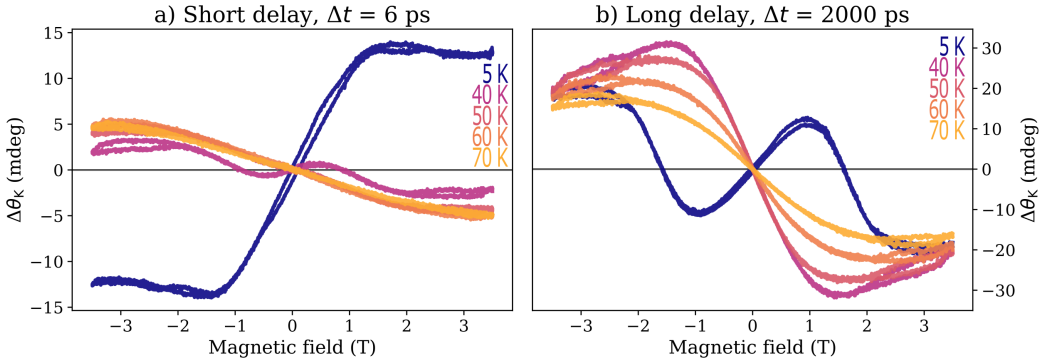

Figure 6.7: Transient hysteresis loops recorded in dependence of the sample temperature at a) a short delay of $\Delta t = 6\,\mathrm{ps}$ and b) a long delay of $\Delta t = 2000\,\mathrm{ps}$. The pump photon energy is set to $\hbar\omega > E_g$ with a fluence of $20\,\mathrm{mJ/cm^2}$.

Temperature-dependent behavior at a short delay

At a delay of $\Delta t = 6\,\mathrm{ps}$, the opening of the hysteresis is clearly visible at $T = 5\,\mathrm{K}$, but it almost completely disappears at $T = 40\,\mathrm{K}$. Increasing the temperature to this value also greatly changes the shape of the transient hysteresis loop. A critical field appears at $B_{\mathrm{Crit}} = 0.8\,\mathrm{T}$, and upon passing this threshold, the previously positive transient rotation becomes negative, similar to measurements performed at a longer delay. In addition, the magnitude of the measured transient rotation is greatly reduced. For $T = 50\,\mathrm{K}$, below the bulk Curie temperature of EuO, no trace of the residual magnetization of the rare earth oxide is visible anymore. There is no opening of the hysteresis, nor positive values of $\Delta\theta_{\mathrm{K}}$ for positive magnetic fields, which would indicate a contribution to the signal from the photoinduced magnetization enhancement of EuO. Instead, the transient rotation is negative for all positive magnetic field values indicating that the Co demagnetization exceeds any residual signal from EuO due to the increased temperature. It is surprising that the signal of the rare earth oxide vanishes almost 20 K below its bulk Curie temperature, but it can be attributed to the direct photoexcitation with a high fluence pump beam. The temperature of the 5d EuO electrons rises sharply, leading to a rapid increase of the 4f electron temperature, which effectively suppresses the EuO magnetization. Similar measurements performed with a pump photon energy

set to $\hbar\omega < E_g$ might avoid this obstacle. The photoexcitation of EuO is not a direct process in this case, but occurs on a longer timescale of a few picoseconds after the demagnetization of the Co layer, as discussed in section 5.4.

Temperature-dependent behavior at a long delay

A similar behavior can be observed in the transient hysteresis loops recorded at a delay of $\Delta t = 2000\,\mathrm{ps}$, depicted in figure 6.7 (b). The transient contribution from EuO is only visible at $T = 5\,\mathrm{K}$, indicated by the positive transient rotation for $B \leq 1\,\mathrm{T}$ and the presence of a critical field at $B_{\mathrm{Crit}} = 1.6\,\mathrm{T}$. For $T \geq 40\,\mathrm{K}$, $\Delta\theta_K$ is negative for all positive magnetic field values, indicating that the transient signal is dominated by the thermal demagnetization of Co. The shape of the transient hysteresis changes slightly for increasing temperatures above 40 K with a decreasing slope of $\Delta\theta_K$ for $B < 1.5\,\mathrm{T}$. The origin of this effect is unknown, but it might be related to a residual magnetization of EuO at $T = 40\,\mathrm{K}$, which gradually decreases upon increasing the temperature.

6.3 Transient hysteresis loops for $\hbar\omega < E_g$

This section discusses the results of the transient hysteresis measurements performed in dependence of the delay, the pump fluence, and the sample temperature using a pump photon energy of 0.83 eV ($\hbar\omega < E_g$) to excite only the Co layer. As discussed in section 5.1.2, the magnetization enhancement of the EuO layer is indirectly induced by a superdiffusive spin current generated by the ultrafast demagnetization of Co. The probe photon energy is set to 1.55 eV with a negligible fluence of $F < 10\,\mu\mathrm{J/cm^2}$. A magnetic field of up to $\pm 3.5\,\mathrm{T}$ is applied perpendicular to the sample surface. The measurements are again conducted with the pump-probe P-MOKE setup described in section 3.5. Due to experimental limitations with the employed pump photon energy, a maximum fluence of $5\,\mathrm{mJ/cm^2}$ could be achieved. Larger values of up to $20\,\mathrm{mJ/cm^2}$ were only possible for the measurements discussed in section 6.3.4. These high fluence measurements are performed to study the oscillations observed in the ultrafast spin dynamics of the EuO/Co bilayer.

6.3.1 Delay dependence

Transient hysteresis loops recorded at $T = 5\,\mathrm{K}$ for increasing delays ranging from 6 ps to 2000 ps are depicted in figure 6.8 (a). The pump photon energy is set to 0.83 eV ($\hbar\omega < E_g$) with a fluence of $5\,\mathrm{mJ/cm^2}$. Figure 6.8 (b) shows a time-resolved

trace measured using the same parameters and a magnetic field of 3.5 T applied perpendicular to the surface.

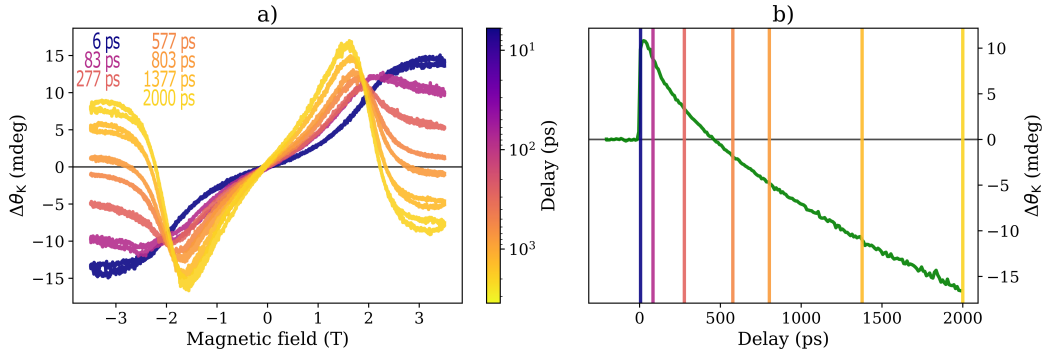

Figure 6.8: a) Transient hysteresis loops recorded on the EuO/Co bilayer in the P-MOKE geometry at $T = 5\,\mathrm{K}$ in dependence of the delay. The pump photon energy is set to $\hbar\omega < E_g$ with a fluence of $5\,\mathrm{mJ/cm^2}$. The delay is gradually increased from 6 ps up to 2000 ps. It is visualized by the equally colored vertical bars in b), where a corresponding time-resolved trace is shown, captured with the same parameters and a field of 3.5 T applied perpendicular to the sample surface. a) is adapted from reference [54].

The behavior of the delay-dependent transient hysteresis loops recorded with $\hbar\omega < E_g$ is consistent with that for a pump photon energy set to $\hbar\omega > E_g$, as discussed in section 6.2.1. For $\Delta t = 6\,\mathrm{ps}$, the transient rotation is positive and increases up to a plateau, which corresponds to the saturation magnetization. At an increased delay of $\Delta t = 83\,\mathrm{ps}$, a maximum of $\Delta\theta_K$ appears at $B = 2\,\mathrm{T}$, and upon passing it, the transient rotation decreases. This magnetic field threshold gradually decreases to lower values with an increasing delay, and simultaneously, the subsequent decrease of $\Delta\theta_K$ strongly increases. For larger delays of at least $\Delta t \geq 800\,\mathrm{ps}$, a critical field B_{Crit} appears, at which the transient rotation changes its sign. This change in sign of $\Delta\theta_K$ is due to the polar component of the thermal demagnetization of Co exceeding that of the EuO magnetization enhancement, as described in figure 6.4. The time-resolved trace shown in figure 6.8 (b) shows a smaller value for crossing zero, which might arise from small variations in the temperature or the pump fluence.

A minor deviation compared to the measurements performed with a photoexcitation of both materials in the EuO/Co bilayer is the height of the transient rotation peak. Unlike in figure 6.5 (a), for a pump photon energy set to $\hbar\omega < E_g$ the peak grows with an increasing delay. This effect is most likely due to the indirect excitation of the rare earth oxide with the superdiffusive spin current generated in the Co

layer, but the exact mechanism remains unclear. As discussed above, the transition metal thermally demagnetizes on a long timescale of hundreds of picoseconds. By increasing the delay, more electrons might contribute to the spin current and thus induce a stronger magnetization enhancement of EuO, leading to a more pronounced peak at increasing delays.

6.3.2 Fluence dependence

Transient hysteresis measurements performed at $T = 5\,\mathrm{K}$ in dependence of the pump fluence are depicted in figure 6.9 (a) and (b) for a short delay of $\Delta t = 6\,\mathrm{ps}$ and a long delay of $\Delta t = 2000\,\mathrm{ps}$, respectively. The pump photon energy is set to $0.83\,\mathrm{eV}$ ($\hbar\omega < E_\mathrm{g}$) with a fluence ranging from $0.5\,\mathrm{mJ/cm^2}$ to $5\,\mathrm{mJ/cm^2}$.

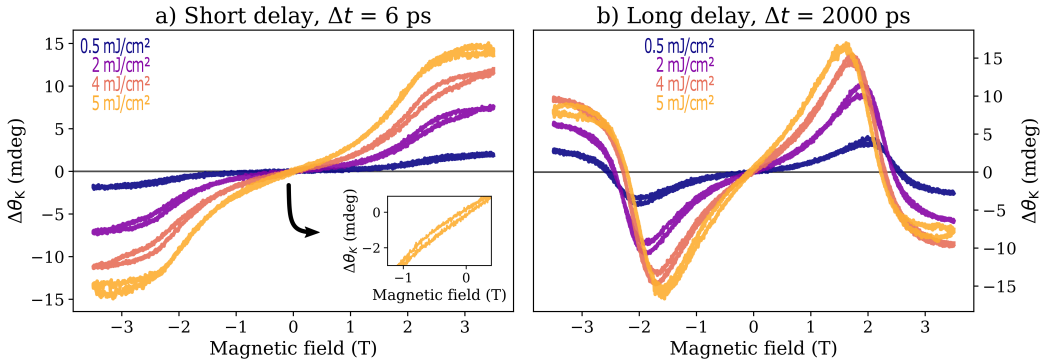

Figure 6.9: Transient hysteresis loops recorded $T = 5\,\mathrm{K}$ in dependence of the pump fluence at a) a short delay of $\Delta t = 6\,\mathrm{ps}$ and b) a long delay of $\Delta t = 2000\,\mathrm{ps}$. The pump photon energy is set to $\hbar\omega < E_\mathrm{g}$. The inset in a) shows a close-up of the measurement conducted with $F = 5\,\mathrm{mJ/cm^2}$ for small magnetic field values. The opening of the hysteresis is attributed to the static EuO magnetization. b) is adapted from reference [54].

Fluence-dependent behavior at a short delay

Due to the smaller maximum fluence, the induced changes for increasing fluences are less pronounced than those discussed in section 6.2.2 for a pump photon energy of $\hbar\omega > E_\mathrm{g}$. Nevertheless, the behavior is similar in the examined fluence range. The measured $\Delta\theta_\mathrm{K}$ is positive for all positive magnetic fields, and its slope and value at the saturation magnetization increase with the fluence. This behavior is due to the indirect EuO magnetization enhancement becoming more pronounced for

an increasing fluence. It exceeds the negative contribution to the transient signal from the thermal Co demagnetization. At $F = 5\,\mathrm{mJ/cm^2}$, the transient hysteresis loop shows a small coercivity, as illustrated by the inset in figure 6.9 (a). This can again be attributed to the EuO magnetization made visible by quenching the Co magnetization.

Fluence-dependent behavior at a long delay

As shown in figure 6.9 (b), increasing the fluence at a long delay of $\Delta t = 2000\,\mathrm{ps}$ has a similar effect on the shape of the transient hysteresis as increasing the delay. The peak of $\Delta\theta_K$ shifts to lower magnetic fields and its subsequent decrease increases with an increasing fluence. While for $F = 0.5\,\mathrm{mJ/cm^2}$, the transient rotation reaches its maximum at $B = 2\,\mathrm{T}$, for $F = 5\,\mathrm{mJ/cm^2}$ it appears already at $B = 1.6\,\mathrm{T}$. The critical field appears independently of the fluence, and its position shifts by the same amount as the shift of the peak of $\Delta\theta_K$. The transient rotation at the peak increases with both, the fluence and the delay, as shown in figure 6.8. As explained above, this effect most likely is due to the indirect excitation mechanism of EuO, since it does not occur for a direct photoexcitation of both layers ($\hbar\omega > E_g$). The increased thermal demagnetization of Co, either by increasing the fluence or the delay, appears to amplify the superdiffusive spin current for $B < B_{\mathrm{Crit}}$.

6.3.3 Temperature dependence

Transient hysteresis loops recorded in dependence of the sample temperature are shown in figure 6.10 (a) for a short delay of $\Delta t = 6\,\mathrm{ps}$ and in figure 6.10 (b) for a long delay of $\Delta t = 2000\,\mathrm{ps}$. The pump photon energy is set to $0.83\,\mathrm{eV}$ ($\hbar\omega < E_g$) with a fluence of $4\,\mathrm{mJ/cm^2}$. The temperature is gradually increased from $5\,\mathrm{K}$ up to $70\,\mathrm{K}$. Similar to the temperature-dependent measurements discussed in section 6.2.3, changes in the behavior of the transient hysteresis loops are most likely to originate from the EuO layer. Since the examined temperature range is far from the T_C of Co [60], the magnetization of the transition metal is not expected to be affected.

Temperature-dependent behavior at a short delay

For a short delay of $\Delta t = 6\,\mathrm{ps}$, increasing the temperature has the opposite effect on the transient rotation than increasing the fluence (see figure 6.9 (a)). The slope of $\Delta\theta_K$, and thus its value at the saturation magnetization, decreases with the temperature. This behavior is attributed to a reduction of the magnetic order of EuO upon approaching its Curie temperature. Unlike the similar measurements

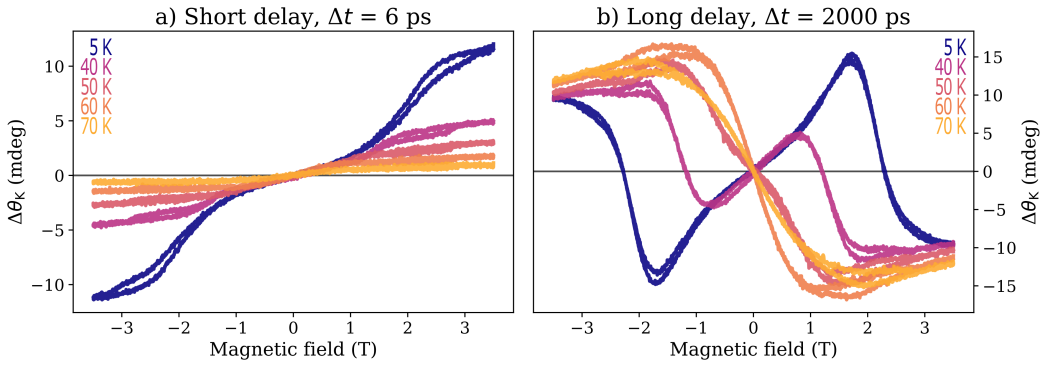

Figure 6.10: Transient hysteresis loops recorded in dependence of the sample temperature at a) a short delay of $\Delta t = 6\,\mathrm{ps}$ and b) a long delay of $\Delta t = 2000\,\mathrm{ps}$. The pump photon energy is set to $\hbar\omega < E_\mathrm{g}$ with a fluence of $4\,\mathrm{mJ/cm^2}$. b) is adapted from reference [54].

performed for a pump photon energy of $\hbar\omega > E_\mathrm{g}$ (see section 6.2.3), $\Delta\theta_\mathrm{K}$ remains positive even at $T = 70\,\mathrm{K}$. Since a positive transient signal from the EuO/Co bilayer is generally attributed to the magnetization enhancement of the rare earth oxide, this indicates a small signal from EuO even above its bulk Curie temperature, which exceeds the thermal demagnetization of the Co layer. As discussed in section 5.4, the photoinduced magnetic polarons responsible for the EuO magnetization enhancement can induce a polarization of the 4f electrons even above its T_C. Therefore, it cannot be taken as evidence for an increased magnetic ordering temperature of the rare earth oxide due to its proximity to Co.

Temperature-dependent behavior at a long delay

Similar to other measurements performed at a long delay of $\Delta t = 2000\,\mathrm{ps}$ at $T = 5\,\mathrm{K}$, $\Delta\theta_\mathrm{K}$ is positive and increases with the field up to a peak, then decreases and changes its sign after passing a critical field B_Crit. As discussed above, a sign change of the transient rotation results from a switch in the dominant transient contribution in the sample system, i.e., when the signal becomes negative, the Co demagnetization exceeds the EuO magnetization enhancement. The critical field is strongly dependent on the temperature, and decreases from $B_\mathrm{Crit} = 2.2\,\mathrm{T}$ at $T = 5\,\mathrm{K}$ to $B_\mathrm{Crit} = 1.2\,\mathrm{T}$ at $T = 40\,\mathrm{K}$. Above this temperature, the transient rotation is negative for all positive magnetic fields. However, the transient contribution of EuO is still visible at $T = 50\,\mathrm{K}$ as a variation of the slope of $\Delta\theta_\mathrm{K}$ for small magnetic fields of $B \leq 0.5\,\mathrm{T}$. This feature vanishes for $T > 50\,\mathrm{K}$, indicating that the residual signal arises solely from the thermal demagnetization of the Co layer.

6.3.4 High fluence measurements

The collective magnetization dynamics of the EuO/Co bilayer exhibit an oscillatory behavior with a frequency of about 1 THz, as demonstrated in section 5.4. It is attributed to the superdiffusive spin current responsible for the indirect EuO magnetization enhancement, which is generated by the ultrafast demagnetization of Co. However, it is unclear why the spin current would induce high frequency oscillations in the transient rotation. The performed time-resolved measurements in dependence of the magnetic field, the fluence and the temperature (see figure 5.9) could only partially explain the observed signal, since the oscillations only were modified by increasing the temperature. They persist at least up to $T = 200\,\mathrm{K}$, together with the simultaneously induced magnetization enhancement.

As described above, a positive transient rotation above the EuO Curie temperature most likely originates from the photoinduced magnetic polarons responsible for the magnetization enhancement, since they can polarize 4f electrons in their vicinity even above $T_C = 69\,\mathrm{K}$ [44]. However, the proximity coupling to Co in the EuO/Co bilayer could also induce an increased magnetic ordering temperature of the rare earth oxide. As demonstrated in section 6.2.2, the magnetic hysteresis of EuO can be accessed by strongly quenching the Co magnetization. Since this feature presumably originates from the static contribution of EuO, it can be used to distinguish between the two possibilities of a transient signal from the rare earth oxide above its bulk Curie temperature. Following this approach, transient hysteresis loops are recorded with a high fluence pump beam for increasing delays up to $\Delta t = 5.8\,\mathrm{ps}$ to study the oscillations and gain insight into their origin. In addition, measurements are conducted in temperature dependence to find evidence of an increased EuO Curie temperature due to proximity to the transition metal cobalt.

Delay-dependent behavior

Transient hysteresis loops are recorded in dependence of the delay at $T = 5\,\mathrm{K}$ with a pump fluence of $20\,\mathrm{mJ/cm^2}$. The pump photon energy is set to 0.83 eV ($\hbar\omega < E_g$) to excite only the Co layer. The EuO magnetization will remain in equilibrium for a short duration after photoexcitation. The measurements are performed with a magnetic field of up to 3.5 T applied perpendicular to the sample surface using the P-MOKE setup described in section 3.5. The results are depicted in figure 6.11 (a). The gradually increasing delay is chosen to match the delay of the maxima and minima of the observed oscillations, as indicated by the equally colored vertical bars in figure 6.11 (b). The latter figure shows a time-resolved trace, which is measured using the same parameters and a static field of 3.5 T. Note that the features near

$\Delta t = 0\,\mathrm{ps}$ are due to a photoinduced change in the optical properties of the sample and do not represent a delay at which a transient hysteresis was recorded.

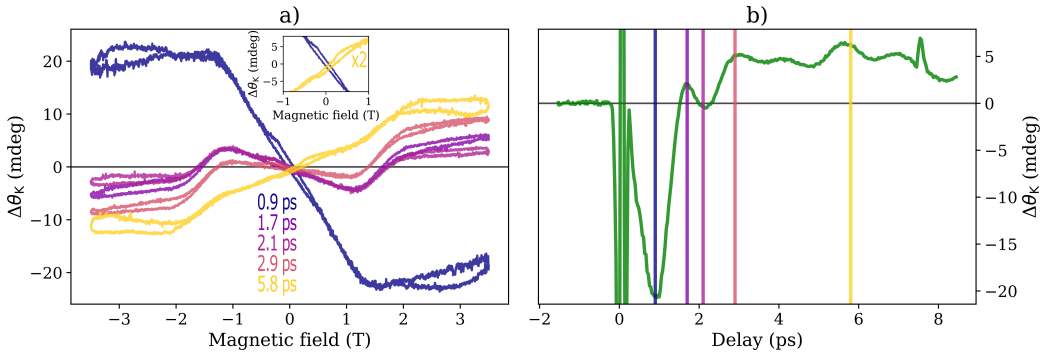

Figure 6.11: a) Transient hysteresis loops recorded on the EuO/Co bilayer in the P-MOKE geometry at $T = 5\,\mathrm{K}$ in dependence of the delay. The pump photon energy is set to $\hbar\omega < E_g$ with a fluence of $20\,\mathrm{mJ/cm^2}$. The delay is gradually increased from $\Delta t = 0.9\,\mathrm{ps}$ up to $\Delta t = 5.8\,\mathrm{ps}$ to examine the maxima and minima of the oscillation occuring in the time-resolved trace depicted in b). The colored vertical bars in b) correspond to the delay of the equally colored transient hysteresis loops. The trace depicted in b) was measured using the same parameters and a static field of $B = 3.5\,\mathrm{T}$. The inset in a) shows a close-up of the opening of the transient hysteresis for $\Delta t = 0.9\,\mathrm{ps}$ (blue) and $\Delta t = 5.8\,\mathrm{ps}$ (yellow). Note that for the latter, the transient rotation is multiplied by 2 to emphasize the shape of the hysteresis at small magnetic fields.

The first minimum of the oscillations at $\Delta t = 0.9\,\mathrm{ps}$ corresponds to the ultrafast demagnetization of the Co layer. The transient signal should be dominated by the transition metal at this delay, because EuO is mostly transparent at the employed pump photon energy. The indirectly induced magnetization enhancement of the rare earth oxide will only be established at a longer delay. The transient hysteresis loop recorded at this delay shows a strong demagnetization signal, i.e., negative values of $\Delta\theta_K$ for positive magnetic fields. As expected, it lacks a transient contribution of EuO, similar to measurements performed at elevated temperatures (see figure 6.10 (b)). However, around zero magnetic field, the transient hysteresis shows a clear opening, which is attributed to the static magnetization of the rare earth oxide. This feature remains visible for all examined delays, although its remanence decreases with an increasing delay. The inset in figure 6.11 (a) shows a close-up of the opening of the transient hysteresis loops recorded at $\Delta t = 0.9\,\mathrm{ps}$ in blue and $\Delta t = 5.8\,\mathrm{ps}$ in yellow. Note that for the latter, $\Delta\theta_K$ is multiplied by two to emphasize its shape.

The transient hysteresis loops recorded at the subsequent oscillations up to $\Delta t = 2.9\,\mathrm{ps}$

show a distinctly different behavior than the measurement conducted at the peak of the ultrafast demagnetization. $\Delta\theta_K$ is negative up to a critical field B_{Crit} and becomes positive for $B > B_{Crit}$. This suggests that the magnetization enhancement of EuO exceeds the Co demagnetization only for sufficiently large magnetic fields, contrary to the behavior observed for long delays at $\Delta t = 2000\,\text{ps}$, where the signal becomes negative for $B > B_{Crit}$. As described in section 6.1.1, the efficiency of the indirect magnetization enhancement is greatly reduced for small magnetic fields. The transfer of majority electrons is suppressed due to the antiparallel coupling between EuO and Co in the in-plane ground state. By increasing the magnetic field, the angle between the two magnetizations of the bilayer shrinks as they rotate toward the field direction. This allows an increasing number of majority electrons from Co to propagate to the EuO layer to form the magnetic polarons and thereby induce the observed magnetization enhancement. $\Delta\theta_K$ becomes positive only upon passing a critical field, when enough electrons contribute to the transient signal of EuO to exceed that of Co. A similar behavior was observed at a negative delay in figure 6.5. Since this effect also appears after a delay of $\Delta t \approx 5\,\mu\text{s}$, the period of the pulsed laser, the generation of the spin current responsible for the indirect EuO magnetization enhancement may not be limited to the ultrafast demagnetization of Co. Instead, the long-lasting demagnetization of the transition metal appears to induce a continuous thermal generation of a spin current of reduced intensity. A similar process, the thermal generation of a spin current by optical means, has been reported in the literature [241].

The critical field shifts with the delay and is reduced from $B_{Crit} = 1.7\,\text{T}$ at $\Delta t = 1.7\,\text{ps}$ to $B_{Crit} = 1.3\,\text{T}$ at $\Delta t = 2.9\,\text{ps}$. This behavior is due to the superdiffusive nature of the spin current generated in Co. The photoexcited hot electrons do not travel directly to the EuO layer, but rather experience many scattering events that influence their direction of propagation [187]. By increasing the delay, an increasing number of electrons is able to reach the rare earth oxide to contribute to the magnetization enhancement. Therefore, the transient contribution of EuO can exceed that of the Co layer even at small magnetic fields for an increased Δt. This can be seen by the transient hysteresis loop recorded at $\Delta t = 5.8\,\text{ps}$, which exhibits a positive $\Delta\theta_K$ up to the saturation magnetization.

Temperature-dependent behavior

Based on these interesting results, additional transient hysteresis loops have been recorded in dependence of the temperature at a fixed delay of $\Delta t = 2.1\,\text{ps}$. The pump photon energy is again set to $0.83\,\text{eV}$ ($\hbar\omega < E_g$) with a fluence of $20\,\text{mJ/cm}^2$. The results for the measurements conducted at $T = 5\,\text{K}$ and $T = 40\,\text{K}$ are depicted

in figure 6.12 (a). The opening of the hysteresis near $B = 0\,\mathrm{T}$ is present in both measurements, although the remanence is significantly smaller at the higher temperature. For a better visualization of this feature, a fit placed through the linear part of the transient hysteresis loops between $B = \pm 1\,\mathrm{T}$ is subtracted from the data, as indicated by the green dashed line. The subtracted data for temperatures up to 300 K are shown in figure 6.12 (b). Note that the opening of the hysteresis at saturation magnetization ($B > 1.5\,\mathrm{T}$) is most likely due to an experimental artifact related to the employed magnet. This feature usually appears in measurements performed as a function of the magnetic field when the field direction begins to reverse.

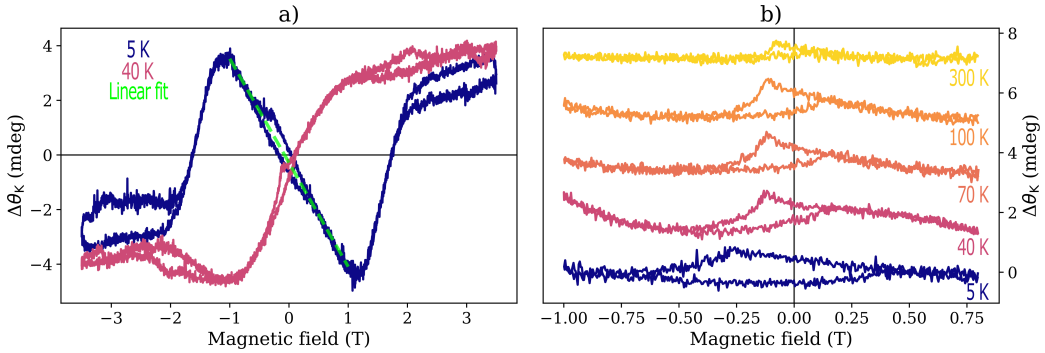

Figure 6.12: Transient hysteresis loops recorded on the EuO/Co bilayer in the P-MOKE geometry at a fixed delay of $\Delta t = 2.1\,\mathrm{ps}$ in dependence of the sample temperature. The pump photon energy is set to $\hbar\omega < E_\mathrm{g}$ with a fluence of $20\,\mathrm{mJ/cm^2}$. The temperature is increased from 5 K to 300 K. a) shows the results for the measurements conducted at $T = 5\,\mathrm{K}$ (blue) and $T = 40$ K (red). For a better visualization of the opening of the hysteresis, a linear fit is placed through the data points between $\pm$ 1 T (green dashed line) and subtracted from the data. The subtracted results up to $T = 300\,\mathrm{K}$ are shown in b). The figure is adapted from reference [54].

Strikingly, the opening of the hysteresis not only persists across the EuO bulk Curie temperature of $T_\mathrm{C} = 69\,\mathrm{K}$, but it is still present at $T = 300\,\mathrm{K}$, albeit with greatly reduced remanence and coercivity. As discussed above, it is highly unlikely that this signal originates from the transient magnetization enhancement of EuO or from the photoinduced magnetic polarons. Instead, it has to be due to a residual magnetization of EuO well above its bulk Curie temperature. It can be concluded, that the recorded transient hysteresis loops provide experimental evidence for a strongly elevated T_C of EuO, induced by magnetic proximity coupling to the transition metal Co. It is unclear whether this coupling effect affects the entire EuO film or only the interface between the two layers.

6.4 Discussion

Transient hysteresis measurements are performed on the EuO/Co bilayer to find evidence for the increased Curie temperature of EuO due to its proximity to Co. This approach offers the possibility to separate the transient contributions of the two layers, which show distinctly different spin dynamics with an ultrafast demagnetization of Co and a magnetization enhancement of EuO on a longer timescale. The transient Kerr rotation $\Delta\theta_\mathrm{K}$ is proportional to the laser-induced change of the magnetization ΔM. Therefore, the transient response of the two layers has opposite signs in the presence of an external magnetic field, which induces a parallel alignment between the magnetization vectors of EuO and Co. Using this information, it is possible to determine which material dominates the transient signal since it is a superposition of the signal from both layers. For positive values of $\Delta\theta_\mathrm{K}$ for $B > 0\,\mathrm{T}$, EuO is the dominant transient contribution, and for negative values, Co is dominant, i.e., $|\Delta M_\mathrm{EuO}| > |\Delta M_\mathrm{Co}|$ and $|\Delta M_\mathrm{EuO}| < |\Delta M_\mathrm{Co}|$, respectively. This interplay between the two materials allows to determine which layer is dominant by varying parameters like the delay, the temperature, the pump fluence, or the magnetic field. Both the sign and the magnitude of the measurable transient rotation of the EuO/Co bilayer can be tuned in this way. It is even possible to find parameters where the transient contributions of the two layers compensate for each other and the measured signal becomes zero.

6.4.1 Indirect excitation of EuO

The comparison of transient hysteresis loops recorded for $\hbar\omega > E_\mathrm{g}$ and $\hbar\omega < E_\mathrm{g}$ provides further insight into the indirect excitation mechanism of the EuO layer. As discussed in section 6.1.1, the photoinduced change of the magnetization ΔM has a longitudinal character, meaning it is parallel to the magnetization M itself. The setup is sensitive only to the polar component of M, and due to the strong in-plane anisotropy of the bilayer, the measured static and transient signals both exhibit zero remanence. Once a magnetic field is applied, the magnetizations of the two layers, and thus also ΔM, rotate toward the field direction and their polar component increases. The slope of the measured transient rotation at a fixed delay of $\Delta t = 6\,\mathrm{ps}$ is strongly dependent on the pump photon energy for small magnetic fields. While it is large for a direct photoexcitation of both layers ($\hbar\omega > E_\mathrm{g}$) even at $B = 0\,\mathrm{T}$, it is vanishingly small for a photoexcitation of Co only ($\hbar\omega < E_\mathrm{g}$), as shown in figure 6.3 (a).

This offset of the slope arises from different excitation processes present for the two different pump photon energies. For $\hbar\omega > E_\mathrm{g}$ the magnetization enhancement

of EuO occurs as a direct process without relying on the coupling to the adjacent Co layer. The slope is therefore large even for small magnetic fields, but is not expected to vary with increasing fields. On the other hand, for a pump photon energy set to $\hbar\omega < E_g$, the direct photoexcitation of EuO is suppressed because the rare earth oxide is mostly transparent. The slope is small for small magnetic fields, but increases as the magnetic field increases. This behavior is consistent with the model of the superdiffusive spin current of majority electrons propagating from Co to the EuO layer, as proposed in section 5.1.2. Due to the antiferromagnetic coupling in the ground state, majority electrons of Co cannot populate the spin-split 5d conduction band of EuO, leading to the vanishing slope of $\Delta\theta_K$ observed for small magnetic fields. However, the slope is finite at $B = 0\,\mathrm{T}$ and not zero. This unexpected feature arises from the mixed nature of the superdiffusive spin current, which consists of both, majority and minority electrons. In the antiparallel ground state, a transfer of minority electrons from Co to majority states of EuO is allowed and can explain the observed signal. Since their lifetime is generally shorter than that of the majority electrons [190], the induced magnetization enhancement of EuO is limited for small magnetic fields. It only increases with increasing fields, as more electrons can contribute to this indirect excitation process. This mechanism is also present for $\hbar\omega > E_g$, since the superdiffusive spin current is generated during the Co demagnetization, independent of the pump photon energy.

6.4.2 Accessing the static EuO magnetization

Transient hysteresis loops performed at a high fluence of about $20\,\mathrm{mJ/cm^2}$ induce a strong demagnetization of the Co layer and reduce the in-plane anisotropy of the sample. Thereby, they provide access to the magnetic hysteresis of the buried EuO layer in the EuO/Co bilayer in the P-MOKE geometry. As demonstrated in section 4.2, this is not possible with static hysteresis measurements in the polar geometry. The signal of EuO becomes visible as a small opening near zero magnetic field, i.e., the transient hysteresis shows a small coercivity and remanence. Due to the strong in-plane anisotropy in equilibrium, both are zero for smaller fluences, as the setup is only sensitive to the polar component of the magnetizations of the sample. The emerging hysteresis can be attributed to EuO, since Co, unlike the rare earth oxide, is reported to exhibit no coercivity along its hard magnetization axis [202]. The opening of the hysteresis is most evident at a short delay of up to a few picoseconds, but it is also observed after a delay of $\Delta t = 2000\,\mathrm{ps}$, as shown in figure 6.6 (b). It appears independent of the employed pump photon energy, since both induce a demagnetization of the Co layer. The efficiency of the superdiffusive spin current, which is responsible for the indirect magnetization enhancement, is strongly suppressed for small magnetic fields, as explained above.

Therefore, it is unlikely that the observed signal is due to a transient change in the EuO magnetization. This is confirmed by a transient hysteresis loop recorded at the delay of the ultrafast demagnetization of Co for a pump photon energy of $\hbar\omega < E_g$. The EuO magnetization is expected to be in equilibrium, but the opening of the hysteresis still occurs and it is even most pronounced at this delay.

Since the magnetic hysteresis of a sample system depends on ferromagnetic ordering, temperature-dependent measurements can be used to determine its Curie temperature T_C. This approach was not successful for the EuO/Co bilayer with static measurements, because any possible residual signal from EuO at an elevated temperature is exceeded by the signal from Co due to its significantly higher Curie temperature. Transient hysteresis loops, on the other hand, are a promising tool to investigate the T_C of EuO, as they rely on a demagnetization of the Co layer to reveal the isolated static signal of the rare earth oxide in a transient measurement. The opening of the hysteresis is well visible at low temperatures, as shown in figure 6.12 (b) with a pump photon energy of $\hbar\omega < E_g$ and a fluence set to $20\,\mathrm{mJ/cm^2}$. Its coercivity and remanence decrease upon increasing the temperature, but strikingly, the signal persists up to at least $T = 300\,\mathrm{K}$. A transient magnetization of EuO above its Curie temperature has already been demonstrated in a pristine reference sample, as shown in figure 5.4 (a). However, as described above, the photoinduced magnetic polarons responsible for this effect are not present at the examined time delay. Furthermore, they are expected to decay after each pulse and thus cannot form the long-range magnetic order necessary for the formation of magnetic hysteresis. It can be concluded that the observed hysteresis at $T = 300\,\mathrm{K}$ originates from the static EuO magnetization. The performed transient hysteresis measurements thereby provide evidence for a magnetic proximity coupling between EuO and Co in the EuO/Co bilayer. This coupling mechanism induces a significant increase of the magnetic ordering temperature of the rare earth oxide. However, it is unclear whether this effect affects the entire EuO film or whether only the interface has an elevated magnetic ordering temperature.

7 Summary and outlook

Europium monoxide (EuO) is a promising material for a new generation of spintronic applications due to its large magnetic moment and strong magneto-optical effects combined with insulating properties. It has already been successfully employed as a magnetic tunnel barrier, generating up to 100 % spin-polarized electrons [26, 45, 46]. Its low Curie temperature of $T_C = 69\,K$ provides a challenge that needs to be overcome before the rare earth oxide can be employed in a broader range of applications. The proximity effect, i.e., the magnetic coupling to a high T_C ferromagnet, is a promising tool to greatly increase the magnetic ordering temperature of EuO, while preserving its stoichiometry and conductivity. This thesis focuses on a sample system consisting of thin films of Co grown on stoichiometric EuO. Changes to the EuO T_C and its spin dynamics induced by the proximity to the transition metal Co are examined by means of the static and time-resolved magneto-optical Kerr effect (MOKE).

Static MOKE measurements on a EuO reference sample show a distinct hysteresis with a broad coercivity and nearly 100 % remanence along both the in-plane and out-of-plane geometry. Both parameters decrease with an increasing temperature and vanish upon approaching the bulk Curie temperature of EuO. The presence of Co drastically changes the magnetic behavior in the EuO/Co bilayer. Along the in-plane geometry, the hysteresis is smaller and vanishes already at $T = 50\,K$. For $T > 50\,K$, it reappears with an inverted orientation. This ferrimagnetic-like behavior suggests an antiferromagnetic coupling between EuO and Co, with the rare earth oxide being the dominant magnetic contribution at low temperatures due to its large magnetic moment. The transition metal becomes dominant at higher temperatures due to its significantly higher T_C [60]. In the out-of-plane geometry, the hysteresis shows no coercivity, indicating an increased in-plane anisotropy induced by the transition metal. Since the measured signal is averaged over both layers, no information can be extracted about the EuO Curie temperature, as any potential residual signal is vastly exceeded by the contribution of Co.

An alternative approach to study the changes induced to EuO by its proximity to Co is to perform time-resolved MOKE measurements, and thereby exploit the intrinsically different spin dynamics of the two materials. As a ferromagnetic transition metal, Co experiences an ultrafast demagnetization within a few hundred

femtoseconds when photoexcited by an ultrashort laser pulse, and remagnetizes within several picoseconds [169]. EuO, on the other hand, undergoes a long-lasting magnetization enhancement, a behavior attributed to an enhanced ferromagnetic exchange interaction by populating 5d states. 4f electrons excited to the 5d conduction band form magnetic polarons, which are reported to induce a transient magnetization enhancement even above T_C [44]. Time-resolved measurements are conducted in the polar geometry with a sufficiently large magnetic field to force a parallel alignment of the EuO and Co magnetizations along the field direction. The spin dynamics of both layers can be observed in the performed measurements and can be distinguished by the sign of the respective transient contribution to the signal. The demagnetization of Co induces a negative contribution to the measured transient Kerr rotation, while the EuO magnetization enhancement provides a positive contribution.

The time-resolved measurements performed on the EuO/Co bilayer show an unexpected long-lasting demagnetization signal, which is still increasing after $\Delta t = 2000\,\mathrm{ps}$. Its origin remains unclear, but it is assumed to originate from the Co layer, since it is interfaced between two insulating materials without heat sinks. However, this signal strongly decreases with increasing temperatures up to at least $T = 200\,\mathrm{K}$, therefore it could also arise from an interface effect between EuO and Co. Interestingly, pump photon energy-dependent measurements show the presence of the EuO magnetization enhancement even when the rare earth oxide is transparent. This behavior is not observed in a pristine EuO reference sample. It is ascribed to a superdiffusive spin current of majority electrons generated during the ultrafast demagnetization of Co. The spin current propagates towards the EuO layer to populate the spin-split 5d conduction band, forming the magnetic polarons responsible for the magnetization enhancement. This process is allowed due to the field-induced parallel alignment between the two magnetizations and greatly diminishes if the magnetic field is reduced. Time-resolved measurements of the ultrafast spin dynamics of the EuO/Co bilayer reveal that the superdiffusive spin current induces oscillations of the transient rotation. They could be related to the coupling between the two ferromagnetic layers, but the exact mechanism remains unclear. The indirectly induced EuO magnetization enhancement occurs during these oscillations and is still present at $T = 200\,\mathrm{K}$. However, it is not possible to distinguish whether this signal is present because EuO is still in a magnetically ordered phase due to the proximity to Co, or whether it originates exclusively from the induced magnetic polarons.

Further insight into the coupling between the two layers and the signal appearing above the EuO T_C can be gained by performing transient hysteresis measurements, i.e., pump-probe measurements at a fixed delay in dependence of the applied field. The different spin dynamics of EuO and Co with positive and negative contributions to the transient Kerr rotation $\Delta\theta_K$, respectively, provide an interesting system,

where the acquired signal can be modified by the sample temperature, the pump fluence, the magnetic field and the delay. Both the sign and the magnitude of $\Delta\theta_K$ are tunable in this way, and it is even possible to find parameters where the transient contributions of the two layers compensate each other. Transient hysteresis measurements performed with a pump fluence of $20\,\mathrm{mJ/cm^2}$ induce a strong demagnetization of the Co layer and thereby reduce the in-plane anisotropy of the EuO/Co bilayer. This approach provides access to the magnetic hysteresis of the buried EuO. It appears as an opening near zero magnetic field, i.e., the hysteresis shows a small coercivity and remanence. Remarkably, this feature persists up to $T = 300\,\mathrm{K}$. This opening of the hysteresis is not expected to arise from the photoinduced magnetic polaron, since it decays after each pulse and thus cannot form the long-range magnetic order required for a magnetic hysteresis. Therefore, the measured signal provides experimental evidence for a residual magnetization of EuO at room temperature, induced by magnetic proximity coupling to the transition metal Co.

It is unclear whether the observed increase of T_C affects the entire EuO film, or if only the interface between the two layers is affected. Due to its element sensitivity, depth-resolved X-ray magnetic circular dichroism (XMCD) performed on specially prepared samples with a wedge-shaped Co layer of increasing thickness could answer this question. Furthermore, time-resolved XMCD measurements can confirm the generation of the superdiffusive spin current responsible for the indirect EuO magnetization enhancement and provide further insight into the oscillations observed on an ultrafast timescale. Such measurements could also shed light on the origin of the long-lasting negative transient rotation, i.e., whether it is really due to an unusually long thermal demagnetization of Co or whether it is an effect of the coupling between the two layers. In addition, further insight on the EuO/Co bilayer can be gained by performing spin- and angle-resolved photoemission spectroscopy (spin ARPES), which allows to study the electronic structure of the interface between the two layers. This approach might provide information about the microscopic origin of the proximity effect presumably responsible for the increase of the EuO Curie temperature.

Bibliography

[1] Nobel Foundation. *The Nobel Prize in Physics*. 1956. URL: https://www.nobelprize.org/prizes/physics/1956/summary/.

[2] Manuel Castells. *The information age: economy, society, and culture. 1, The rise of the network society*. 2nd ed., with a new pref. Wiley-Blackwell, 2010. ISBN: 9781405196864.

[3] I.M. Ross. "The invention of the transistor." In: *Proceedings of the IEEE* 86.1 (1998), pp. 7–28. DOI: 10.1109/5.658752.

[4] TORMEKA. *Advantages of Integrated Circuits ICs*. 2023. URL: https://tormeka.com/mastering-the-fundamentals-everything-you-need-to-know-about-integrated-circuits-ics/ (visited on 05/24/2023).

[5] Gordon E. Moore. "Cramming more Components onto Integrated Circuits." In: *Electronics* 38.8 (1965), 114ff.

[6] Paul S. Peercy. "The drive to miniaturization." In: *Nature* 406 (6799 2000), pp. 1023–1026. DOI: 10.1038/35023223.

[7] M. Mitchell. Waldrop. "The chips are down for Moore's law." In: *Nature* 530 (2016), pp. 144–147. DOI: 10.1038/530144a.

[8] IEEE. *IEEE International Roadmap for Devices and Systems*. 2022. URL: https://irds.ieee.org/ (visited on 05/24/2023).

[9] Graeme A Stewart, Walter Lampl, and for the ATLAS Collaboration. "How to review 4 million lines of ATLAS code." In: *Journal of Physics: Conference Series* 898.7 (Oct. 2017), p. 072013. DOI: 10.1088/1742-6596/898/7/072013.

[10] Thomas N. Theis and H.-S. Philip Wong. "The End of Moore's Law: A New Beginning for Information Technology." In: *Computing in Science and Engineering* 19.2 (2017), pp. 41–50. DOI: 10.1109/MCSE.2017.29.

[11] Klaus Mogensen. *The End of Moore's Law*. 2022. URL: https://farsight.cifs.dk/are-we-at-the-end-of-moores-law/ (visited on 05/24/2023).

[12] Nvidia. *GeForce RTX 4090*. 2022. URL: https://www.nvidia.com/de-de/geforce/graphics-cards/40-series/rtx-4090/ (visited on 05/24/2023).

[13] GadgetVersus. *Nvidia GeForce GTX 1080 Ti vs Nvidia GeForce RTX 4090*. 2022. URL: https://gadgetversus.com/graphics-card/nvidia-geforce-gtx-1080-ti-vs-nvidia-geforce-rtx-4090/ (visited on 05/24/2023).

[14] UserBenchmark. *Nvidia GeForce GTX 1080 Ti vs Nvidia GeForce RTX 4090*. 2022. URL: https://gpu.userbenchmark.com/Compare/Nvidia-RTX-4090-vs-Nvidia-GTX-1080-Ti/4136vs3918 (visited on 05/24/2023).

[15] S. A. Wolf, D. D. Awschalom, R. A. Buhrman, J. M. Daughton, S. von Molnár, M. L. Roukes, A. Y. Chtchelkanova, and D. M. Treger. "Spintronics: A Spin-Based Electronics Vision for the Future." In: *Science* 294.5546 (2001), pp. 1488–1495. DOI: 10.1126/science.1065389.

[16] M. N. Baibich, J. M. Broto, A. Fert, F. Nguyen Van Dau, F. Petroff, P. Etienne, G. Creuzet, A. Friederich, and J. Chazelas. "Giant Magnetoresistance of (001)Fe/(001)Cr Magnetic Superlattices." In: *Phys. Rev. Lett.* 61 (21 Nov. 1988), pp. 2472–2475. DOI: 10.1103/PhysRevLett.61.2472.

[17] G. Binasch, P. Grünberg, F. Saurenbach, and W. Zinn. "Enhanced magnetoresistance in layered magnetic structures with antiferromagnetic interlayer exchange." In: *Phys. Rev. B* 39 (7 Mar. 1989), pp. 4828–4830. DOI: 10.1103/PhysRevB.39.4828.

[18] Nobel Foundation. *The Nobel Prize in Physics*. 2009. URL: http://nobelprize.org/nobel_prizes/physics/laureates/2007/index.html.

[19] Claude Chappert, Albert Fert, and Frédéric Nguyen Van Dau. "The emergence of spin electronics in data storage." In: *Nature Materials* 6 (11 Nov. 2007), pp. 813–823. DOI: 10.1038/nmat2024.

[20] Albert Fert and Frédéric Nguyen Van Dau. "Spintronics, from giant magnetoresistance to magnetic skyrmions and topological insulators." In: *Comptes Rendus Physique* 20.7 (2019), pp. 817–831. ISSN: 1631-0705. DOI: https://doi.org/10.1016/j.crhy.2019.05.020.

[21] M. Julliere. "Tunneling between ferromagnetic films." In: *Physics Letters A* 54.3 (1975), pp. 225–226. ISSN: 0375-9601. DOI: https://doi.org/10.1016/0375-9601(75)90174-7.

[22] Shinji Yuasa, Taro Nagahama, Akio Fukushima, Yoshishige Suzuki, and Koji Ando. "Giant room-temperature magnetoresistance in single-crystal Fe/MgO/Fe magnetic tunnel junctions." In: *Nature Materials* 3.12 (2004), pp. 868–871. ISSN: 1476-4660. DOI: 10.1038/nmat1257.

[23] Xiaofeng Yao, Jonathan Harms, Andrew Lyle, Farbod Ebrahimi, Yisong Zhang, and Jian-Ping Wang. "Magnetic Tunnel Junction-Based Spintronic Logic Units Operated by Spin Transfer Torque." In: *IEEE Transactions on Nanotechnology* 11.1 (2012), pp. 120–126. DOI: 10.1109/TNANO.2011.2158848.

[24] Xuanyao Fong, Yusung Kim, Karthik Yogendra, Deliang Fan, Abhronil Sengupta, Anand Raghunathan, and Kaushik Roy. "Spin-Transfer Torque Devices for Logic and Memory: Prospects and Perspectives." In: *IEEE Transactions on Computer-Aided Design of Integrated Circuits and Systems* 35.1 (2016), pp. 1–22. DOI: 10.1109/TCAD.2015.2481793.

[25] J. S. Moodera, X. Hao, G. A. Gibson, and R. Meservey. "Electron-Spin Polarization in Tunnel Junctions in Zero Applied Field with Ferromagnetic EuS Barriers." In: *Phys. Rev. Lett.* 61 (5 Aug. 1988), pp. 637–640. DOI: 10.1103/PhysRevLett.61.637.

[26] Tiffany S. Santos and Jagadeesh S. Moodera. "Observation of spin filtering with a ferromagnetic EuO tunnel barrier." In: *Physical Review B* 69.24 (June 2004), p. 241203. ISSN: 1098-0121, 1550-235X. DOI: 10.1103/PhysRevB.69.241203.

[27] M. Gajek, M. Bibes, A. Barthélémy, K. Bouzehouane, S. Fusil, M. Varela, J. Fontcuberta, and A. Fert. "Spin filtering through ferromagnetic $BiMnO_3$ tunnel barriers." In: *Phys. Rev. B* 72 (2 July 2005), p. 020406. DOI: 10.1103/PhysRevB.72.020406.

[28] Satoshi Sugahara and Junsaku Nitta. "Spin-Transistor Electronics: An Overview and Outlook." In: *Proceedings of the IEEE* 98.12 (2010), pp. 2124–2154. DOI: 10.1109/JPROC.2010.2064272.

[29] Pojen Chuang, Sheng-Chin Ho, L. W. Smith, et al. "All-electric all-semiconductor spin field-effect transistors." In: *Nature Nanotechnology* 10.1 (2015), pp. 35–39. DOI: 10.1038/nnano.2014.296.

[30] Shengwei Jiang, Lizhong Li, Zefang Wang, Jie Shan, and Kin Fai Mak. "Spin tunnel field-effect transistors based on two-dimensional van der Waals heterostructures." In: *Nature Electronics* 2.4 (2019), pp. 159–163. DOI: 10.1038/s41928-019-0232-3.

[31] M. E. Flatté and G. Vignale. "Unipolar spin diodes and transistors." In: *Appl. Phys. Lett.* 78.9 (2001), pp. 1273–1275. DOI: 10.1063/1.1348317.

[32] Minggang Zeng, Lei Shen, Miao Zhou, Chun Zhang, and Yuanping Feng. "Graphene-based bipolar spin diode and spin transistor: Rectification and amplification of spin-polarized current." In: *Phys. Rev. B* 83 (11 Mar. 2011), p. 115427. DOI: 10.1103/PhysRevB.83.115427.

[33] Atsufumi Hirohata and Koki Takanashi. "Future perspectives for spintronic devices." In: *Journal of Physics D: Applied Physics* 47.19 (Apr. 2014), p. 193001. DOI: 10.1088/0022-3727/47/19/193001.

[34] David D. Awschalom and Michael E. Flatté. "Challenges for semiconductor spintronics." In: *Nature Physics* 3.3 (2007), pp. 153–159. DOI: 10.1038/nphys551.

[35] Masaaki Tanaka. "Recent progress in ferromagnetic semiconductors and spintronics devices." In: *Japanese Journal of Applied Physics* 60.1 (Dec. 2020), p. 010101. DOI: 10.35848/1347-4065/abcadc.

[36] Nils C. Gerhardt and Martin R. Hofmann. "Spin-Controlled Vertical-Cavity Surface-Emitting Lasers." In: *Advances in Optical Technologies* 2012 (2012), p. 268949. DOI: 10.1155/2012/268949.

[37] Claudia Felser, Gerhard H. Fecher, and Benjamin Balke. "Spintronics: A Challenge for Materials Science and Solid-State Chemistry." In: *Angewandte Chemie International Edition* 46.5 (2007), pp. 668–699. DOI: https://doi.org/10.1002/anie.200601815.

[38] Tomasz Dietl and Hideo Ohno. "Dilute ferromagnetic semiconductors: Physics and spintronic structures." In: *Rev. Mod. Phys.* 86 (1 Mar. 2014), pp. 187–251. DOI: 10.1103/RevModPhys.86.187.

[39] B. Dieny, I. L. Prejbeanu, K. Garello, et al. "Opportunities and challenges for spintronics in the microelectronics industry." In: *Nature Electronics* 3.8 (2020), pp. 446–459. DOI: 10.1038/s41928-020-0461-5.

[40] Günther M. Prinz, Timm Gerber, Axel Lorke, and Martina Müller. "Quantum confinement in EuO heterostructures." In: *Applied Physics Letters* 109.20 (Jan. 2016), p. 202401. ISSN: 0003-6951, 1077-3118. DOI: 10.1063/1.4966223.

[41] J. H. Greiner and G. J. Fan. "Longitudinal magneto-optical Kerr Effect in EuO and EuS." In: *Applied Physics Letters* 9.1 (July 1966), pp. 27–29. ISSN: 0003-6951, 1077-3118. DOI: 10.1063/1.1754584.

[42] J. C. Suits and Kenneth Lee. "Giant Magneto-Optical Kerr Effect in EuO." In: *Journal of Applied Physics* 42.8 (July 1971), pp. 3258–3260. ISSN: 0021-8979, 1089-7550. DOI: 10.1063/1.1660721.

[43] K. Y. Ahn and M. W. Shafer. "Relationship Between Stoichiometry and Properties of EuO Films." In: *Journal of Applied Physics* 41.3 (Mar. 1970), pp. 1260–1262. ISSN: 0021-8979, 1089-7550. DOI: 10.1063/1.1658902.

[44] F. Liu, T. Makino, T. Yamasaki, K. Ueno, A. Tsukazaki, T. Fukumura, Y. Kong, and M. Kawasaki. "Ultrafast Time-Resolved Faraday Rotation in EuO Thin Films." In: *Physical Review Letters* 108.25 (June 2012), p. 257401. ISSN: 0031-9007, 1079-7114. DOI: 10.1103/PhysRevLett.108.257401.

[45] Martina Müller, Guo-Xing Miao, and Jagadeesh S. Moodera. "Exchange splitting and bias-dependent transport in EuO spin filter tunnel barriers." In: *EPL (Europhysics Letters)* 88.4 (Nov. 2009), p. 47006. ISSN: 0295-5075, 1286-4854. DOI: 10.1209/0295-5075/88/47006.

[46] Christian Caspers, Andrei Gloskovskij, Wolfgang Drube, Claus M. Schneider, and Martina Müller. "Heteroepitaxy and ferromagnetism of EuO/MgO (001): A route towards combined spin- and symmetry-filter tunneling." In: *Physical Review B* 88.24 (Dec. 2013), p. 245302. ISSN: 1098-0121, 1550-235X. DOI: 10.1103/PhysRevB.88.245302.

[47] J. B. Torrance, M. W. Shafer, and T. R. McGuire. "Bound Magnetic Polarons and the Insulator-Metal Transition in EuO." In: *Physical Review Letters* 29.17 (Oct. 1972), pp. 1168–1171. ISSN: 0031-9007. DOI: 10.1103/PhysRevLett.29.1168.

[48] J. Schoenes and P. Wachter. "Exchange optics in Gd-doped EuO." In: *Physical Review B* 9.7 (Apr. 1974), pp. 3097–3105. ISSN: 0556-2805. DOI: 10.1103/PhysRevB.9.3097.

[49] A. Mauger and C. Godart. "The magnetic, optical, and transport properties of representatives of a class of magnetic semiconductors: The europium chalcogenides." In: *Physics Reports* 141.2–3 (Aug. 1986), pp. 51–176. ISSN: 03701573. DOI: 10.1016/0370-1573(86)90139-0.

[50] H. Ott, S. J. Heise, R. Sutarto, Z. Hu, C. F. Chang, H. H. Hsieh, H.-J. Lin, C. T. Chen, and L. H. Tjeng. "Soft x-ray magnetic circular dichroism study on Gd-doped EuO thin films." In: *Physical Review B* 73.9 (Mar. 2006), p. 094407. ISSN: 1098-0121, 1550-235X. DOI: 10.1103/PhysRevB.73.094407.

[51] Bingqian Song, Mingchang Wang, Xianjie Wang, Yu Sui, and Jinke Tang. "Positive exchange bias of EuO1—x films." In: *Journal of Magnetism and Magnetic Materials* 496 (Feb. 2020), p. 165900. ISSN: 03048853. DOI: 10.1016/j.jmmm.2019.165900.

[52] P. Fumagalli, A. Schirmeisen, and R. J. Gambino. "Exchange-induced enhancement of T C in Co 1 − x (EuS) x macroscopic ferrimagnets." In: *Physical Review B* 57.22 (June 1998), pp. 14294–14298. ISSN: 0163-1829, 1095-3795. DOI: 10.1103/PhysRevB.57.14294.

[53] C. Müller, H. Lippitz, J. J. Paggel, and P. Fumagalli. "Evidence of exchange-induced spin polarization in the magnetic semiconductor EuS." In: *Journal of Applied Physics* 95.11 (June 2004), pp. 7172–7174. ISSN: 0021-8979, 1089-7550. DOI: 10.1063/1.1688652.

[54] David Mönkebüscher, Paul Rosenberger, Fabian Mertens, Roman Adam, Claus M Schneider, Umut Parlak, Martina Müller, and Mirko Cinchetti. "Modulation of the Transient Magnetization of an EuO/Co Bilayer Tuned by Optical Excitation." In: *Advanced Materials Interfaces* (2023), p. 2300236.

[55] Joachim Stöhr and Hans Christoph Siegmann. *Magnetism: from fundamentals to nanoscale dynamics*. Springer series in solid-state sciences. Berlin; New York: Springer, 2006. ISBN: 978-3-540-30282-7.

[56] Daniel C. Mattis. *The Theory of Magnetism I: Statics and Dynamics*. Vol. 17. Springer Series in Solid-State Sciences. Berlin, Heidelberg: Springer Berlin Heidelberg, 1981. ISBN: 978-3-540-18425-6. DOI: 10.1007/978-3-642-83238-3. URL: https://link.springer.com/10.1007/978-3-642-83238-3.

[57] *Scientific and Clinical Applications of Magnetic Carriers*. Boston, MA: Springer US, 1997. ISBN: 978-1-4419-3283-9. DOI: 10.1007/978-1-4757-6482-6. URL: http://link.springer.com/10.1007/978-1-4757-6482-6.

[58] Zvonimir Z. Bandic and Randall H. Victora. "Advances in Magnetic Data Storage Technologies." In: *Proceedings of the IEEE* 96.11 (Nov. 2008), pp. 1749–1753. ISSN: 1558-2256. DOI: 10.1109/JPROC.2008.2004308.

[59] J. M. D. Coey. *Magnetism and Magnetic Materials*. Cambridge University Press, 2010. DOI: 10.1017/CBO9780511845000.

[60] Rudolf Gross and Achim Marx. *Festkörperphysik*. München: Oldenbourg, 2012. ISBN: 978-3-486-71294-0.

[61] Kannan M. Krishnan. *Fundamentals and applications of magnetic materials*. First edition. Oxford, United Kingdom: Oxford University Press, 2016. ISBN: 978-0-19-957044-7.

[62] E. Lenz. "Ueber die Bestimmung der Richtung der durch elektodynamische Vertheilung erregten galvanischen Ströme." In: *Annalen der Physik und Chemie* 107.31 (1834), pp. 483–494.

[63] Charles Kittel. *Introduction to solid state physics*. 8th ed. Hoboken, NJ: Wiley, 2005. ISBN: 978-0-471-41526-8.

[64] Robin Bläsing, Tianping Ma, See-Hun Yang, Chirag Garg, Fasil Kidane Dejene, Alpha T N'Diaye, Gong Chen, Kai Liu, and Stuart SP Parkin. "Exchange coupling torque in ferrimagnetic Co/Gd bilayer maximized near angular momentum compensation temperature." In: *Nature communications* 9.1 (2018), p. 4984.

[65] Thomas J Kools, Marnix C van Gurp, Bert Koopmans, and Reinoud Lavrijsen. "Magnetostatics of room temperature compensated Co/Gd/Co/Gd-based synthetic ferrimagnets." In: *Applied Physics Letters* 121.24 (2022).

[66] Takaya Okuno. "Introduction." In: *Magnetic Dynamics in Antiferromagnetically-Coupled Ferrimagnets: The Role of Angular Momentum*. Springer Singapore, 2020, pp. 1–24. ISBN: 9789811591754.

[67] P. W. Anderson. "Antiferromagnetism. Theory of Superexchange Interaction." In: *Physical Review* 79.2 (July 1950), pp. 350–356. ISSN: 0031-899X. DOI: 10.1103/PhysRev.79.350.

[68] P. Böni and G. Shirane. "Paramagnetic neutron scattering from the Heisenberg ferromagnet EuO." In: *Phys. Rev. B* 33 (5 Mar. 1986), pp. 3012–3019. DOI: 10.1103/PhysRevB.33.3012.

[69] Edmund C. Stoner. "Collective electron ferromagnetism." In: *Proceedings of the Royal Society A* 165.922 (1938), pp. 372–414.

[70] Alex Hubert and Rudolf Schäfer. *Magnetic domains: the analysis of magnetic microstructures*. Berlin; New York: Springer, 1998. ISBN: 978-3-540-64108-7.

[71] Giorgio Bertotti. *Hysteresis in magnetism: for physicists, materials scientists, and engineers*. Electromagnetism. San Diego: Academic Press, 1998. ISBN: 978-0-12-093270-2.

[72] T. R. McGuire and M. W. Shafer. "Ferromagnetic Europium Compounds." In: *Journal of Applied Physics* 35.3 (Mar. 1964), pp. 984–988. ISSN: 0021-8979, 1089-7550. DOI: 10.1063/1.1713568.

[73] T. Kasuya and A. Yanase. "Anomalous Transport Phenomena in Eu-Chalcogenide Alloys." In: *Reviews of Modern Physics* 40.4 (Oct. 1968), pp. 684–696. ISSN: 0034-6861. DOI: 10.1103/RevModPhys.40.684.

[74] P. Schwob and O. Vogt. "Magnetic Properties of the Europium Chalcogenides under Hydrostatic Pressure." In: *Journal of Applied Physics* 40.3 (Mar. 1969), pp. 1328–1329. ISSN: 0021-8979, 1089-7550. DOI: 10.1063/1.1657657.

[75] T. Kasuya. "Exchange Mechanisms in Europium Chalcogenides." In: *IBM Journal of Research and Development* 14.3 (May 1970), pp. 214–223. ISSN: 0018-8646, 0018-8646. DOI: 10.1147/rd.143.0214.

[76] G. Güntherodt, P. Wachter, and D. M. Imboden. "Energy level scheme and the effect of magnetic order on the optical transitions in europium chalcogenides." In: *Physik der Kondensierten Materie* 12.4 (May 1971), pp. 292–310. ISSN: 1434-6028, 1434-6036. DOI: 10.1007/BF02422557.

[77] P. Wachter. "The optical electrical and magnetic properties of the europium chalcogenides and the rare earth pnictides." In: *C R C Critical Reviews in Solid State Sciences* 3.2 (July 1972), pp. 189–241. ISSN: 0011-085X. DOI: 10.1080/10408437208244865.

[78] A. Kornblit, G. Ahlers, and E. Buehler. "Heat capacity of RbMnF3 and EuO near the magnetic phase transitions." In: *Physics Letters A* 43.6 (Apr. 1973), pp. 531–532. ISSN: 03759601. DOI: 10.1016/0375-9601(73)90027-3.

[79] G. Güntherodt. "Optical properties and electronic structure of europium chalcogenides." In: *Physics of Condensed Matter* 18.1 (July 1974), pp. 37–78. ISSN: 1434-6028, 1434-6036. DOI: 10.1007/BF01950500.

[80] D.D. Berkner. "Magneto-optic study of the critical region of EuS." In: *Physics Letters A* 54.5 (Oct. 1975), pp. 396–398. ISSN: 03759601. DOI: 10.1016/0375-9601(75)90785-9.

[81] W. Zinn. "Microscopic studies of magnetic properties and interactions recent results on europium-monochalcogenides." In: *Journal of Magnetism and Magnetic Materials* 3.1–2 (Mar. 1976), pp. 23–36. ISSN: 03048853. DOI: 10.1016/0304-8853(76)90007-X.

[82] H. G. Bohn, W. Zinn, B. Dorner, and A. Kollmar. "Neutron scattering study of spin waves and exchange interactions in ferromagnetic EuS." In: *Physical Review B* 22.11 (Dec. 1980), pp. 5447–5452. ISSN: 0163-1829. DOI: 10.1103/PhysRevB.22.5447.

[83] Paul Fumagalli and Joachim Schoenes. *Magneto-optics*. De Gruyter, Dec. 2021. ISBN: 978-3-11-063530-0. DOI: 10.1515/9783110635300-202. URL: https://www.degruyter.com/document/doi/10.1515/9783110635300-202/html.

[84] P. G. Steeneken. "New light on EuO thin films: preparation, transport, magnetism and spectroscopy of a ferromagnetic semiconductor." PhD thesis. Groningen, Netherlands: Universiteit Groningen, Mar. 2002.

[85] W Reim and J. Schoenes. "Magneto-optical spectroscopy of f-electron systems." In: *Handbook of Ferromagnetic Materials, Vol. 5*. Ed. by K. H. J. Buschow and E. P. Wohlfarth. Springer International Publishing, 1990. ISBN: 978-0-444-87477-1. URL: https://www.sciencedirect.com/handbook/handbook-of-ferromagnetic-materials/vol/5/suppl/C.

[86] B. T. Matthias, R. M. Bozorth, and J. H. Van Vleck. "Ferromagnetic Interaction in EuO." In: *Physical Review Letters* 7.5 (Sept. 1961), pp. 160–161. ISSN: 0031-9007. DOI: 10.1103/PhysRevLett.7.160.

[87] J. Lettieri, V. Vaithyanathan, S. K. Eah, J. Stephens, V. Sih, D. D. Awschalom, J. Levy, and D. G. Schlom. "Epitaxial growth and magnetic properties of EuO on (001) Si by molecular-beam epitaxy." In: *Applied Physics Letters* 83.5 (Aug. 2003), pp. 975–977. ISSN: 0003-6951, 1077-3118. DOI: 10.1063/1.1593832.

[88] R. W. Ulbricht, A. Schmehl, T. Heeg, J. Schubert, and D. G. Schlom. "Adsorption-controlled growth of EuO by molecular-beam epitaxy." In: *Applied Physics Letters* 93.10 (Sept. 2008), p. 102105. ISSN: 0003-6951, 1077-3118. DOI: 10.1063/1.2973180.

[89] R. Sutarto, S. G. Altendorf, B. Coloru, et al. "Epitaxial and layer-by-layer growth of EuO thin films on yttria-stabilized cubic zirconia (001) using MBE distillation." In: *Physical Review B* 79.20 (May 2009), p. 205318. ISSN: 1098-0121, 1550-235X. DOI: 10.1103/PhysRevB.79.205318.

[90] A. G. Swartz, J. Ciraldo, J. J. I. Wong, et al. "Epitaxial EuO thin films on GaAs." In: *Applied Physics Letters* 97.11 (Sept. 2010), p. 112509. ISSN: 0003-6951, 1077-3118. DOI: 10.1063/1.3490649.

[91] Andreas Schmehl, Venu Vaithyanathan, Alexander Herrnberger, et al. "Epitaxial integration of the highly spin-polarized ferromagnetic semiconductor EuO with silicon and GaN." In: *Nature Materials* 6.11 (Nov. 2007), pp. 882–887. ISSN: 1476-1122, 1476-4660. DOI: 10.1038/nmat2012.

[92] Raghava P. Panguluri, T. S. Santos, E. Negusse, J. Dvorak, Y. Idzerda, J. S. Moodera, and B. Nadgorny. "Half-metallicity in europium oxide conductively matched with silicon." In: *Physical Review B* 78.12 (Sept. 2008), p. 125307. ISSN: 1098-0121, 1550-235X. DOI: 10.1103/PhysRevB.78.125307.

[93] Yu Song and Gang Dai. "Spin filter and spin valve in ferromagnetic graphene." In: *Applied Physics Letters* 106.22 (June 2015), p. 223104. ISSN: 0003-6951, 1077-3118. DOI: 10.1063/1.4921668.

[94] Vladimir N. Kats, Sergey G. Nefedov, Leonid A. Shelukhin, et al. "Giant quadratic magneto-optical Kerr effect in (Eu,Gd)O films for magnetic field sensing." In: *Applied Materials Today* 19 (June 2020), p. 100640. ISSN: 23529407. DOI: 10.1016/j.apmt.2020.100640.

[95] Masakazu Matsubara, Andreas Schmehl, Jochen Mannhart, Darrell G. Schlom, and Manfred Fiebig. "Large nonlinear magneto-optical effect in the centrosymmetric ferromagnetic semiconductor EuO." In: *Physical Review B* 81.21 (June 2010), p. 214447. ISSN: 1098-0121, 1550-235X. DOI: 10.1103/PhysRevB.81.214447.

[96] Masakazu Matsubara, Carsten Becher, Andreas Schmehl, Jochen Mannhart, Darrell G. Schlom, and Manfred Fiebig. "Optical second- and third-harmonic generation on the ferromagnetic semiconductor europium oxide." In: *Journal of Applied Physics* 109.7 (Apr. 2011), p. 07C309. ISSN: 0021-8979, 1089-7550. DOI: 10.1063/1.3540685.

[97] Masakazu Matsubara, Andreas Schmehl, Jochen Mannhart, Darrell G. Schlom, and Manfred Fiebig. "Giant third-order magneto-optical rotation in ferromagnetic EuO." In: *Physical Review B* 86.19 (Nov. 2012), p. 195127. ISSN: 1098-0121, 1550-235X. DOI: 10.1103/PhysRevB.86.195127.

[98] Y. Shapira, S. Foner, and T. B. Reed. "EuO. I. Resistivity and Hall Effect in Fields up to 150 kOe." In: *Physical Review B* 8.5 (Sept. 1973), pp. 2299–2315. ISSN: 0556-2805. DOI: 10.1103/PhysRevB.8.2299.

[99] W. Nolting and A.M. Oles. "Red shift of the optical absorption edge of ferromagnetic semiconductors." In: *Solid State Communications* 35.12 (Sept. 1980), pp. 1007–1010. ISSN: 00381098. DOI: 10.1016/0038-1098(80)91007-8.

[100] P. G. Steeneken, L. H. Tjeng, I. Elfimov, G. A. Sawatzky, G. Ghiringhelli, N. B. Brookes, and D.-J. Huang. "Exchange Splitting and Charge Carrier Spin Polarization in EuO." In: *Physical Review Letters* 88.4 (Jan. 2002), p. 047201. ISSN: 0031-9007, 1079-7114. DOI: 10.1103/PhysRevLett.88.047201.

[101] T. Mairoser, A. Schmehl, A. Melville, et al. "Is There an Intrinsic Limit to the Charge-Carrier-Induced Increase of the Curie Temperature of EuO?" In: *Physical Review Letters* 105.25 (Dec. 2010), p. 257206. ISSN: 0031-9007, 1079-7114. DOI: 10.1103/PhysRevLett.105.257206.

[102] J. M. An and K. D. Belashchenko. "Electronic structure and magnetic properties of Gd-doped and Eu-rich EuO." In: *Physical Review B* 88.5 (Aug. 2013), p. 054421. ISSN: 1098-0121, 1550-235X. DOI: 10.1103/PhysRevB.88.054421.

[103] Nuttachai Jutong, Ulrich Eckern, Thomas Mairoser, and Udo Schwingenschlögl. "Effect of Gd doping and O deficiency on the Curie temperature of EuO." In: *Scientific Reports* 5.1 (Jan. 2015), p. 8038. ISSN: 2045-2322. DOI: 10.1038/srep08038.

[104] M. W. Shafer and T. R. McGuire. "Studies of Curie Point Increases in EuO." In: *Journal of Applied Physics* 39.2 (Feb. 1968), pp. 588–590. ISSN: 0021-8979, 1089-7550. DOI: 10.1063/1.2163533.

[105] S. von Molnar and M. W. Shafer. "Transport in Gd Doped EuO." In: *Journal of Applied Physics* 41.3 (Mar. 1970), pp. 1093–1094. ISSN: 0021-8979, 1089-7550. DOI: 10.1063/1.1658826.

[106] Tetsuro Matsumoto, Katsuhiko Yamaguchi, Masatada Yuri, Kenji Kawaguchi, Naoto Koshizaki, and Koji Yamada. "Preparation of Gd-doped EuO 1 x thin films and the magnetic and magneto-transport properties." In: *Journal of Physics: Condensed Matter* 16.34 (Sept. 2004), pp. 6017–6028. ISSN: 0953-8984, 1361-648X. DOI: 10.1088/0953-8984/16/34/003.

[107] R. Sutarto, S. G. Altendorf, B. Coloru, et al. "Epitaxy, stoichiometry, and magnetic properties of Gd-doped EuO films on YSZ (001)." In: *Physical Review B* 80.8 (Aug. 2009), p. 085308. ISSN: 1098-0121, 1550-235X. DOI: 10.1103/PhysRevB.80.085308.

[108] Xianjie Wang, Pan Liu, Kyle A. Fox, Jinke Tang, Juan A. Colon Santana, Kirill Belashchenko, Peter A. Dowben, and Yu Sui. "Effects of Gd Doping and Oxygen Vacancies on the Properties of EuO Films Prepared via Pulsed Laser Deposition." In: *IEEE Transactions on Magnetics* 46.6 (June 2010), pp. 1879–1882. ISSN: 0018-9464. DOI: 10.1109/TMAG.2010.2046314.

[109] Masao Takahashi. "Electronic and magnetic properties of Gd-doped EuO." In: *Physical Review B* 86.16 (Oct. 2012), p. 165208. ISSN: 1098-0121, 1550-235X. DOI: 10.1103/PhysRevB.86.165208.

[110] O. Massenet, Y. Capiomont, and Nguyen Van Dang. "Effects of high non-stoichiometry on EuO properties." In: *Journal of Applied Physics* 45.8 (Aug. 1974), pp. 3593–3599. ISSN: 0021-8979, 1089-7550. DOI: 10.1063/1.1663822.

[111] Toyohiko J. Konno, Norihiro Ogawa, Kimio Wakoh, Kenji Sumiyama, and Kenji Suzuki. "Synthesis and Magnetic Properties of Non-Equilibrium Eu-Rich EuO Thin Films." In: *Japanese Journal of Applied Physics* 35.Part 1, No. 12A (Dec. 1996), pp. 6052–6056. ISSN: 0021-4922, 1347-4065. DOI: 10.1143/JJAP.35.6052.

[112] M. Barbagallo, N. D. M. Hine, J. F. K. Cooper, et al. "Experimental and theoretical analysis of magnetic moment enhancement in oxygen-deficient EuO." In: *Physical Review B* 81.23 (June 2010), p. 235216. ISSN: 1098-0121, 1550-235X. DOI: 10.1103/PhysRevB.81.235216.

[113] Pan Liu and Jinke Tang. "A magnetic polaron model for the enhanced Curie temperature of EuO 1− x." In: *Journal of Physics: Condensed Matter* 25.12 (Mar. 2013), p. 125802. ISSN: 0953-8984, 1361-648X. DOI: 10.1088/0953-8984/25/12/125802.

[114] M. R. Oliver, J. A. Kafalas, J. O. Dimmock, and T. B. Reed. "Pressure Dependence of the Electrical Resistivity of EuO." In: *Physical Review Letters* 24.19 (May 1970), pp. 1064–1067. ISSN: 0031-9007. DOI: 10.1103/PhysRevLett.24.1064.

[115] M. R. Oliver, J. O. Dimmock, A. L. McWhorter, and T. B. Reed. "Conductivity Studies in Europium Oxide." In: *Physical Review B* 5.3 (Feb. 1972), pp. 1078–1098. ISSN: 0556-2805. DOI: 10.1103/PhysRevB.5.1078.

[116] A Mauger and C Godart. "Metal-Insulator transition in Eu rich EuO." In: *Solid State Communications* 35.10 (1980), pp. 785–788.

[117] P. Sinjukow and W. Nolting. "Metal-insulator transition in EuO." In: *Physical Review B* 68.12 (Sept. 2003), p. 125107. ISSN: 0163-1829, 1095-3795. DOI: 10.1103/PhysRevB.68.125107.

[118] Dmitri R. Yakovlev and Wolfgang Ossau. "Magnetic Polarons." In: *Introduction to the Physics of Diluted Magnetic Semiconductors*. Ed. by Jan A. Gaj and Jacek Kossut. Springer Series in Materials Science, 2010. ISBN: 978-3-642-15855-1. DOI: 10.1007/978-3-642-15856-8_7.

[119] J.P. Lascaray, J.P. Desfours, and M. Averous. "Bound magnetic polaron evidence in EuO." In: *Solid State Communications* 19.7 (July 1976), pp. 677–679. ISSN: 00381098. DOI: 10.1016/0038-1098(76)91103-0.

[120] D. B. McWhan, P. C. Souers, and G. Jura. "Magnetic and Structural Properties of Europium Metal and Europium Monoxide at High Pressure." In: *Physical Review* 143.2 (Mar. 1966), pp. 385–389. ISSN: 0031-899X. DOI: 10.1103/PhysRev.143.385.

[121] D. DiMarzio, M. Croft, N. Sakai, and M. W. Shafer. "Effect of pressure on the electrical resistance of EuO." In: *Physical Review B* 35.16 (June 1987), pp. 8891–8893. ISSN: 0163-1829. DOI: 10.1103/PhysRevB.35.8891.

[122] V. G. Tissen and E. G. Poinyatowskii. "Behaviour of the Curie temperature of EuO at pressures up to 20 GPa." In: *JETP Letters* 46.7 (1987). URL: http://jetpletters.ru/ps/1230/article_18586.pdf.

[123] W. Söllinger, W. Heiss, R. T. Lechner, K. Rumpf, P. Granitzer, H. Krenn, and G. Springholz. "Exchange interactions in europium monochalcogenide magnetic semiconductors and their dependence on hydrostatic strain." In: *Physical Review B* 81.15 (Apr. 2010), p. 155213. ISSN: 1098-0121, 1550-235X. DOI: 10.1103/PhysRevB.81.155213.

[124] N. J. C. Ingle and I. S. Elfimov. "Influence of epitaxial strain on the ferromagnetic semiconductor EuO : First-principles calculations." In: *Physical Review B* 77.12 (Mar. 2008), p. 121202. ISSN: 1098-0121, 1550-235X. DOI: 10.1103/PhysRevB.77.121202.

[125] Pan Liu, Juan A.Colón Santana, Qilin Dai, Xianjie Wang, Peter A. Dowben, and Jinke Tang. "Sign of the superexchange coupling between next-nearest neighbors in EuO." In: *Physical Review B* 86.22 (Dec. 2012), p. 224408. ISSN: 1098-0121, 1550-235X. DOI: 10.1103/PhysRevB.86.224408.

[126] Hari Babu Vasili, Matheus Gamino, Jaume Gazquez, Florencio Sanchez, Manuel Valvidares, Pierluigi Gargiani, Eric Pellegrin, and Josep Fontcuberta. "Magnetoresistance in hybrid Pt/CoFe2O4 bilayers controlled by competing spin accumulation and interfacial chemical reconstruction." In: *ACS applied materials & interfaces* 10.14 (2018), pp. 12031–12041.

[127] J. J. Hauser. "Magnetic Proximity Effect." In: *Physical Review* 187.2 (Nov. 1969), pp. 580–583. ISSN: 0031-899X. DOI: 10.1103/PhysRev.187.580.

[128] F. Wilhelm, P. Poulopoulos, G. Ceballos, et al. "Layer-Resolved Magnetic Moments in Ni / Pt Multilayers." In: *Physical Review Letters* 85.2 (July 2000), pp. 413–416. ISSN: 0031-9007, 1079-7114. DOI: 10.1103/PhysRevLett.85.413.

[129] F. Wilhelm, P. Poulopoulos, A. Scherz, H. Wende, K. Baberschke, M. Angelakeris, N. K. Flevaris, J. Goulon, and A. Rogalev. "Interface magnetism in 3d/5d multilayers probed by X-ray magnetic circular dichroism." In: *physica status solidi (a)* 196.1 (Mar. 2003), pp. 33–36. ISSN: 00318965, 1521396X. DOI: 10.1002/pssa.200306346.

[130] H. X. Yang, A. Hallal, D. Terrade, X. Waintal, S. Roche, and M. Chshiev. "Proximity Effects Induced in Graphene by Magnetic Insulators: First-Principles Calculations on Spin Filtering and Exchange-Splitting Gaps." In: *Physical Review Letters* 110.4 (Jan. 2013), p. 046603. ISSN: 0031-9007, 1079-7114. DOI: 10.1103/PhysRevLett.110.046603.

[131] Jackson J. Bauer, Patrick Quarterman, Alexander J. Grutter, Bharat Khurana, Subhajit Kundu, K. Andre Mkhoyan, Julie A. Borchers, and Caroline A. Ross. "Magnetic proximity effect in magnetic-insulator/heavy-metal heterostructures across the compensation temperature." In: *Physical Review B* 104.9 (Sept. 2021), p. 094403. ISSN: 2469-9950, 2469-9969. DOI: 10.1103/PhysRevB.104.094403.

[132] Miguel Kiwi. "Origin of the magnetic proximity effect." In: *MRS Online Proceedings Library (OPL)* 746 (2002).

[133] PK Manna and SM Yusuf. "Two interface effects: Exchange bias and magnetic proximity." In: *Physics Reports* 535.2 (2014), pp. 61–99.

[134] F Garcia, J Sort, B Rodmacq, S Auffret, and B Dieny. "Large anomalous enhancement of perpendicular exchange bias by introduction of a nonmagnetic spacer between the ferromagnetic and antiferromagnetic layers." In: *Applied physics letters* 83.17 (2003), pp. 3537–3539.

[135] RL Stamps. "Mechanisms for exchange bias." In: *Journal of Physics D: Applied Physics* 33.23 (2000), R247.

[136] F. Maccherozzi, M. Sperl, G. Panaccione, et al. "Evidence for a Magnetic Proximity Effect up to Room Temperature at Fe / (Ga , Mn) As Interfaces." In: *Physical Review Letters* 101.26 (Dec. 2008), p. 267201. ISSN: 0031-9007, 1079-7114. DOI: 10.1103/PhysRevLett.101.267201.

[137] M. Sperl, F. Maccherozzi, F. Borgatti, et al. "Identifying the character of ferromagnetic Mn in epitaxial Fe/(Ga,Mn)As heterostructures." In: *Physical Review B* 81.3 (Jan. 2010), p. 035211. ISSN: 1098-0121, 1550-235X. DOI: 10.1103/PhysRevB.81.035211.

[138] C. Song, M. Sperl, M. Utz, M. Ciorga, G. Woltersdorf, D. Schuh, D. Bougeard, C. H. Back, and D. Weiss. "Proximity Induced Enhancement of the Curie Temperature in Hybrid Spin Injection Devices." In: *Physical Review Letters* 107.5 (July 2011), p. 056601. ISSN: 0031-9007, 1079-7114. DOI: 10.1103/PhysRevLett.107.056601.

[139] Ivana Vobornik, Unnikrishnan Manju, Jun Fujii, Francesco Borgatti, Piero Torelli, Damjan Krizmancic, Yew San Hor, Robert J. Cava, and Giancarlo Panaccione. "Magnetic Proximity Effect as a Pathway to Spintronic Applications of Topological Insulators." In: *Nano Letters* 11.10 (Oct. 2011), pp. 4079–4082. ISSN: 1530-6984, 1530-6992. DOI: 10.1021/nl201275q.

[140] Yan Zhang, Keisuke Shinokita, Kenji Watanabe, et al. "Controllable Magnetic Proximity Effect and Charge Transfer in 2D Semiconductor and Double Layered Perovskite Manganese Oxide van der Waals Heterostructure." In: *Advanced Materials* 32.50 (Dec. 2020), p. 2003501. ISSN: 0935-9648, 1521-4095. DOI: 10.1002/adma.202003501.

[141] V. V. Volobuev, A. N. Stetsenko, and J. van Lierop. "Film thickness dependence of the enhanced EuS interface ordering temperature in EuS/Co thin films." In: *Journal of Applied Physics* 103.7 (Apr. 2008), p. 07C905. ISSN: 0021-8979, 1089-7550. DOI: 10.1063/1.2832627.

[142] M. Szot, L. Kowalczyk, T. Story, V. Domukhovski, W. Knoff, K. Gas, V.V. Volobuev, A.Yu. Sipatov, and A.G. Fedorov. "Magnetic Properties of EuS/Co Multilayers on KCl and BaF Substrates." In: *Acta Physica Polonica A* 114.5 (Nov. 2008), pp. 1397–1402. ISSN: 0587-4246, 1898-794X. DOI: 10.12693/APhysPolA.114.1397.

[143] B. Lewitz, A. Straub, V. Kapaklis, P. Poulopoulos, A. Delimitis, S. D. Pappas, and P. Fumagalli. "Proximity effects and Curie temperature enhancment in Co/EuS and Fe/EuS multilayers." In: *SPIN* 02.04 (Dec. 2012), p. 1250016. ISSN: 2010-3247, 2010-3255. DOI: 10.1142/S2010324712500166.

[144] S. D. Pappas, P. Poulopoulos, B. Lewitz, A. Straub, A. Goschew, V. Kapaklis, F. Wilhelm, A. Rogalev, and P. Fumagalli. "Direct evidence for significant spin-polarization of EuS in Co/EuS multilayers at room temperature." In: *Scientific Reports* 3.1 (Dec. 2013), p. 1333. ISSN: 2045-2322. DOI: 10.1038/srep01333.

[145] A. Goschew, M. Scott, and P. Fumagalli. "Verification of antiferromagnetic exchange coupling at room temperature using polar magneto-optic Kerr effect in thin EuS/Co multilayers with perpendicular magnetic anisotropy." In: *Applied Physics Letters* 109.6 (Aug. 2016), p. 062401. ISSN: 0003-6951, 1077-3118. DOI: 10.1063/1.4960794.

[146] M S S Brooks, O Eriksson, and B Johansson. "3d-5d band magnetism in rare earth transition metal intermetallics: LuFe 2." In: *Journal of Physics: Condensed Matter* 1.34 (Aug. 1989), pp. 5861–5874. ISSN: 0953-8984, 1361-648X. DOI: 10.1088/0953-8984/1/34/004.

[147] Dmitry V. Averyanov, Andrey M. Tokmachev, Oleg E. Parfenov, et al. "Probing proximity effects in the ferromagnetic semiconductor EuO." In: *Applied Surface Science* 488 (Sept. 2019), pp. 107–114. ISSN: 01694332. DOI: 10.1016/j.apsusc.2019.05.191.

[148] Patrick Lömker. "Interfacing EuO in confined oxide and metal heterostructures." PhD thesis. TU Dortmund, 2018. ISBN: 9783958063372.

[149] Michael Faraday. "On the magnetization of light and the illumination of magnetic lines of force." In: *Philosophical Transactions of the Royal Society of London* 136 (Dec. 1846), pp. 1–20. ISSN: 0261-0523, 2053-9223. DOI: 10.1098/rstl.1846.0001.

[150] K. Shinagawa. "Faraday and Kerr Effects in Ferromagnets." In: *Magneto-Optics*. Ed. by Satoru Sugano and Norimichi Kojima. Vol. 128. Springer Series in Solid-State Sciences. Berlin, Heidelberg: Springer Berlin Heidelberg, 2000. ISBN: 978-3-642-08523-9. DOI: 10.1007/978-3-662-04143-7. URL: http://link.springer.com/10.1007/978-3-662-04143-7.

[151] John Kerr. "XLIII. On rotation of the plane of polarization by reflection from the pole of a magnet." In: *The London, Edinburgh, and Dublin Philosophical Magazine and Journal of Science* 3.19 (May 1877), pp. 321–343. ISSN: 1941-5982, 1941-5990. DOI: 10.1080/14786447708639245.

[152] Wolfgang Demtröder. *Experimentalphysik 2*. Springer-Lehrbuch. Berlin, Heidelberg: Springer Berlin Heidelberg, 2013. ISBN: 978-3-642-29943-8. DOI: 10.1007/978-3-642-29944-5.

[153] A. K. Zvezdin and V. A. Kotov. *Modern magnetooptics and magnetooptical materials*. CRC Press, 1997. ISBN: 978-0-367-80260-8.

[154] P. M. Oppeneer. "Magneto-Optical Kerr Spectra." In: *Handbook of Magnetic Materials*. Vol. 13. Elsevier, Amsterdam, 2001, pp. 229–422.

[155] Haibin Zhao. "4. Photo-induced spin dynamics in spintronic materials." In: *Advances in Condensed Matter Optics*. DE GRUYTER, Dec. 2015, pp. 139–190. ISBN: 978-3-11-030693-4. DOI: 10.1515/9783110307023.139. URL: https://www.degruyter.com/document/doi/10.1515/9783110307023.139/html.

[156] Mark L.M. Lalieu and Bert Koopmans. "Magneto-optics and Laser-Induced Dynamics of Metallic Thin Films." In: *Handbook of Magnetism and Magnetic Materials*. Ed. by J. M. D. Coey and Stuart S.P. Parkin. Springer International Publishing, 2021. ISBN: 978-3-030-63208-3. DOI: 10.1007/978-3-030-63210-6. URL: https://link.springer.com/10.1007/978-3-030-63210-6.

[157] P S Pershan. "Magneto-Optical Effects." In: *Journal of Applied Physics* 38.3 (1967).

[158] M. Freiser. "A survey of magnetooptic effects." In: *IEEE Transactions on Magnetics* 4.2 (June 1968), pp. 152–161. ISSN: 1941-0069. DOI: 10.1109/TMAG.1968.1066210.

[159] W. Wettling. "Magneto-optics of ferrites." In: *Journal of Magnetism and Magnetic Materials* 3.1–2 (Mar. 1976), pp. 147–160. ISSN: 03048853. DOI: 10.1016/0304-8853(76)90026-3.

[160] G A Smolenskii, R V Pisarev, and I G Sinn. "Birefringence of light in magnetically ordered crystals." In: *Soviet Physiscs Uspekhi* 18.6 (1975), p. 21.

[161] Lev Davidovič Landau, Evgenij M. Lifšic, Lev P. Pitaevskij, and Lev Davidovič Landau. *Electrodynamics of continuous media*. 2. ed., rev.enlarged, repr. Course of theoretical physics / L. D. Landau and E. M. Lifshitz. Amsterdam Heidelberg: Elsevier Butterworth-Heinemann, 2009. ISBN: 978-0-7506-2634-7.

[162] Lars Onsager. "Reciprocal Relations in Irreversible Processes. I." In: *Physical Review* 37.4 (Feb. 1931), pp. 405–426. ISSN: 0031-899X. DOI: 10.1103/PhysRev.37.405.

[163] Lars Onsager. "Reciprocal Relations in Irreversible Processes. II." In: *Physical Review* 38.12 (Dec. 1931), pp. 2265–2279. ISSN: 0031-899X. DOI: 10.1103/PhysRev.38.2265.

[164] Toshihiko Yokoyama, Takeshi Nakagawa, and Yasumasa Takagi. "Magnetic circular dichroism for surface and thin film magnetism: Measurement techniques and surface chemical applications." In: *International Reviews in Physical Chemistry* 27.3 (July 2008), pp. 449–505. ISSN: 0144-235X, 1366-591X. DOI: 10.1080/01442350802127608.

[165] Seung-gi Gang, Roman Adam, Moritz Plötzing, et al. "Element-selective investigation of femtosecond spin dynamics in NiPd magnetic alloys using extreme ultraviolet radiation." In: *Phys. Rev. B* 97 (6 Feb. 2018), p. 064412. DOI: 10.1103/PhysRevB.97.064412.

[166] David J Hilton. "Ultrafast Pump–Probe Spectroscopy." In: *Optical Techniques for Solid-State Materials Characterization*. Ed. by Rohit P. Prasankumar and Antoinette J. Taylor. 1st Edition. CRC Press, 2012, p. 42. ISBN: 978-0-429-19291-3.

[167] Andrei Kirilyuk, Alexey V. Kimel, and Theo Rasing. "Ultrafast optical manipulation of magnetic order." In: *Reviews of Modern Physics* 82.3 (Sept. 2010), pp. 2731–2784. ISSN: 0034-6861, 1539-0756. DOI: 10.1103/RevModPhys.82.2731.

[168] D Bossini, M Pancaldi, L Soumah, M Basini, F Mertens, M Cinchetti, T Satoh, O Gomonay, and S Bonetti. "Ultrafast Amplification and Nonlinear Magnetoelastic Coupling of Coherent Magnon Modes in an Antiferromagnet." In: *PHYSICAL REVIEW LETTERS* 127.077202 (2021), p. 6.

[169] E. Beaurepaire, J.-C. Merle, A. Daunois, and J.-Y. Bigot. "Ultrafast Spin Dynamics in Ferromagnetic Nickel." In: *Physical Review Letters* 76.22 (May 1996), pp. 4250–4253. ISSN: 0031-9007, 1079-7114. DOI: 10.1103/PhysRevLett.76.4250.

[170] J. Hohlfeld, E. Matthias, R. Knorren, and K. H. Bennemann. "Nonequilibrium Magnetization Dynamics of Nickel." In: *Physical Review Letters* 78.25 (June 1997), pp. 4861–4864. ISSN: 0031-9007, 1079-7114. DOI: 10.1103/PhysRevLett.78.4861.

[171] J. Güdde, U. Conrad, V. Jähnke, J. Hohlfeld, and E. Matthias. "Magnetization dynamics of Ni and Co films on Cu(001) and of bulk nickel surfaces." In: *Physical Review B* 59.10 (Mar. 1999), R6608–R6611. ISSN: 0163-1829, 1095-3795. DOI: 10.1103/PhysRevB.59.R6608.

[172] B. Koopmans, M. Van Kampen, J. T. Kohlhepp, and W. J. M. De Jonge. "Ultrafast Magneto-Optics in Nickel: Magnetism or Optics?" In: *Physical Review Letters* 85.4 (July 2000), pp. 844–847. ISSN: 0031-9007, 1079-7114. DOI: 10.1103/PhysRevLett.85.844.

[173] H.-S. Rhie, H. A. Dürr, and W. Eberhardt. "Femtosecond Electron and Spin Dynamics in N i / W (110) Films." In: *Physical Review Letters* 90.24 (June 2003), p. 247201. ISSN: 0031-9007, 1079-7114. DOI: 10.1103/PhysRevLett.90.247201.

[174] T. Ogasawara, K. Ohgushi, Y. Tomioka, K. S. Takahashi, H. Okamoto, M. Kawasaki, and Y. Tokura. "General Features of Photoinduced Spin Dynamics in Ferromagnetic and Ferrimagnetic Compounds." In: *Physical Review Letters* 94.8 (Mar. 2005), p. 087202. ISSN: 0031-9007, 1079-7114. DOI: 10.1103/PhysRevLett.94.087202.

[175] Ganping Ju, Julius Hohlfeld, Bastiaan Bergman, René J. M. Van De Veerdonk, Oleg N. Mryasov, Jai-Young Kim, Xiaowei Wu, Dieter Weller, and Bert Koopmans. "Ultrafast Generation of Ferromagnetic Order via a Laser-Induced Phase Transformation in FeRh Thin Films." In: *Physical Review Letters* 93.19 (Nov. 2004), p. 197403. ISSN: 0031-9007, 1079-7114. DOI: 10.1103/PhysRevLett.93.197403.

[176] M. Van Kampen, C. Jozsa, J. T. Kohlhepp, P. LeClair, L. Lagae, W. J. M. De Jonge, and B. Koopmans. "All-Optical Probe of Coherent Spin Waves." In: *Physical Review Letters* 88.22 (May 2002), p. 227201. ISSN: 0031-9007, 1079-7114. DOI: 10.1103/PhysRevLett.88.227201.

[177] C. D. Stanciu, F. Hansteen, A. V. Kimel, A. Kirilyuk, A. Tsukamoto, A. Itoh, and Th. Rasing. "All-Optical Magnetic Recording with Circularly Polarized Light." In: *Physical Review Letters* 99.4 (July 2007), p. 047601. ISSN: 0031-9007, 1079-7114. DOI: 10.1103/PhysRevLett.99.047601.

[178] I. Radu, K. Vahaplar, C. Stamm, et al. "Transient ferromagnetic-like state mediating ultrafast reversal of antiferromagnetically coupled spins." In: *Nature* 472.7342 (Apr. 2011), pp. 205–208. ISSN: 0028-0836, 1476-4687. DOI: 10.1038/nature09901.

[179] A. J. Schellekens, K. C. Kuiper, R.R.J.C. De Wit, and B Koopmans. "Ultrafast spin-transfer torque driven by femtosecond pulsed-laser excitation." In: *Nature Communications* 5.1 (July 2014), p. 4333. ISSN: 2041-1723. DOI: 10.1038/ncomms5333.

[180] Gyung-Min Choi, Byoung-Chul Min, Kyung-Jin Lee, and David G. Cahill. "Spin current generated by thermally driven ultrafast demagnetization." In: *Nature Communications* 5.1 (July 2014), p. 4334. ISSN: 2041-1723. DOI: 10.1038/ncomms5334.

[181] W. Hübner and G. P. Zhang. "Ultrafast spin dynamics in nickel." In: *Phys. Rev. B* 58 (10 Sept. 1998), R5920–R5923. DOI: 10.1103/PhysRevB.58.R5920.

[182] Jean-Yves Bigot, Mircea Vomir, and Eric Beaurepaire. "Coherent ultrafast magnetism induced by femtosecond laser pulses." In: *Nature Physics* 5 (7 July 2009), pp. 515–520. DOI: 10.1038/nphys1285.

[183] R. J. Elliott. "Theory of the Effect of Spin-Orbit Coupling on Magnetic Resonance in Some Semiconductors." In: *Phys. Rev.* 96 (2 Oct. 1954), pp. 266–279. DOI: 10.1103/PhysRev.96.266.

[184] Y. Yafet. "g Factors and Spin-Lattice Relaxation of Conduction Electrons**Part of the work connected with the preparation of this article, in particular the work on spin-lattice relaxation, was done while the author was at the Westinghouse Research Laboratories, Pittsburgh, Pennsylvania." In: ed. by Frederick Seitz and David Turnbull. Vol. 14. Solid State Physics. Academic Press, 1963, pp. 1–98. DOI: https://doi.org/10.1016/S0081-1947(08)60259-3.

[185] B. Koopmans, G. Malinowski, F. Dalla Longa, D. Steiauf, M. Fähnle, T. Roth, M. Cinchetti, and M. Aeschlimann. "Explaining the paradoxical diversity of ultrafast laser-induced demagnetization." In: *Nature Materials* 9 (3 Mar. 2010), pp. 259–265. DOI: 10.1038/nmat2593.

[186] B. Koopmans, J. J. M. Ruigrok, F. Dalla Longa, and W. J. M. de Jonge. "Unifying Ultrafast Magnetization Dynamics." In: *Phys. Rev. Lett.* 95 (26 Dec. 2005), p. 267207. DOI: 10.1103/PhysRevLett.95.267207.

[187] M. Battiato, K. Carva, and P. M. Oppeneer. "Superdiffusive Spin Transport as a Mechanism of Ultrafast Demagnetization." In: *Physical Review Letters* 105.2 (July 2010), p. 027203. ISSN: 0031-9007, 1079-7114. DOI: 10.1103/PhysRevLett.105.027203.

[188] M. Battiato, K. Carva, and P. M. Oppeneer. "Theory of laser-induced ultrafast superdiffusive spin transport in layered heterostructures." In: *Physical Review B* 86.2 (July 2012), p. 024404. ISSN: 1098-0121, 1550-235X. DOI: 10.1103/PhysRevB.86.024404.

[189] M. Battiato, P Maldonado, and P. M. Oppeneer. "Treating the effect of interface reflections on superdiffusive spin transport in multilayer samples." In: *Journal of Applied Physics* 115 (2014), p. 172611. DOI: 10.1063/1.4870589.

[190] M. Aeschlimann, M. Bauer, S. Pawlik, W. Weber, R. Burgermeister, D. Oberli, and H. C. Siegmann. "Ultrafast Spin-Dependent Electron Dynamics in fcc Co." In: *Physical Review Letters* 79.25 (Dec. 1997), pp. 5158–5161. ISSN: 0031-9007, 1079-7114. DOI: 10.1103/PhysRevLett.79.5158.

[191] G. Malinowski, F. Dalla Longa, J. H. H. Rietjens, P. V. Paluskar, R. Huijink, H. J. M. Swagten, and B. Koopmans. "Control of speed and efficiency of ultrafast demagnetization by direct transfer of spin angular momentum." In: *Nature Physics* 4.11 (Nov. 2008), pp. 855–858. ISSN: 1745-2473, 1745-2481. DOI: 10.1038/nphys1092.

[192] Dennis Rudolf, Chan La-O-Vorakiat, Marco Battiato, et al. "Ultrafast magnetization enhancement in metallic multilayers driven by superdiffusive spin current." In: *Nature Communications* 3.1 (Sept. 2012), p. 1037. ISSN: 2041-1723. DOI: 10.1038/ncomms2029.

[193] Emrah Turgut, Chan La-o-vorakiat, Justin M. Shaw, et al. "Controlling the Competition between Optically Induced Ultrafast Spin-Flip Scattering and Spin Transport in Magnetic Multilayers." In: *Phys. Rev. Lett.* 110 (19 May 2013), p. 197201. DOI: 10.1103/PhysRevLett.110.197201.

[194] Pavel Balaz, Maciej Zwierzycki, Francesco Cosco, Karel Carva, Pablo Maldonado, and Peter M. Oppeneer. "Theory of superdiffusive spin transport in noncollinear magnetic multilayers." In: *Phys. Rev. B* 107 (17 May 2023), p. 174418. DOI: 10.1103/PhysRevB.107.174418.

[195] M. L. M. Lalieu, P. L. J. Helgers, and B. Koopmans. "Absorption and generation of femtosecond laser-pulse excited spin currents in noncollinear magnetic bilayers." In: *Phys. Rev. B* 96 (1 July 2017), p. 014417. DOI: 10.1103/PhysRevB.96.014417.

[196] P. Balaz, M. Zonda, K. Carva, P. Maldonado, and P. M. Oppeneer. "Transport theory for femtosecond laser-induced spin-transfer torques." In: *Journal of Physics: Condensed Matter* 30 (2018), p. 115801. DOI: 10.1088/1361-648X/aaad95.

[197] Pavel Balaz, Karel Carva, Ulrike Ritzmann, Pablo Maldonado, and Peter M. Oppeneer. "Domain wall dynamics due to femtosecond laser-induced superdiffusive spin transport." In: *Phys. Rev. B* 101 (17 May 2020), p. 174418. DOI: 10.1103/PhysRevB.101.174418.

[198] M. Hofherr, P. Maldonado, O. Schmitt, et al. "Speed and efficiency of femtosecond spin current injection into a nonmagnetic material." In: *Phys. Rev. B* 96 (10 Sept. 2017), p. 100403. DOI: 10.1103/PhysRevB.96.100403.

[199] Alexey Melnikov, Liane Brandt, Niklas Liebing, Mirko Ribow, Ingrid Mertig, and Georg Woltersdorf. "Ultrafast spin transport and control of spin current pulse shape in metallic multilayers." In: *Phys. Rev. B* 106 (10 Sept. 2022), p. 104417. DOI: 10.1103/PhysRevB.106.104417.

[200] M. Battiato and K. Held. "Ultrafast and Gigantic Spin Injection in Semiconductors." In: *Phys. Rev. Lett.* 116 (19 May 2016), p. 196601. DOI: 10.1103/PhysRevLett.116.196601.

[201] M. Battiato. "Spin polarisation of ultrashort spin current pulses injected in semiconductors." In: *Journal of Physics: Condensed Matter* 29 (Mar. 2017), p. 174001. DOI: 10.1088/1361-648X/aa62de.

[202] F. Mertens, M. Terschanski, D. Mönkebüscher, S. Ponzoni, D. Bossini, and M. Cinchetti. "Wide spectral range ultrafast pump–probe magneto-optical spectrometer at low temperature, high-magnetic and electric fields." In: *Review of Scientific Instruments* 91.11 (Nov. 2020), p. 113001. ISSN: 0034-6748, 1089-7623. DOI: 10.1063/5.0024449.

[203] Marc Terschanski. "Phononkopplung an Spins und Ladungen auf der ultraschnellen Zeitskala im antiferromagnetischen Halbleiter MnTe." PhD thesis. Dortmund, Germany: Technische Universität Dortmund, 2022.

[204] C. M. Schneider, P. Bressler, P. Schuster, J. Kirschner, J. J. de Miguel, and R. Miranda. "Curie temperature of ultrathin films of fcc-cobalt epitaxially grown on atomically flat Cu(100) surfaces." In: *Physical Review Letters* 64.9 (Feb. 1990), pp. 1059–1062. ISSN: 0031-9007. DOI: 10.1103/PhysRevLett.64.1059.

[205] T.J. Konno, N. Ogawa, K. Wakoh, K. Sumiyama, and K. Suzuki. "Structure and magnetic properties of Fe/EuO granular films." In: *Materials Science and Engineering: A* 217-218 (1996). International Conference on Nano-Clusters and Granular Materials, pp. 331–335. ISSN: 0921-5093. DOI: https://doi.org/10.1016/S0921-5093(96)10328-2.

[206] V. V. Volobuev, A. N. Stetsenko, A. Yu. Sipatov, and J. van Lierop. "Magnetic exchange effects in PbS/Fe/EuS/PbS thin films." In: *Phys. Rev. B* 81 (13 Apr. 2010), p. 134430. DOI: 10.1103/PhysRevB.81.134430.

[207] P Poulopoulos, A Goschew, Vassilios Kapaklis, et al. "Induced spin-polarization of EuS at room temperature in Ni/EuS multilayers." In: *Applied Physics Letters* 104.11 (2014).

[208] Paul Rosenberger, Matthias Opel, Stephan Geprägs, Hans Huebl, Rudolf Gross, Martina Müller, and Matthias Althammer. "Quantifying the spin mixing conductance of EuO/W heterostructures by spin Hall magnetoresistance experiments." In: *Applied Physics Letters* 118.19 (May 2021), p. 192401. ISSN: 0003-6951, 1077-3118. DOI: 10.1063/5.0049235.

[209] Paul Rosenberger and Martina Müller. "Europium oxide: Growth guide for the first monolayers on oxidic substrates." In: *Physical Review Materials* 6.4 (Apr. 2022), p. 044404. ISSN: 2475-9953. DOI: 10.1103/PhysRevMaterials.6.044404.

[210] R. P. Ingel and D. Leiws III. "Journal of the American Ceramic Society - April 1986 - INGEL - Lattice Parameters and Density for Y2O3 Stabilized ZrO2." In: *J. Am. Ceram. Soc.* 69.325 (1986).

[211] C. Caspers, A. Gloskovskii, W. Drube, C. M. Schneider, and M. Müller. ""Conductive" yttria-stabilized zirconia as an epitaxial template for oxide heterostructures." In: *Journal of Applied Physics* 115.17 (May 2014), p. 17C111. ISSN: 0021-8979, 1089-7550. DOI: 10.1063/1.4863803.

[212] Martina Müller, Patrick Lömker, Paul Rosenberger, Mai Hussein Hamed, David N. Mueller, Ronja A. Heinen, Thomas Szyjka, and Lutz Baumgarten. "Hard x-ray photoelectron spectroscopy of tunable oxide interfaces." In: *Journal of Vacuum Science and Technology A* 40.1 (Jan. 2022), p. 013215. ISSN: 0734-2101, 1520-8559. DOI: 10.1116/6.0001491.

[213] Martina Müller, Guo-Xing Miao, and Jagadeesh S. Moodera. "Thickness dependence of ferromagnetic- and metal-insulator transition in thin EuO films." In: *Journal of Applied Physics* 105.7 (Apr. 2009), p. 07C917. ISSN: 0021-8979, 1089-7550. DOI: 10.1063/1.3063673.

[214] Kenji Kawaguchi, Mitsugu Sohma, and Y. Oosawa. "Magnetic properties of Fe/EuO multilayered films." In: *Journal of Magnetism and Magnetic Materials* 156.1–3 (Apr. 1996), pp. 235–236. ISSN: 03048853. DOI: 10.1016/0304-8853(95)00851-9.

[215] Jinke Tang, Li Feng, C.J. O'Connor, and Sichu Li. "Antiferromagnetic coupling in a macroscopic ferrimagnet EuS-Co." In: *IEEE Transactions on Magnetics* 33.5 (Sept. 1997), pp. 3739–3741. ISSN: 00189464. DOI: 10.1109/20.619556.

[216] Jinke Tang, Christine E O'Connor, and Li Feng. "Magnetotransport and antiferromagnetic coupling in nanocomposites EuS–Co." In: *Journal of Alloys and Compounds* 275–277 (July 1998), pp. 606–610. ISSN: 09258388. DOI: 10.1016/S0925-8388(98)00402-2.

[217] M. S. S. Brooks, L. Nordström, and B. Johansson. "Magnetism of RFe 2 compounds." In: *Journal of Applied Physics* 69.8 (Apr. 1991), pp. 5683–5684. ISSN: 0021-8979, 1089-7550. DOI: 10.1063/1.347937.

[218] M. Binder, A. Weber, O. Mosendz, et al. "Magnetization dynamics of the ferrimagnet CoGd near the compensation of magnetization and angular momentum." In: *Phys. Rev. B* 74 (13 Oct. 2006), p. 134404. DOI: 10.1103/PhysRevB.74.134404.

[219] Do Bang, Pham Van Thach, and Hiroyuki Awano. "Current-induced domain wall motion in antiferromagnetically coupled structures: Fundamentals and applications." In: *Journal of Science: Advanced Materials and Devices* 3.4 (2018), pp. 389–398. ISSN: 2468-2179. DOI: https://doi.org/10.1016/j.jsamd.2018.09.003.

[220] A. B. Drovosekov, D. I. Kholin, and N. M. Kreinies. "Magnetic Properties of Layered Ferrimagnetic Structures Based on Gd and Transition 3d Metals." In: *Journal of Experimental and Theoretical Physics* 131.1 (2020), pp. 149–159. ISSN: 1090-6509. DOI: 10.1134/S1063776120070031.

[221] M. Cinchetti, M. Sánchez Albaneda, D. Hoffmann, et al. "Spin-Flip Processes and Ultrafast Magnetization Dynamics in Co: Unifying the Microscopic and Macroscopic View of Femtosecond Magnetism." In: *Physical Review Letters* 97.17 (Oct. 2006), p. 177201. ISSN: 0031-9007, 1079-7114. DOI: 10.1103/PhysRevLett.97.177201.

[222] Michael Krauß, Tobias Roth, Sabine Alebrand, Daniel Steil, Mirko Cinchetti, Martin Aeschlimann, and Hans Christian Schneider. "Ultrafast demagnetization of ferromagnetic transition metals: The role of the Coulomb interaction." In: *Physical Review B* 80.18 (Nov. 2009), p. 180407. ISSN: 1098-0121, 1550-235X. DOI: 10.1103/PhysRevB.80.180407.

[223] Vivek Unikandanunni, Rajasekhar Medapalli, and Eric E Fullerton. "Anisotropic ultrafast spin dynamics in epitaxial cobalt." In: *Applied Physics Letters* 118 (2021), p. 232404.

[224] M. C. Donker. "Ultrafast Carrier and Magnetization Dynamics in EuO." Master thesis. Groningen, Netherlands: University of Groningen, 2006.

[225] S. A. McGill, R. I. Miller, O. N. Torrens, A. Mamchik, I-Wei Chen, and J. M. Kikkawa. "Optical evidence for transient photoinduced magnetization in $La_{0.7}Ca_{0.3}MnO_3$." In: *Phys. Rev. B* 71 (7 Feb. 2005), p. 075117. DOI: 10.1103/PhysRevB.71.075117.

[226] J. Wang, I. Cotoros, K. M. Dani, X. Liu, J. K. Furdyna, and D. S. Chemla. "Ultrafast Enhancement of Ferromagnetism via Photoexcited Holes in GaMnAs." In: *Phys. Rev. Lett.* 98 (21 May 2007), p. 217401. DOI: 10.1103/PhysRevLett.98.217401.

[227] M. Matsubara, Y. Okimoto, T. Ogasawara, Y. Tomioka, H. Okamoto, and Y. Tokura. "Ultrafast Photoinduced Insulator-Ferromagnet Transition in the Perovskite Manganite $Gd_{0.55}Sr_{0.45}MnO_3$." In: *Phys. Rev. Lett.* 99 (20 Nov. 2007), p. 207401. DOI: 10.1103/PhysRevLett.99.207401.

[228] Subodha Mishra and Sashi Satpathy. "Photoinduced Magnetism in the Ferromagnetic Semiconductors." In: *International Journal of Modern Physics B* 24.03 (2010), pp. 359–367. DOI: 10.1142/S0217979210055068.

[229] Antonio Caretta, Michiel C. Donker, Alexey O. Polyakov, Thomas T. M. Palstra, and Paul H. M. van Loosdrecht. "Photoinduced magnetization enhancement in two-dimensional weakly anisotropic Heisenberg magnets." In: *Phys. Rev. B* 91 (2 Jan. 2015), p. 020405. DOI: 10.1103/PhysRevB.91.020405.

[230] Li-Zhen Cai, Ming-Sheng Wang, and Guo-Cong Guo. "Photoinduced Significant Magnetization Enhancement in a Viologen-Based Photochromic Compound." In: *American Chemical Society* 23 (3 Mar. 2023), pp. 1592–1597. DOI: doi:10.1021/acs.cgd.2c01223.

[231] Richard C. Prince, Renee R. Frontiera, and Eric O. Potma. "Stimulated Raman Scattering: From Bulk to Nano." In: *Chemical Reviews* 117.7 (Apr. 2017), pp. 5070–5094. ISSN: 0009-2665, 1520-6890. DOI: 10.1021/acs.chemrev.6b00545.

[232] Filippo Glerean, Stefano Marcantoni, Giorgia Sparapassi, Andrea Blason, Martina Esposito, Fabio Benatti, and Daniele Fausti. "Quantum model for impulsive stimulated Raman scattering." In: *Journal of Physics B: Atomic, Molecular and Optical Physics* 52.14 (July 2019), p. 145502. ISSN: 0953-4075, 1361-6455. DOI: 10.1088/1361-6455/ab0bdc.

[233] Wolfgang SM Werner, Kathrin Glantschnig, and Claudia Ambrosch-Draxl. "Optical constants and inelastic electron-scattering data for 17 elemental metals." In: *Journal of Physical and Chemical Reference Data* 38.4 (2009), pp. 1013–1092.

[234] Santanu Pan, Olav Hellwig, and Anjan Barman. "Controlled coexcitation of direct and indirect ultrafast demagnetization in Co/Pd multilayers with large perpendicular magnetic anisotropy." In: *Phys. Rev. B* 98 (21 Dec. 2018), p. 214436. DOI: 10.1103/PhysRevB.98.214436.

[235] MV Lebedev, Oleg V Misochko, Thomas Dekorsy, and Nikolai Georgiev. "On the nature of "coherent artifact"." In: *Journal of Experimental and Theoretical Physics* 100 (2005), pp. 272–282.

[236] D. L. Wood and K. Nassau. "Refractive index of cubic zirconia stabilized with yttria." In: *Appl. Opt.* 21.16 (Aug. 1982), pp. 2978–2981. DOI: 10.1364/AO.21.002978. URL: https://opg.optica.org/ao/abstract.cfm?URI=ao-21-16-2978.

[237] Tom Lichtenberg, Youri LW Van Hees, Maarten Beens, Caspar J Levels, Reinoud Lavrijsen, Rembert A Duine, and Bert Koopmans. "Probing laser-induced spin-current generation in synthetic ferrimagnets using spin waves." In: *Physical Review B* 106.9 (2022), p. 094436.

[238] Julian Hintermayr, Youri LW van Hees, and Bert Koopmans. "Exploring terahertz-scale exchange resonances in synthetic ferrimagnets with ultrashort optically induced spin currents." In: *Physical Review B* 108.2 (2023), p. 024401.

[239] Daniel C Ralph and Mark D Stiles. "Spin transfer torques." In: *Journal of Magnetism and Magnetic Materials* 320.7 (2008), pp. 1190–1216.

[240] Fangzhou Wang, Daniel E. Bürgler, Roman Adam, Umut Parlak, Derang Cao, Christian Greb, Sarah Heidtfeld, and Claus M. Schneider. "Magnetization relaxation dynamics in [Co / Pt] 3 multilayers on pico- and nanosecond timescales." In: *Physical Review Research* 3.3 (July 2021), p. 033061. ISSN: 2643-1564. DOI: 10.1103/PhysRevResearch.3.033061.

[241] M Agrawal, VI Vasyuchka, AA Serga, et al. "Role of bulk-magnon transport in the temporal evolution of the longitudinal spin-Seebeck effect." In: *Physical Review B* 89.22 (2014), p. 224414.

Danksagung

Abschließend möchte ich gerne all denen danken, die mich während der letzten Jahre begleitet, und zum erfolgreichen Abschluss meiner Promotion beigetragen haben. An erster Stelle sei da mein Doktorvater Mirko Cinchetti genannt, der mir die Möglichkeit eröffnet hat meine Dissertation in einer angenehmen Arbeitsumgebung über ein interessantes Thema zu schreiben. Vielen Dank für die Betreuung meiner Arbeit und die vielen fachlichen Diskussionen, die zum Verständnis unserer Messergebnisse führten. Ebenfalls möchte ich Martina Müller, welche die Zweitkorrektur übernommen hat und stets mit fachlichem Rat über Europiumoxid hilfreich zur Seite stand, und Paul Rosenberger, der unsere vermessenen Proben hergestellt hat, danken.

Desweiteren möchte ich mich für die erfolgreiche Zusammenarbeit und die gute Arbeitsatmosphäre bei dem gesamtem Lehrstuhl bedanken. Insbesondere sei hier Fabian Mertens genannt, von dem ich sehr viel über die Laborarbeit gelernt habe und der mir stets bei Problemen hilfsbereit zur Seite stand - gerne auch um 3 Uhr morgens. Ebenfalls möchte ich Umut Parlak danken, der es mir ermöglicht hat zusätzliche Messungen am FZ Jülich durchzuführen, und der stehts ein offenes Ohr für Fragen und Diskussionen hatte. Auch bei Marc Terschanski und Sophie Bork möchte ich mich bedanken, mit denen die langwierige Arbeit im Labor nie langweilig wurde. Vielen Dank euch allen, für die schöne Zeit in den letzten Jahren!

Natürlich möchte ich auch meiner Familie danken, die in meinen 10 Jahren an der TU Dortmund immer hinter mir stand und mich unterstützt hat. Abschließend möchte ich mich bei Julia, meiner Frau, bedanken. Vielen Dank für deine Unterstützung und deine Geduld in den letzten Jahren.